Low-current behaviour and current chopping of vacuum arcs

LOW-CURRENT BEHAVIOUR AND CURRENT CHOPPING OF VACUUM ARCS

RENE SMEETS

LOW-CURRENT BEHAVIOUR AND CURRENT CHOPPING OF VACUUM ARCS

CIP-GEGEVENS KONINKLIJKE BIBLIOTHEEK, DEN HAAG

Smeets, René Peter Paul

Low-current behaviour and current chopping
of vacuum arcs / René Peter Paul Smeets.-
[S.l. : s.n.]. - Fig., tab.
Proefschrift Eindhoven. - Met lit. opg., reg.
ISBN 90-9001649-X
SISO 661.52 UDC 621.316.57.064.26(043.3) NUGI 832
Trefw.: hoogspanningsschakelaars / gasontladingen.

LOW-CURRENT BEHAVIOUR AND CURRENT CHOPPING OF VACUUM ARCS

PROEFSCHRIFT

ter verkrijging van de graad van doctor aan de Technische Universiteit Eindhoven, op gezag van de rector magnificus, prof.dr. F.N. Hooge, voor een commissie aangewezen door het college van decanen in het openbaar te verdedigen op vrijdag 19 juni 1987 te 16.00 uur

door

RENE PETER PAUL SMEETS

geboren te Venlo

Druk: Dissertatiedrukkerij Wibro, Helmond.

Dit proefschrift is goedgekeurd door de promotoren:

Prof.dr.ir. W.M.C. van den Heuvel
en
Prof.dr. M.P.H. Weenink

"Statt eines Ganzen, Abgeschlossenen, wie ich geträumt, hinterlasse ich Stückwerk, Unvollendetes: wie es dem Menschen bestimmt ist"

Gustav Mahler

Aan mijn ouders, die mij op een gelukkige dag een mikroskoop kochten

Table of contents:

Parts of this thesis have been published elsewhere in a summarized form:

- Smeets R.P.P. and Schulpen F.J.H., "Extinction of low-current vacuum arcs", XVIIth Int. Conf. on Phen. in Ion. Gases, Budapest (1985) 795-7
- Smeets R.P.P., "Stability of low-current vacuum arcs", J. Phys. D: Appl. Phys., vol. 19 (1986) 575-87
- Smeets R.P.P., "Electron shield currents following forced decline of vacuum arc current", XIIth Int. Symp. on Disch. and Elec. Insul. in Vac., Shoresh (1986) 205-8
- Smeets R.P.P., "Transient electron shield currents in vacuum arcs", J. Phys. D: Appl. Phys., vol. 19 (1986) 2401-13

DANKWOORD

Het werk, beschreven in dit proefschrift, is uitgevoerd in de vakgroep "Elektrische Energiesystemen" van de Fakulteit Elektrotechniek van de Technische Universiteit Eindhoven.

De eerste stappen op dit voor mij nieuwe werkterrein werden gezet aan de bekwame hand van dr.ir. Jaap Daalder. Van diens baanbrekende werk heb ik uitermate kunnen profiteren. Bovenal ben ik dank verschuldigd aan prof.dr.ir. Wil van den Heuvel. Zijn wetenschappelijke, didaktische en menselijke kwaliteiten hebben mij zeer gesteund. Grote waardering gaat uit naar de manier waarop hij de teugels van de direkte toepasbaarheid niet strak hanteerde. Zeer nuttig waren ook de diskussies met prof.dr. M.P.H. Weenink en prof.dr. F.J. de Hoog.

Geen promotie-onderzoek zonder technische bijstand. De heren Arie van Staalduinen als kundig vakuum-specialist, Ton Wilmes als bekwaam elektronicus en ing. Hans Vossen als experimentator, leverden belangrijke bijdragen. In een aanzienlijk stuk computerwerk wist ik me verzekerd van de steun van dr.ir. Vlastimil Kalasek en ir. Joop Sloot. De tekst van het proefschrift werd getypt door mevr. Jeanne Loonen; andere administratieve hulp kreeg ik van mevr. Miep Marrevée.

Een niet te onderschatten deel van het werk heb ik te danken aan (ex-)studenten. Met name zij genoemd de afstudeerders:

Ir. Theo Meeks, die knap ingenieurswerk afleverde; de gedegen aanpak van ir. Jack Doomernik heeft geresulteerd in waardevolle metingen; ir. Huub Reijnders, wiens veelzijdigheid me meer dan eens trof. Als laatste maar niet de minste ir. Frans Schulpen, die door zijn positief kritische instelling een uitmuntend stuk werk verrichtte. Verder ben ik dank verschuldigd aan de 7 stagiairs, die bij het projekt betrokken waren.

Fu Yan hong M. Sc. bedank ik voor de interessante bijdragen. Ik wens haar veel sukses. The cover artwork is performed by Mr. Shi hong.

Tot slot gaat mijn erkentelijkheid uit naar de medewerkers van HOLEC Innovatie en Technologie Oost, met name naar ir. Jer Lipperts en later dr.ir. Hans Schellekens, die door diskussie en het ter beschikking stellen van (uiteenlopende) middelen de praktische waarde van het werk hebben doen vergroten.

April 1987 *René Smeets*

1. INTRODUCTION

Circuit breaking

The principle of current interruption by means of an electrical conducting plasma between separating contacts is in use for just over a hundred years. Since the introduction of large scale power networks, circuit breakers are among the most important elements for protection of power transmission- and distribution systems.

The interruption process is characterized by a change of impedance of the interrupting medium within microseconds. Before interruption, when contacts are butted together, impedance is less than a mΩ whereas an almost infinite impedance must be attained in opened position after interruption. The transition between these extremes must be achieved in such a way, that reliable interruption is achieved under all possible network conditions.

Demands are extremely severe in modern AC power networks, especially in case of short circuits, when currents of up to several tens of kA must be switched off within milliseconds. Besides that, transient recovery voltages with rates of rise of some kV/μs must be withstood immediately after interruption.

In the history of circuit breaker technology, the major breakthroughs are accomplished by the introduction of novel interrupting media. Very early designs simply use atmospheric air, in the late 1920's revolutionarized by the introduction of forced cooling of switching arcs by air blast.

By this time, the advantages of interruption in oil were recognized. Development of this method of circuit-breaking has been directed towards the reduction of the oil volume.

Since the early 1960's a simultaneous evolution of two new, additional "interrupting media" can be recognized: the isolating, electro-negative gas SF_6 in SF_6 breakers, and the metal vapour released by a discharge in vacuum, formed in the vacuum interrupter.

The vacuum interrupter

At the high voltage (> 72 kV) side of power supply systems gas- and oil breakers still are employed exclusively, while in the medium voltage range (3-70 kV) of power distribution the vacuum interrupter is enjoying a rapidly growing popularity. The advantage of the vacuum interrupter above other types of breakers does not lie so much in the interruption characteristics itself but predominantly in its mechanical simplicity, ease of maintenance, compactness and uncomplicated environmental applicability.

In 1985 its share in world market of medium voltage interrupters amounted to 46% against 19% in 1980 (Fink 86). With an annual sale of many tenthousands of vacuum interrupters, it will be clear that research effort is considerable in this field.

The development of arc physics is greatly accelerated due to the applicability of arc plasmas in circuit breakers. For a conventional (gas, oil-) breaker, consistent and manageable physical models are available and are widely used. Physical processes in the metal vapour discharge in a vacuum interrupter, however, are much less understood and are subject of controversy. This is because the relevant physical processes in the metal vapour discharge in vacuum, or for the sake of simplicity called "vacuum arc", occur in very localized, so-called cathode spots. These cathode spots are very inaccessible to direct measurement because of their dimensions of fractions of mm, their rapid displacement over the cathode surface and the inherent extreme plasma conditions.

Unlike a typical gas-discharge, the behaviour of a vacuum arc is largely determined by the cathode material that must supply the arcing medium. It is widely accepted that the number of simultaneously active cathode spots increases stepwise with arc current. For copper, one cathode spot for every 100 A is reported by various authors (Lafferty 80). Because of the low ionization potential of metal vapours, arc voltage is only some tens of volts. Contrary to a gas-discharge the voltage-current characteristic has a (slightly) positive slope.

For very high currents (>1 kA), anode phenomena come into play, and the domination of cathode processes no longer holds.

Current chopping, overview of the investigation

For low currents (<100 A for copper), it is known that only one cathode spot is active at a time, sustaining the entire discharge. The stability of the discharge therefore, is governed by this one and only emission structure. Whenever power input becomes too low (for copper about 40-50 W) the discharge tends to be highly instable and collapses spontaneously.

In the case of AC power current interruption, this critical point will always be reached sooner or later on the falling sine slope resulting in extinction of the discharge prior to the sine-zero. This phenomenon is called "current chopping". The rapidity of the associated fall of current is such, that large overvoltages can arise endangering network components at the load side of the interrupter.

The vast majority of switching operations "in vacuum" is performed by vacuum switches. These are distinguished from vacuum circuit breakers only by the inability to break large fault currents. It is also in these vacuum switches, that generation of overvoltages caused by current chopping can be troublesome. This applies especially when switching off inductive loads, such as locked motors and transformers in no-load operation during their inrush period.

In modern vacuum interrupters, generation of overvoltages is rarely a serious problem. Due to the careful selection of special metals for contact material, these switching overvoltages can be handled by standard surge protection techniques. Chopping current levels of 3-8 A for breakers and approx. 1 A for motor switches are common, against 15-20 A in early designs.

Investigation of vacuum arc behaviour at low currents, where only one cathode spot is active, can reveal important information about the discharge in a state where the essential current zero phenomena like current chopping and the interruption itself are located.

It is this objective, that forms the foundation of the present work. Starting point is the finite lifetime of a vacuum arc at low currents (chapter 2). Taking this finite lifetime as a basis, two different directions will be pursued.

The first one will lead in a quantitative sense from the observed dependence of lifetime on current up to its resultant practical important current chopping level in vacuum interrupters (chapter 3).
The second one goes down into the detailed micro-structure of instability behaviour that apparently explains finiteness of lifetime (chapter 4) and leads further (in a more qualititative sense) into the fundamental physical processes that may cause arc instability (chapter 5 and 7).
After the chopping of the arc current, the insulating capacity of the contact gap is not instantaneously restored. Chapter 6 gives an analysis of post current-zero recovery of the vacuum gap, together with some associated phenomena. Some (more general) conclusions that emerge from this present work are drawn in chapter 8.

Physical theories about cathode spot processes are extraordinary numerous, often mutually exclusive and insufficiently supported by experimental evidence (Lafferty 80). Therefore, the need was felt not to add another closed physical theory, but rather to present new measurements and to explain these where possible within the limited but firm framework of generally accepted principles.

It must be stressed that the understanding of the vacuum arc is not only advantageous in the development of circuit breakers. Through the arcing process, electrode mass is transported in ionized or neutral form (Daalder 78). This is exploited in vacuum arc deposition techniques, but is highly undesirable in nuclear fusion devices where plasma-wall arcs supply metallic mass into the fusion plasma, leading to excessive radiation losses.

References:

- Daalder J.E., Ph.D. Thesis, Eindhoven University of Technology (1978)
- Fink H., Plattner H., Elektrizitätswirtschaft. Jg. 85 (1986) 589-92
- Lafferty J.M., "Vacuum arcs, theory and application", Wiley & Sons, New York (1980)

2. DC ARC LIFETIME; EXPERIMENTAL RESULTS

a. Introduction

In practical power circuits, a vacuum arc current will mostly have a sinusoidal course. In this chapter, however, only DC vacuum arcs will be considered. The reason for this approach is of fundamental value, because a DC current study permits to examine the behaviour of the discharge as a function of current, uncomplicated by circuit imposed variations with time. Later on, in chapter 3, conclusions mainly drawn on the basis of this current dependence, will be used for a time dependent approach in 50 Hz circuits.

It is a well-known fact that the current sustained by one single cathode spot has an approximate maximum value, solely determined by cathode material (Agarwal 84). For copper, the material mainly used as a cathode in this work, this maximum is approx. 100 A. For currents well below (more than say 50%) this average current per spot it was observed that a discharge, once ignited, spontaneously extinguishes after having maintained itself a measurable length of time. This occurs without change of any of the external parameters. Throughout this thesis the duration from ignition to spontaneous extinction will be called (DC) arc lifetime.

Copeland and Sparing (45) were the first to study this phenomenon (in a Hg discharge), and noted a strong current dependence of arc lifetime, as well as a large spread in lifetimes obtained in successive trials. Later, a number of measurements were undertaken in order to establish the current dependence of solid metal arc lifetime (Cobine 60, Farrall 61, Kesaev 63, 64, Attia 73, Jüttner 75, Filip 84, Smeets 86). Some of the well documented results for the Cu vapour arc are put together in fig. 2.1, merely to illustrate the large discrepancy between the various individual results.
This divergence is caused by the large number of parameters involved,

such as parameters of the circuitry, method of arc initiation, electrode distance, -size and less controllable ones like surface roughness and cleanliness. It will be clear that experiments must be undertaken under well-defined, reproducible and statistically justifiable conditions.

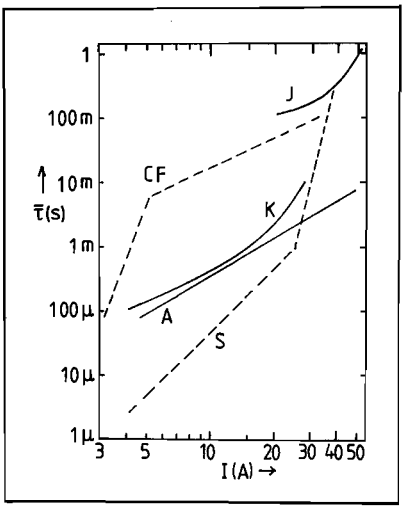

Fig. 2.1: Survey of lifetime ($\bar{\tau}$) vs. current (I) relations for copper electrodes. CF: Cobine and Farrall (60); K: Kesaev (63); A: Attia (73); J: Juettner (75); S: Smeets (86).

In this chapter, only experimental results will be presented. After a discussion of the experimental set-up (section b), measured data are given of copper DC arc lifetimes under the variation of the most relevant parameters such as current (section c), circuit parameters (section e, f) and electrode distance (section g). The effect of different degrees of cathode surface roughness on lifetime is discussed in section h. Conclusive rather than explanatory remarks are given in section j. This is because some characteristics of the measuring results will be used directly in chapter 3, whereas a detailed interpretation of the instability microstructure leading to a finite lifetime is postponed to chapter 4.

Vacuum interrupters nowadays are equipped with (empirically) selected copper alloys as contacts. Nevertheless, the copper vapour arc is chosen as a subject of study favouring an unambiguous comprehensibility of phenomena. Besides, there is a larger volume of relevant data available on copper than on any other solid metal.

b. Outline of the basic DC experimental circuit

The experimental circuit for lifetime measurements is shown in fig. 2.2. Power was supplied by a 72 V storage battery. Current was regulated by means of a variable carbon moulded resistor R_v. All parts of the feeding circuit (except the power source) were built in a shielding box thus bringing about a coaxial arrangement: after the passage through the measuring shunts R_s, the current return path is through the test vacuum interrupter housing and the shielding box. In this way, shielding of high-frequency interference as well as a minimum circuit inductance was obtained. Inherent capacitance is about 400 pF, the effective inductance, verified by HF resonance techniques, is 6 μH. Both reactances are parasitic, but treated in the following as lumped elements (C_p, L_v in fig. 2.2). A surge impedance $Z_o = \sqrt{(L_v/C_p)}$ is defined, and equals 122 Ω for this basic circuit.

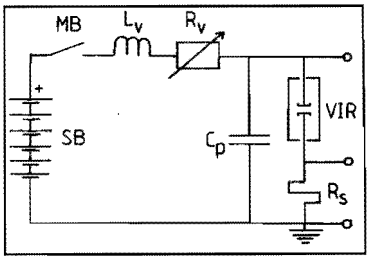

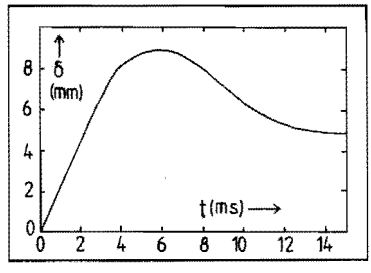

Fig. 2.2: Basic circuit. MB: master breaker; L_v,C_p: parasitic inductance (6 μH), capacitance (400 pF); R_v: variable resistor; R_s: measuring shunt; SB: storage battery (72 V); VIR: vacuum interrupter.
Fig. 2.3: Contact distance (δ) to time (t) characteristic.

The vacuum interrupter (VIR) has a stainless-steel housing with demountable flanges provided with ceramic bushings. No internal shield is used. The ultra high vacuum is sealed by copper gaskets and maintained at better than 5.10^{-8} torr by an ion getter pump. The vacuum housing is always grounded.

The arc was ignited in two different ways.

In the majority of cases, arc initiation was achieved by contact separation after 30 ms of current passage through closed contacts. This separation was effectuated by means of a spring driven, pneumatically operated opening mechanism. Fig 2.3 shows the electrode distance (δ) to time characteristic. Final contact distance is (unless stated otherwise)

5 mm. The initial opening speed is 2 m/s.

The contacts (or electrodes) are made of OFHC copper and measure 30 mm in diameter and 3 mm in thickness. The anode has a slightly rounded surface to ensure arc initiation at the cathode's center. Prior to mounting, the two contacts are acid etched and degreased. After assembling and evacuation the vacuum housing was baked out for at least 12 hours at 400 °C. After the method of arc initiation, the thus started arcs will be referred to as "drawn arcs".

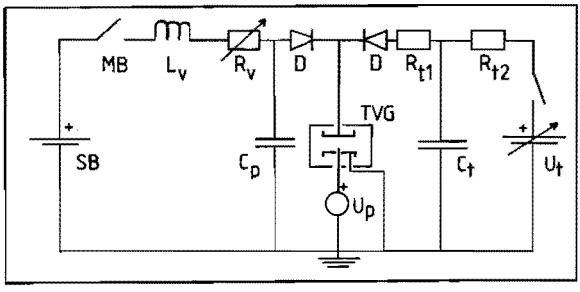

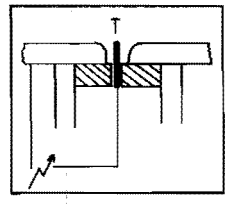

Fig: 2.4a: TVG-circuit. MB, L_v, C_p, R_v as in fig. 2.2. SB: battery (144 V); D: diode; $R_{t1,2}$: resistor (3 Ω, 1 MΩ); C_t: capacitor (5 μF); U_t: charg. source (0-1 kV); U_p: HV pulser (15 kV); TVG: Trig. vac. gap. Fig. 2.4b: Trigger-cathode. T: W-Trigger pin; shaded: Al_2O_3 insulator.

In the cases that contact motion is unwanted, the principle of a triggered vacuum gap (TVG) is applied (Lafferty 66). A 15 kV pulse initiates breakdown between a trigger pin, located in the center of the cathode, and the cathode (fig. 2.4). The resultant pulsed plasma bridges the anode-cathode gap whereupon a vacuum arc can establish.

It was found necessary to extend the basic circuit of fig. 2.2 with an extra capacitor branch and some diodes, as outlined in fig. 2.4. Before triggering, capacitor C_t was charged to some hundreds of volts thus facilitating transition of the gap into the conducting state at triggering. Thereafter, a current pulse of 15 μs duration and approx. 100 A amplitude from the secondary circuit feeds the arc during the first microseconds when the main circuit inductance L_v prevents a sufficiently rapid rise of circuit current.

The contacts that were installed in the TVG underwent the same cleaning procedure as the "drawn arc" contacts, except for the bake-out temperature. Due to the presence of insulating PTFE in the TVG housing, bake-out was performed at 125 °C.

After the principle of arc initiation, arcs produced in a TVG will be called "triggered arcs".
Although maximum attention has been given to a proper contact cleaning, formation of dielectric layers and the adsorbtion of gas can hardly be avoided in UHV systems. In order to eliminate their highly undesired effect on the arcing process (Jüttner 81), further in situ cleaning was done by the arcing process itself. At least a 500 C charge was transferred before serious measuring started, both in the triggered as in the drawn arc configuration.
For the ease of survey, detailed discussion of signal transducers as well as recording equipment will be given at the appropriate sections.

c. DC arc lifetime: dependence on current

DC arc lifetime is an easily measurable quantity that expresses the macroscopic result of a large number of repetitive arc processes. When arc current and voltage are recorded on an appropriate time base, a distinct start and end of the discharge can be noted. This is shown in fig. 2.5 where a typical oscillogram of arc current and voltage is given. The start of a lifetime is identified by the onset of arc voltage (approx. 20 V for copper), while the end is defined by a (high) di/dt of some 100 A/µs bringing arc current to zero.

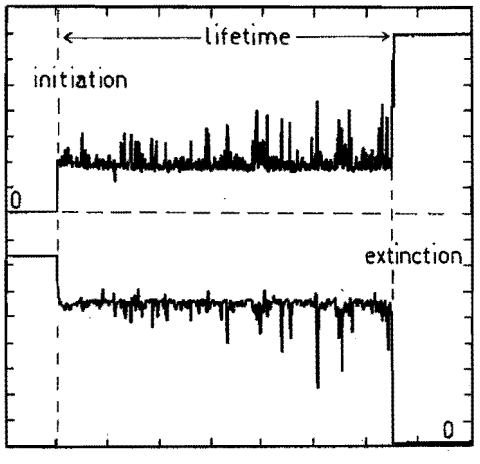

Fig: 2.5: Typical oscillogram for arc lifetime measurement. Upper trace: Voltage over the interrupter (10 V/div); lower trace: Arc current (4 A/div). Time: 200 µs/div.

The behaviour in between reveals a seemingly noisy character, which will not be considered in detail at this point.

Of all the parameters that affect arc lifetime, arc current is the most decisive one for a given cathode material. For a number of current values, 100 arc lifetimes were measured per current value. A sufficiently large number of data is necessitated by an inherent large statistical spread (Filip 84), treated in detail in the next section. The experiments were carried out in the (drawn arc) circuit of fig 2.2 with a parallel capacitance of 7 nF added to the inherent C_p.
The current signal from the measuring shunt was recorded with a pair of two analogue storage oscilloscopes, each employing a different (factor 5) time base. Both very short and long lifetimes could so be measured accurately.
Results are given in fig. 2.6 presenting the average lifetime ($\bar{\tau}$) as a function of DC arc current (I). Inaccuracy is between 3 and 9%.
As can been seen, two branches can be distinguished, each of which can be approximately described by an exponential relation:

$$\bar{\tau} = \alpha\ (I')^{\beta} \qquad (2.1)$$

I', τ' (and every other primed symbol in this thesis) is a dimensionless quantity, the numerical value of which is equal to the value in ampere, second, etc. of the corresponding unprimed current, time etc. $I' = I/I_n$, with $I_n = 1$ A. The background is a correct use of empirically found relations.
The constants in eq. (2.1) are:

$4 < I < 25$ A : $\alpha = 1.8\ 10^{-8}$ s; $\beta = 3.4$

$25 \leq I < 40$ A : $\alpha = 2.6\ 10^{-27}$ s; $\beta = 16.5$

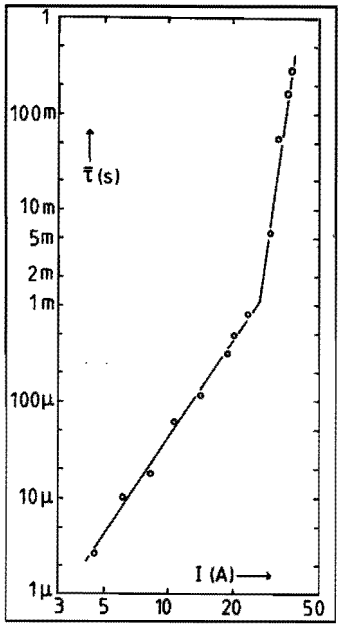

Fig: 2.6 Average DC arc lifetime ($\bar{\tau}$) vs. arc current (I) for the circuit of fig. 2.2 with an extra parallel capacitance of 7 nF.

For a variation in arc lifetime of almost 6 orders of magnitude it thus

seems possible to characterize its dependence on current by two sets of two parameters.
Comparing these results with earlier studies for copper (cf. fig. 2.1) gives a striking discrepancy between all the curves obtained. Even qualitatively, relations of the form ln $\bar{\tau}$' proportional to I (Kesaev 63, Jüttner 75) as well as ln $\bar{\tau}$' proportional to ln I' (Cobine 61, Attia 73) are encountered. As stated earlier, the apparent lack of congruence merely reflects the very strong lifetime dependence on (more or less controllable) experimental conditions. It must be stressed therefore that the $\bar{\tau}$ vs. I characteristic so obtained is pertinent to only one combination of parameters. Reproducibility was verified, using a second circuit with the same parameters, and a second pair of contacts, treated similarly. Results were in accordance with the first series.

d. Statistical analysis

The question of continued survival of the discharge is determined largely by the statistical nature of the arc cathode processes.
A statistical inspection of the lifetime data is desirable for practical reasons. An important quantity for vacuum arc stability, and thus for the level at which an AC current is chopped before a natural zero, is the probability that a DC arc at a relatively high current extinguishes after a short lifetime. It is especially under such circumstances that unacceptably high overvoltages can be generated by vacuum arc interruptions in AC circuits.

Copeland and Sparing (45) reasoned that the number of arcs dN that extinguishes in a time interval dt should be proportional to the product of the number of arcs N - active at a given instant - and the time interval dt. Thus they derived an exponential distribution function for arc lifetimes: $F_1(\tau) = 1 - \exp(-\tau/\bar{\tau})$, with $\bar{\tau}$ the average lifetime. Later, this was found to describe lifetime distributions of solid metal arcs satisfactorily (Cobine 61). It must be remarked however, that the number of trials (40) was rather small for an unambiguous conclusion.
Filip (84) suggests a log-normal distribution after extensive measurements using copper-chromium contacts.

On the basis of a sufficiently large number of samples (200 data at I = 23.4 A), three types of distributions were checked:

Exponential distribution :

$$F_1(\tau) = 1 - \exp(-\tau/\bar{\tau}) \qquad (2.2)$$

Normal distribution :

$$F_2(\tau) = [\sigma\sqrt{(2\pi)}]^{-1} \int_{-\infty}^{\tau} \exp\left[-\tfrac{1}{2}\left(\frac{u-\bar{\tau}}{\sigma}\right)^2\right] du \qquad (2.3)$$

Log-normal distribution :

$$F_3(\tau) = [\sigma\sqrt{(2\pi)}]^{-1} \int_{0}^{\tau} \frac{1}{u} \exp\left[-\tfrac{1}{2}\left(\frac{\ln u - \bar{\tau}}{\sigma}\right)^2\right] du \qquad (2.4)$$

with σ the usual standard deviation.

A chi-square goodness-of-fit test was applied to the 200 data, leading to the rejection of F_1, F_3 and acceptance of the normal distribution. A significance level of 5% was adopted. This is further illustrated in fig. 2.7 where the cumulative lifetime distribution is plotted on an exponential, "normal" and "log normal" scale.

Probably the best way to describe the distribution of lifetime data is to use the two parameter Weibull distribution (Mann 74), often used in lifetime statistics. Its distribution function $F_4(\tau)$ is given by:

Weibull distribution: $F_4(\tau) = 1 - \exp(-\tau/\bar{\tau})^b$. (2.5)

This function has the features of all the distribution functions mentioned earlier. For b = 1 exponential, for b values between 1 and 2 approximately log-normal, between 2 and 3 approximately normal. For the correct description of the results for a wide range of currents it appeared necessary to adopt a dependence of b on arc current: b $\approx$ 1.5 for I < 8 A; b $\approx$ 2 for 8 < I < 20 A and b $\approx$ 2.5 for I > 20 A.

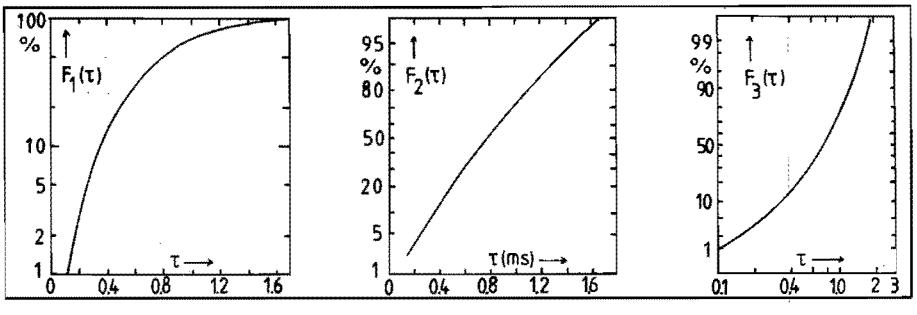

Fig: 2.7: Cumulative distribution (in percentage "smaller than") for exponential (F_1), normal (F_2) and log-normal distribution (F_3). N = 200.

For the sake of simplicity however, in the following all lifetimes are assumed to be distributed normally with a mean value ($\bar{\tau}$) and a standard deviation (σ).

The inaccuracy of a measurement of $\bar{\tau}$ in this connection is given by $\Delta\bar{\tau} = \sigma/\sqrt{N}$ (N = number of data). An impression of this inaccuracy relative to average lifetime ($\Delta\bar{\tau}/\bar{\tau}$) for different arc currents can be obtained from fig. 2.8.

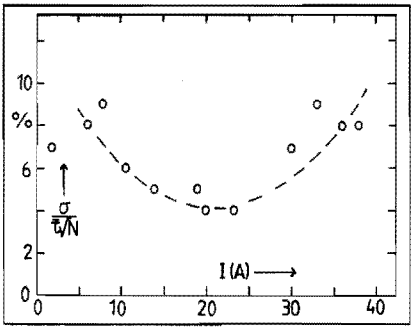

Fig: 2.8: Relative inaccuracy $[\sigma/(\bar{\tau}\sqrt{N})]$ *as a function of current* (I).

e. Dependence on circuit inductance and capacitance

As can been seen in fig. 2.5, arcing activity is attended with rapid changes of arc current and voltage. Therefore, it is important for the discharge how the feeding circuit responds to these changes. As might be expected, there must be an intimate coupling between the arcing behaviour and the electrical circuit parameters, reflected in the resultant arc lifetime.

This was checked by measurements of lifetimes in the "drawn arc" circuit under variation of series inductance L_v while keeping parallel capacitance C_p constant and the other way round. Purpose was not to establish a precise curve of the inductive/capacitive influence. In that case, a possible current dependence should be incorporated as well, making the number of parameter combinations too large.

Fig. 2.9 shows an increase of average arc lifetime with increasing series inductance in a limited number of steps.

Fig. 2.10 alternatively, reveals a gradual decrease of lifetime as a function of additional parallel capacitance. In both cases current was approx. 20 A; 100 measurements per point were averaged over.

The tendency to prolonged arc lifetime at higher circuit inductances was noted in earlier investigations. However, Cobine (60) only perceived a significant increase in (CuBi) arc lifetime after adding 1 mH. This finding was corroborated by Kesaev (60) in Hg arc experiments. In both experiments however, the number of data points may have been too small to discriminate between random fluctuations of data and clear trends.

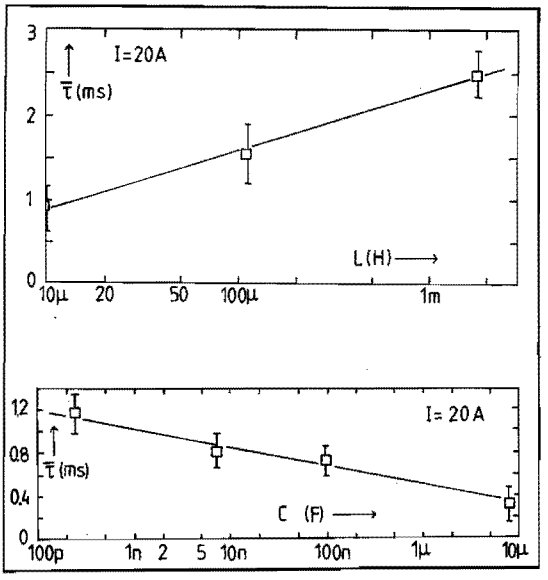

Fig: 2.9: Average lifetime ($\bar{\tau}$) as a function of additional series inductance L.

Fig: 2.10: Average lifetime ($\bar{\tau}$) as a function of additional parallel capacitance C.

Arc lifetime shortening by adding parallel capacitance is a common outcome of all reported experiments. Filip (84) finds a very drastic lifetime reduction for a CuCr DC arc by adding only 1 nF; Cobine (60) concludes a similar shortening in a range from 0 - 1 mF capacitance paralleled to a copper DC arc. From the same experiment, it may be inferred that the relative lifetime reduction is independent of current.

f. Dependence on parallel resistance

Shunting the arc by a low ohmic resistor can be a powerful tool to study circuit influences on the arcing behaviour. A resistor placed parallel to the arc will shield off the reactive part of the feeding circuit provided that $R_p \ll Z_o$, with R_p the value of the parallel resistor. The high-frequency oscillatory components of arc current and voltage will be effectively damped.

In order to check the consequences for arc lifetime, a low inductive resistor R_p was mounted over the vacuum housing in such a way that the inductance of the loop formed by arc and resistor was about 1.5 µH, much smaller than the circuit (parasitic) inductance L_v.

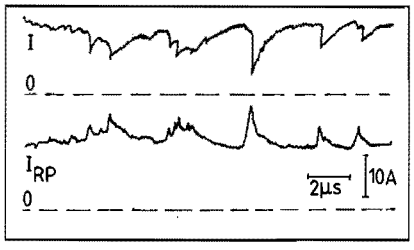

Fig: 2.11: Rapid commutation of arc current (I) into the parallel resistor branch. I_{Rp}: current in the parallel resistor.

If resistors R_v (cf. fig. 2.2) and R_p are chosen such as to achieve approximate equality of arc current I and current through parallel resistor I_{Rp}, a rapid commutation takes place from the arc branch into the parallel branch at rapid changes in the arc current. This can be seen in the oscillogram of fig. 2.11. The main feeding circuit can be treated as a constant current source in this case.
The resultant effect on the total arc lifetime is plotted in fig. 2.12.

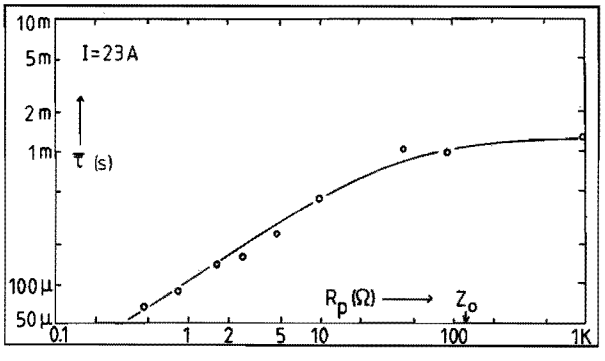

Fig: 2.12: Arc lifetime ($\bar{\tau}$) at I = 23 A as a function of parallel resistance (R_p).
$Z_o = \sqrt{(L_v/C_p)}$.

It can be observed that reduction of the shunt resistor considerably reduces arc lifetime. Throughout the measurements, the arc current is kept at a constant value of 23 A. As might be expected, a large shunt resistor ($R_p > Z_o$) does not affect arc behaviour, and the situation of fig. 2.2 is restored.
The imposed monotonous decrease of the value of R_p can be interpreted in terms of a gradual transition of effective circuit inductance from L_v to a value well below this parasitic one. The resultant lifetime reduction strengthens the indication that arc lifetime is susceptible to small changes of the inductance.

g. Dependence on contact motion and distance

In a vacuum interrupter, an arc is always ignited by means of contact separation. For a predictive model relating DC arc lifetime to AC arc behaviour in such an interrupter, it is unavoidable to study the influence of contact motion on arc lifetime.
For that purpose, the opening mechanism that "draws" the arc in the circuit of fig. 2.2 was equipped with a variable opening speed in the range 0.8 - 2.5 m/s, based on figures encountered in practice.
For a number of speed values in this range, 50 lifetimes were measured per speed at a fixed current of 27 A. This current is such, that arc lifetimes were sufficiently short, guaranteeing arc extinction before standstill of the contacts. Contact travel against time was recorded preceeding each series of trials, and was found to be reasonably linear during the first 4 ms after separation (cf. fig. 2.3).
The outcome of this experiment is plotted in fig. 2.13.

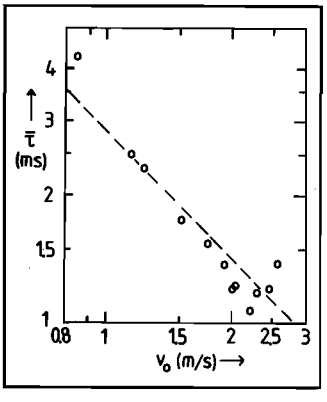

Fig: 2.13: Average lifetime ($\bar{\tau}$) at I = 27 A as a function of contact opening speed (v_o).

For low contact speed (v_o < 1.5 m/s) a strong influence on arc lifetime is clearly recognized. In first approximation, the results can be represented on a log-log scale by a straight line having a 45° slope. This implies that the product of opening speed and average lifetime is approximately a constant. Physically, this means that the discharge continues to survive, until a certain contact distance has been reached. For this "average survival length" a figure of (2.8 ± 0.5) mm is found. The same experiment was repeated at a current of 24 A, yielding a similar qualitative trend and an average survival length (2.0 ± 0.1) mm.

From these results, one might conclude that conditions for a sustained arcing process are deteriorated after the excess of a certain electrode distance.

The study of Cobine and Farrall (60) compares lifetime data of (drawn) copper arcs for some final contact distances between 1.2 and 5.9 mm. No evidence of some distance effects was found. Their measurements are difficult to compare with the ones described here, as opening speed was about 1/100 of the values in our experiment. This low opening speed can very well account for the reported lifetimes, much larger compared to ours (cf. fig. 2.1).
A similar experiment was carried out by Jüttner (75) who studied the lifetime of arcs between CuMo contacts as a function of distance. A strong dependence on distance was observed (distance < 3 - 5 mm) as well as on current (10 - 15 A), qualitatively in accordance with the Cu arc results presented here. Jüttner's contact speed is not specified, but the very long arc lifetimes (> 1 s) make it reasonable to suppose that a variation in lifetime results from a differing final contact distance.
In order to eliminate contact motion effects, the necessity was felt to establish a vacuum arc between fixed contacts. This is possible with a triggered vacuum gap, globally outlined in section b. The measuring circuit was according to the original drawn arc circuit of fig. 2.4, slightly adapted to facilitate high voltage triggering. For a number of currents, the dependence of arc lifetime on contact distance was investigated with electrode distance as a parameter.
The results are shown in fig. 2.14; the curves show a clear tendency for the arc to maintain itself longer between closely spaced contacts, especially at higher currents. Although this tendency clearly emerges, the existence of a certain "average survival length", as suspected in the drawn arc experiments applying a variable contact separation speed, is not confirmed by this experiment.
Plotted in the same figure 2.14 is the lifetime vs. current relationship of the drawn arc in a similar circuit. It is evident that average lifetimes of "drawn arcs" exceed these of "triggered arcs" many times.
This can now be interpreted as follows: the probability that an arc extinguishes spontaneously seems to be a function of contact distance. Short distance corresponds to low probability, longer distance to higher

probability. In this interpretation it is (qualitatively) clear that an arc between contacts with a spacing varying between zero and a final distance has a higher survival probability than an arc struck between contacts, fixed at this final distance.

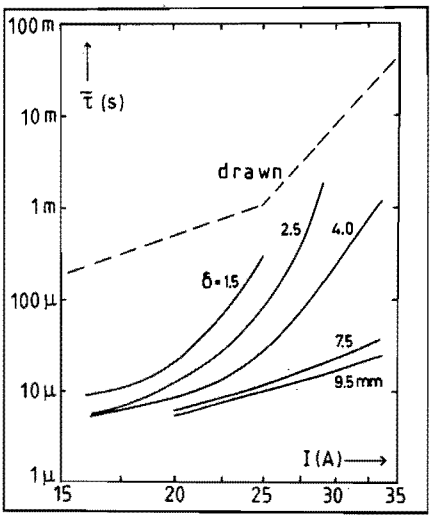

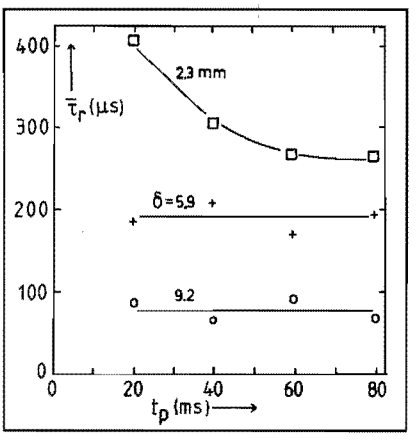

Fig: 2.14: Arc lifetime ($\bar{\tau}$) vs. current (I) at different fixed contact distances (δ) in the TVG and in the drawn arc.
Fig: 2.15: Residual arc lifetimes ($\bar{\tau}_r$) for a Cd arc as a function of pre-reduction time (t_p) at various fixed contact distances (δ).

In a third way, evidence was acquired of contact distance effects. For this experiment, cadmium contacts were employed. This metal has a much higher vapour pressure than copper, resulting in a higher density of metal vapour at a given cathode surface temperature. This material parameter primarily accounts for the very long lifetime of Cd arcs compared to Cu arcs at a given current. A copper arc reaches a lifetime of 1 ms at approx. 24 A, a cadmium arc does so already at 1.5 A. This makes cadmium arcs, from a viewpoint of experimental ease, attractive to study.

The following experiment was performed: By means of a transistor parallel to the drawn arc, current was suddenly reduced, after a certain arcing time t_p. Initially, during a time t_p arc current (2.7 A) was such that average lifetime at this current is greater than 100 ms.

The reduced current (1.8 A) corresponded to a lifetime less than 1 ms,

to be called residual lifetime. In order to avoid influence of contact motion, t_p was greater than 15 ms, i.e. exceeding the contact travelling time. In this way, residual arc lifetime at reduced current can be measured with contacts fixed at their final distance. Besides, a possible effect of the time t_p can be tracked.
These investigations are summarized in fig. 2.15, that gives average residual lifetimes of a Cd arc as a function of the final contact distance and pre-reduction time t_p.
Again, an unambiguous dependence of lifetime on contact distance can be noted. The "history" of the arc prior to the moment of current reduction, as expressed by differing values of t_p seems not be of relevance as long as the distance is not too short.

h. Dependence on cathode surface roughness

Cathode surface roughness is an important parameter in lifetime studies, more from a fundamental point of view, however, than prompted by practical application. In a usual interrupter, repeated arcing shapes the microscopic surface structure of the electrodes.
Lifetime measurements were performed using four flat cathodes, only differing in the way the surface was treated. Their resultant surface roughness is here characterized by the average field intensification factor β_a. This factor can be taken as a measure for the sharpness of microprotrusions, present on any surface. Its value can be determined by studying the dependence of the current (carried by electrons emitted by the field intensificating protrusions) on the voltage over the anode-cathode gap (e.g. Latham 81).
The treatment of the 4 surfaces under test was as follows:

(1) A very rough surface was obtained by using abrasive paper (P220), leaving a dead and extremely scratched surface; HV-measurements yielded a value of $\beta_a \approx 800$.
(2) A glossy surface was created with a finer paper (P800); $\beta_a \approx 400$.
(3) A diamond paper (grain size $< 1\ \mu m$) abrasive disk was used to obtain a mirror-like surface; besides, this cathode was conditioned by a high voltage until a value $\beta_a \approx 100$ had been reached.
(4) One cathode was eroded by arcing, using 540 C of charge transfer. Around 80% of the surface was covered with the erosion pattern.

This cathode could serve as a reference, as it is treated the same as described elsewhere in this thesis.

Chemical cleaning was the same in all four cases; after mounting, evacuation, bake-out (and electrical treatment for no. 3 and 4), lifetime data were collected, starting at the lowest current.

The circuit parameters were L_v = 12 μH; C_p = 500 pF (cf. fig. 2.2).

The results are represented in fig. 2.16; the inaccuracy of the individual points is around 8%; 25 measurements were averaged per point.

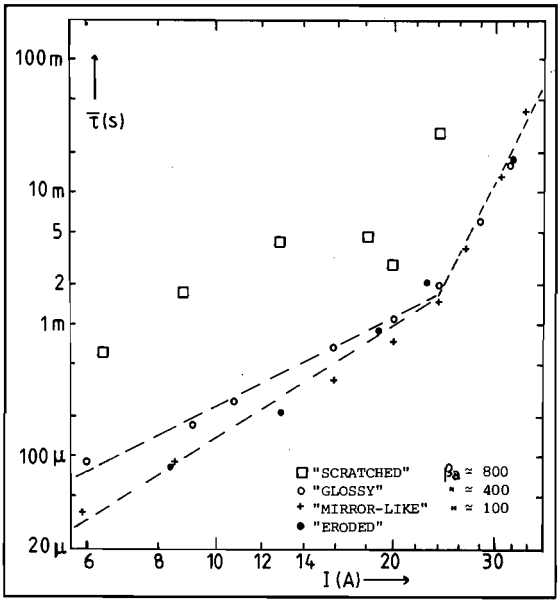

Fig. 2.16: Average arc lifetimes ($\bar{\tau}$) vs. current (I) for 4 different degrees of cathode surface roughness.
(measurements: Fu Yan hong)

It can be clearly seen, that the higher the value of β_a is, the higher the arc lifetime is. The similarity of arc lifetimes on "mirror like" and "eroded" surface is surprising. On first sight the "eroded" surface is very coarse, but the apparent "smoothness", as suggested by the comparative lifetime data, may be explainable by the fact that a thin surface layer has been molten by the pre-measurement arc charge transfer. After solidification, protrusions are left over that are much less sharp than those, left after mechanical treatment. Besides, impurities still present before the start of measurement in case (1), (2) and (3) are removed by the pre-measurement arcs.

The percentage of surface area, eroded by the measurement arcs, is determined for cathodes (1), (2) and (3), with the charge transferred during the measurement series given as a parameter: Scratched: (32 C) giving 60% eroded area; glossy: (34 C) 30%; mirror-like: (50 C) 15%.

It is clear that on a smooth cathode, the arc has the tendency to confine itself to a smaller area.
Qualitatively similar results are reported by Farrall (61), observing that arcs on solid surfaces appear to have a longer life than on a liquid surface of the same metal. Sena (71) also reports an increased stability of an arc on a rough cathode.

j. Concluding remarks

The tendency of a DC vacuum arc, once ignited to continue its activity, can be expressed in a measurable quantity called average arc lifetime.
First of all, the arc lifetime is dependent on the cathode material. Examination of the metal properties reveals that the most significant factor affecting lifetime is vapour pressure of the cathode material (Cobine 60).
Low heat conductivity as well as low work function also favour sustained arcing (Hammann 80, Kurakina 68).

In this work, carefully cleaned and pre-arced copper cathodes were used. The lifetime dependence on arc current is quantitatively expressed as a pair of relations of the form $\bar{\tau} = \alpha\ (I')^{\beta}$.
The existence of two separate branches in the corresponding curve is hard to explain. This might be an effect of contact motion: the low current branch ($I < 25$ A) of the curve can be seen as originating from a competition of increase in lifetime through an increment of arc current and a decrease through a steadily growing contact distance. After a time of approx. 1 - 2 ms, a contact distance of 2 - 4 mm has been reached, above which a further increase of distance only slightly affects arc lifetime. The higher current branch $I > 25$ A reflects - in this hypothesis - the increase of arc lifetime with current only. This increase is here steeper because of the virtual absence of a widening contact gap.
Cobine and Farrall (60) observed a similar crack in a number of lifetime curves. In their case however, the curve continued less steeply. They supposed a change in structure of active cathode spots, but later experiments (Djakov 71) made this assumption rather improbable.

The work of Kesaev (63) explains the lifetime vs. current relationship on theoretical grounds, based on the probability that a cathode spot temporarily splits into fragmentary subcells. Nowadays, a subdivision of cathode spot on clean metal surfaces is far from being proved, and must be attributed to surface contaminations (Rakhovskii 76, Jüttner 81).

Apart from these internal parameters, a number of external ones can be mentioned. The feeding circuit predominantly acts through parallel capacitance and series inductance. Qualitatively speaking, their combined action can be summarized by a net increase in arc lifetime at higher surge impedance Z_0. As will be made plausible in chapter 4, a circuit having larger Z_0 is able to react in a more favourable way on tendencies to extinguish so giving the discharge a higher probability to survive.

A large difference between arc voltage and available power source voltage also seems to enhance chances for arc survival (Cobine 60). It can be said that there is more "reserve" voltage in the system to meet the demands of the arc in case of a threatening extinction.

The geometry of the electrode configuration is important too. This was proved here in three ways for the contact distance.

A study by Kutzner (80) suggests the existence of a critical solid angle Ω_{cr} subtended by the anode seen from the cathode center. By underpassing Ω_{cr} he observed a different behaviour of the arc, possibly associated with a higher probability for extinction. Whereas he found Ω_{cr} = 1 - 1.5 sr, a significant decrease in arc lifetime was noted in the present study by a change (for example) from 5.9 to 5.5 sr (1 and 2 mm distance respectively). A large relative change in lifetime (over 100%) can more easily be explained by an equally large change in contact distance (100%) than by a small change (7%) in solid angle. Therefore, a lifetime dependence on distance alone will be assumed.

In this work it was demonstrated that a (microscopic) rough cathode surface increases the arc lifetime relative to smooth-cathode lifetimes, with the same degree of surface contamination.

The last influential parameter encountered in literature is ambient gas pressure (Farrall 65). The presence of each of a number of gases caused an increase in lifetime with respect to the "vacuum" situation.

Lifetime data of arcs in atmospheric air between copper contacts are (among others) produced by Barrault (82).

References:

- Agarwal M.S. and Holmes R., J. Phys. D: Appl. Phys., vol. 17 (1984) 757-67
- Attia E.A., Proc. IEEE (1973) 1156-8
- Barrault M.R., Haug R. and Maftoul J., IEEE Trans. on Plasma Sci., PS - 10 (1982) 130-5
- Cobine J.D. and Farrall G.A., J. Appl. Phys., vol. 31 (1960) 2296-304
- Cobine J.D. and Farrall G.A., Proc. Int. Res. Symp. on Electric Contact Phen., Univ. of Maine, (1961) 263-83
- Copeland P. and Sparing W.H., J. Appl. Phys., vol. 16 (1945) 302-8
- Djakov B.E. and Holmes R., J. Phys. D: Appl. Phys., vol. 4 (1971) 504-9
- Farrall G.A. and Reiling G.H., J. Appl. Phys., vol. 32 (1961) 1528-34
- Farrall G.A. and Cobine J.D., J. Appl. Phys., vol. 36 (1965) 53-6
- Filip G., Thesis, Technical University of Vienna (1984)
- Hammann J.F., Kippenberg H., Häßler H. and Schreiner H., Siemens Forsch. u. Entw. Ber. Bd. 9 (1980) 210-6
- Jüttner B. and Freund E., Beitr. Plasmaph. 15 (1975) 47-61
- Jüttner B., Beitr. Plasmaph. (1981) 217-32
- Kesaev I.G., Sov. Phys. - Techn. Phys. 4 (1960) 1351-8
- Kesaev I.G., Sov. Phys. - Techn. Phys. 8 (1963) 447-56
- Kesaev I.G., Sov. Phys. - Techn. Phys. 8 (1963) 457-62
- Kesaev I.G., "Cathode processes in the Mercury Arc", Consultants Bureau, New York (1964)
- Kurakina T.S., Potokin V.S. and Rakhovskii V.I., El. Techn. USSR, vol. 4 (1968) 140-6
- Kutzner J., Physica 104 C (1981) 116-23
- Lafferty J.M., Proc. IEEE, vol. 54 (1966) 23-32
- Latham R.V., Ch. 2, "High Voltage Vacuum Insulation", Academic Press, London (1981)
- Mann N.R., Schafer R.E., "Methods for statistical analysis of reliability and life data", Wiley and sons, New York (1974)
- Rakhovskii V.I., IEEE Trans. on Plasma Sci., PS - 4 (1976) 81-102
- Sena L.A., Pranevichius L.I. and Fursey G.N., Xth Int. Conf. on Phen. in Ion. Gases, Oxford (1971) 105
- Smeets R.P.P., J. Phys. D: Appl. Phys., vol. 19 (1986) 575-87

3. CURRENT CHOPPING IN VACUUM INTERRUPTERS

a. Introduction

Ideally, in a power interrupter called upon to switch an AC current, a stable discharge should persist between its separating contacts until the current reaches the first sine- or "natural" zero. In practice however, the current flow is interrupted prior to this moment. Failure to carry the current gradually to zero is called "current chopping".

Current chopping is extensively studied in circuit breakers employing air, oil and SF_6 as an interrupting medium. It has been shown that precocious arc extinction herein can be attributed to a number of causes:

1. Strong motion of the ambient gas lengthens the arc. In high pressure arcs, the voltage drop over the arc columm is considerable. Under circumstances, the arc length and thus arc voltage becomes higher than the available circuit voltage. This causes arc cessation.
2. In a high pressure arc, lowering of current results in an increased arc voltage. Hence, a negative dynamic resistance can be attributed to the arc. Due to this negative arc resistance, "instability oscillations" with an increasing amplitude can make the arc current reach zero so that the arc extinguishes and the main circuit current is chopped. This is generally accepted as the principle cause of current chopping in gasblast and oil circuit breakers. Instability theories of this kind are commonly divided into static (Baltensperger 50) and (the more realistic) dynamic theories (Rizk 64).
3. An abrupt decrease of arc resistance, for example caused by sudden short circuits of the curled arc path in a turbulent medium may give rise to an oscillating discharge of circuit capacitance into the arc path. This oscillation can force the main current to zero and thus causes current chopping (van den Heuvel 80).
4. At sufficiently low currents, the character of the discharge can be altered from arc discharge into glow discharge. The latter requires a much higher voltage. When such a sudden voltage increase is prevented by the circuit, the discharge vanishes (van den Heuvel 66).

Each of these current chopping provoking mechanisms, is based on arc properties inherent to the high pressure arc, but not belonging to the vacuum arc. For the latter does not apply that arc elongation yields a higher arc voltage (Rondeel 75); that a negative voltage vs. current characteristic holds (Reece 63), nor that a glow discharge can be established.
Whereas chopping in high pressure arcs is governed by arc columnar effects, the absence of such effects at low currents in vacuum arcs suggests a dominant cathode determined current chopping process.

Depending on the surge impedance and damping of the circuit, a large transient voltage may follow a current chop. Under the - hypothetical - condition that an arc is brought to a (natural) current zero, this transient voltage over the breaker may amount to about twice the momentary source voltage. A current chop however, augments this voltage. Fig. 3.1 expresses this case.

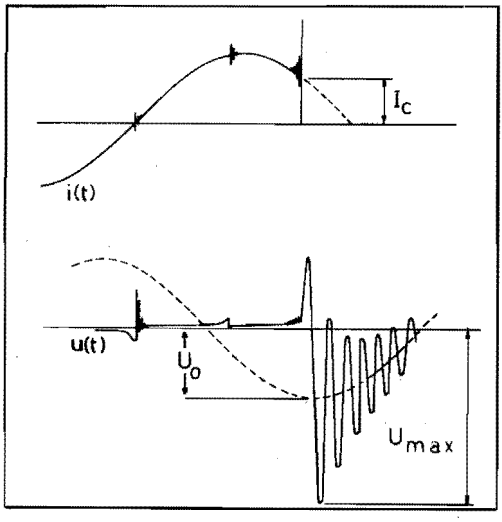

Fig. 3.1: Current chopping due to an instability oscillation during interruption of an inductive load (from Electra 91 p. 13). Current through the breaker [i(t), top] and voltage over the breaker [u(t), bottom]. I_c: chopping current; U_o: source voltage at chopping; U_{max}: overvoltage.

Neglecting damping, the maximum voltage (U_{max}) over the breaker can be quantified in a rough approximation as:

$$U_{max} = \sqrt{[U_o^2 + (I_c Z_o)^2]} + U_o \qquad (3.1)$$

With I_c being the chopped current, U_o the source voltage at occurrence of chopping and $Z_o = \sqrt{(L/C)}$ surge impedance of the circuit having

capacitance C and inductance L. A refined treatment is given by van den Heuvel (66).

Overvoltages following current chopping in conventional circuit breakers incorporated in practical networks are usually not higher than 3 to 4 pu (1 pu being equal to the source voltage, in three phase circuits being the phase voltage). In principle, much higher values can be reached, but are often suppressed automatically by reignitions inside the breaker. This is because a hot arc columm retains a slower vanishing conductivity a certain time after current zero, resulting in a decreased breakdown voltage.

Such a voltage limiting mechanism is active to a lesser extent in a vacuum breaker. Recovery to the situation where no arcing activity is present proceeds on a much faster time scale in a vacuum breaker than in any other type. Evaluation of an experiment after several millions of vacuum switching operations by Holmes (74) resulted in average overvoltages between 2 and 7 pu, depending on circuit surge impedance.

Since large transient voltages can damage the circuit insulation, it is important to understand the chopping phenomenon and to minimize the chopping current. Comparing the progress, made in each of these fields, one must conclude that through considerable research effort, acceptable values of chopping current have been made possible in modern vacuum interrupters. This development is greatly accelerated by the introduction of special alloys and mixtures of pure metals as a contact material. A contact composed of copper and a chromium additive, sintered together, has emerged as the most attractive one, fulfilling a number of conflicting demands. Farrall (63), Burrage (73), Holmes (74), Hammann (80), Néveri (80), Reininghaus (83), Filip (84), Frey (84), Sämann (84), and Czarnecki (86) present comparative measurements of chopping currents. They employ copper as a basis with one metallic additive, variable in character as well as in quantity. Kurosawa (85) reports a further reduction of chopping current, realized by ternary contact systems. Slade (73) reviews the (equally important) requirements that a suitable contact material must fulfil for mechanical reasons.

However, fundamental insight in the current chopping phenomenon has proceeded far from proportional to the progress made in the

applicational field. This is probably due to the lack of both experimental and theoretical knowledge of the vacuum arc in a current region where instability sets on, and limits the lifetime of the discharge. It is this region, whereupon this present work is focussed. In this chapter, DC arc lifetime will be taken as a measure for arc stability in DC as well as in AC circuits. In section b, a quantitative relationship will be established between DC arc lifetime and AC chopping current. Section c gives details of the experimental set-up, used to verify the validity of the DC - AC relation. Experimental results will be presented and compared to literature in section d. Section e discusses circuit influences while the conclusive section f enters into the limitation of the model.

b. The relation between DC arc lifetime and AC chopping current

In chapter 2, it was found that the DC arc lifetime at a given combination of parameters can be represented by a reproducible number $\bar{\tau}$, average lifetime. Most of all, this average lifetime appeared to depend strongly on arc current I. Fig. 3.2 shows this relation $\bar{\tau}$ (I) for the low current branch of fig. 2.6, together with the course of some sinusoidal currents: $i(\vartheta) = \hat{\imath} \sin(\pi - \omega\vartheta)$.
Herein, $\hat{\imath}$ is the amplitude of the AC current; ω = 314 rad/s (industrial frequency); ϑ is the time remaining until the first coming current zero. For a certain critical current value I_{cr}, average arc lifetime $\bar{\tau}$ equals the remaining time ϑ. For higher currents, the expected lifetime exceeds the remaining time ($\bar{\tau} > \vartheta$), while the opposite is true below I_{cr}: $\bar{\tau} < \vartheta$. It will be clear that a natural zero will never be reached, because expected arc lifetime diminishes at a faster rate with current than the circuit imposed time to attain the sine zero gradually.
Prospective chopping current (I_{pc}) is defined by:

$$I_{pc} = \hat{\imath} \sin \omega (\vartheta - \bar{\tau}) \qquad (3.2)$$

This quantity is to be interpreted as the current that - starting at ϑ - will be reached in a time $\bar{\tau}$, with $\bar{\tau}$ determined by the corresponding DC value (I) of the actual current (i) at time ϑ.

The latter current is:

$$i(\vartheta) = \hat{i} \sin (\pi - \omega \vartheta) = \hat{i} \sin \omega \vartheta \qquad (3.3)$$

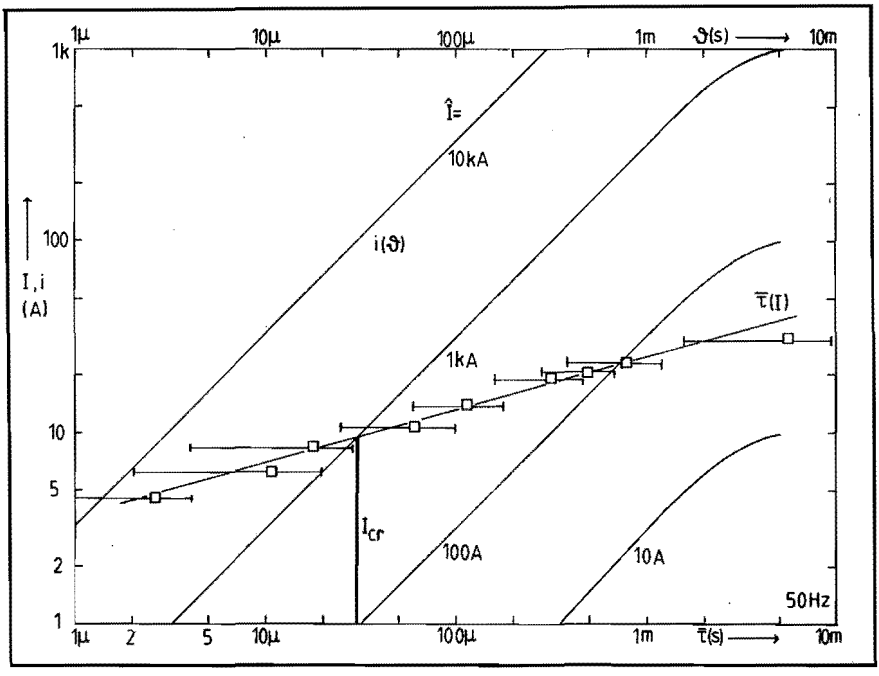

Fig. 3.2: Pre-current zero course of AC current [$i(\vartheta)$] and DC arc lifetime vs. current [$\bar{\tau}(I)$]. $\hat{i}$: AC amplitude; ϑ: time before current zero; I_{cr}: critical current.

Time is eliminated from eq. (3.2) by substitution of the empirically found lifetime vs. current relation (cf. sect. 2c):

$$\bar{\tau} = \alpha \, (I')^{\beta}, \qquad (3.4)$$

and the inverted time vs. actual current relation from eq. (3.3):

$$\vartheta = (\omega)^{-1} \sin^{-1} (i/\hat{i}), \qquad (3.5)$$

so that the prospective chopping current can be expressed in current exclusively (i' is the dimensionless equivalent of i):

$$I_{pc} = \hat{\imath} \sin \{\sin^{-1} (i/\hat{\imath}) - \omega \alpha (i')^{\beta}\}, \qquad \text{with } i \equiv I. \qquad (3.6)$$

In fig. 3.3, relations (3.3), (3.4) as well as (3.6) are plotted, based on an AC amplitude $\hat{\imath}$ = 1 kA and DC parameters α, β from the results, presented in sect. 2c: $\alpha = 1.8\ 10^{-8}$ s, $\beta = 3.4$.

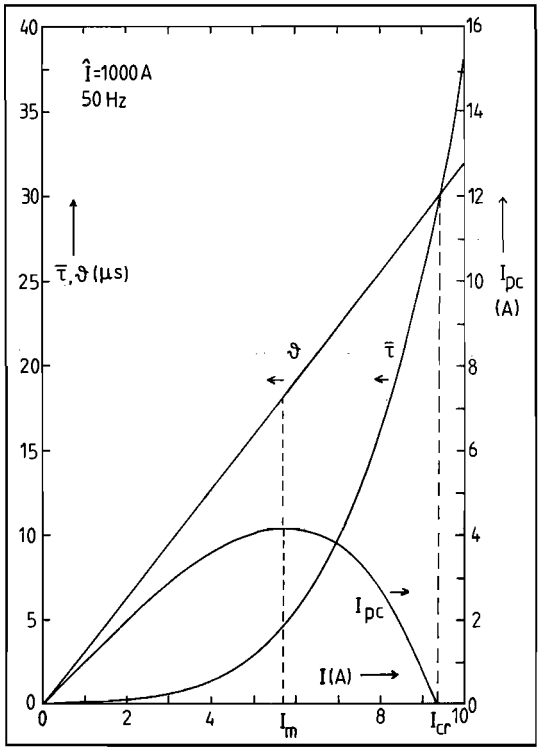

Fig. 3.3: DC arc lifetime ($\bar{\tau}$) and time before current zero (ϑ) of a 50 Hz, 1 kA current. Also plotted is the prospective chopping current (I_{pc}), reaching its maximum at I_m. I_{cr}: critical current.

At current I_{cr}, the remaining time $\vartheta_{cr} = (\omega)^{-1}\sin^{-1}(I_{cr}/\hat{\imath})$ equals the lifetime $\bar{\tau}_{cr} = \alpha(I'_{cr})^{\beta}$ that a DC arc at a current I_{cr} would have. So:

$$I_{pc}(I_{cr}) = 0 \qquad (I \neq 0) \qquad (3.7)$$

This leads to an implicit equation (3.6) that defines I_{cr} at a given ω, $\hat{\imath}$, α, β. Continuing to approach current zero, at a certain moment the current will reach a value I_m where the prospective chopping current attains a maximum.

The adequate definitions are:

$$\left.\frac{dI_{pc}}{di}\right|_{I_m} = \left[\hat{i}'\cos\left[\sin^{-1}(I_m/\hat{i}) - \omega\,\alpha\, I_m'^{\beta}\right]\right]\left[(\hat{i}'^2 - I_m'^2)^{-1/2} - \omega\,\alpha\,\beta I_m'^{\beta-1}\right] = 0 \tag{3.8}$$

When the actual circuit current has reached the value I_m, the prospective chopping current is at its maximum. It is expected, that current chopping will occur near this value at a level I_c:

$$I_m < I_c < I_{cr} \tag{3.9}$$

In general, it is not possible to solve I_m analytically from eq. (3.8) for a given set of ω, $\hat{i}$, α, β. For relevant small pre-current zero times and currents however, eq. (3.3) through (3.8) can be linearized by taking $\sin\delta = \delta$, as $\delta \ll 1$. This is allowed in most cases, except when chopping currents become as large as the amplitude:

$I_c \approx \hat{i}$.

With the aid of this simplification I_{cr} [eq. (3.7)] and I_m [eq. (3.8)] are expressable as simple explicit functions of the parameters:

$$I_{cr}' = (\omega\,\hat{i}'\alpha)^q \tag{3.10}$$

$$I_m' = (\omega\,\hat{i}'\alpha\,\beta)^q \qquad q = (1-\beta)^{-1} \tag{3.11}$$

According to this set of characteristic currents, the chopping current I_c will have a value close to the current I_m where the prospective chopping current has a maximum:

$$I_m < I_c \ll \beta^{-q} I_m \tag{3.12}$$

A simple equation (3.11) now links the DC lifetime data (α, β) and AC data (ω, $\hat{i}$) to a resultant chopping current.

Running ahead of confrontation of this model with direct experimental results, some characteristics strike the eye. As $\beta > 1$, it is clear from eq. (3.11) that lower amplitude values of AC currents result in higher chopping currents. This is a common outcome of a large number of experiments, of which the best documented ones are reported by Farrall

(62) and (71), Holmes (74) and Froncek (85). Through this mechanism, current chopping can only be a problem when switching low currents (like in vacuum switches) and not for short circuit interruptions.
Further, it can be seen that the AC parameters ω and $\hat{i}$ enter the equation (3.10) as the combination $\omega\hat{i}$, i.e. the near-current zero value of di/dt. An elegant experiment by Yano (70) showed a dependence of I_c on $\hat{i}$ (keeping f constant) as expected. However, if $\hat{i}$ is varied under the condition of a constant di/dt (with a variable frequency) no change of I_c was observed.

c. Experimental set-up

The measurement of chopping currents involves the use of voluminous circuits, compared to the simple circuits that yield DC lifetime data. Rather high AC currents are necessary to study a possible dependence of chopping current (I_c) on amplitude ($\hat{i}$).
Two different vacuum interrupters were used. The first one (to be called VI 1) is a demountable interrupter, equipped with OFHC copper contacts and similar to the one described in sect. 2b.
The second one (VI 2) is a commercially available type (Holec VB 21/12) having contacts made of a (chopping current reducing) copper-chromium composite.
Both interrupters underwent a thorough cleaning procedure by chemical cleaning, bake-out and arcing.
As it is one of the purposes to measure both AC chopping currents and DC lifetimes in the same circuit, a circuit was set up such, that use could be made of a DC- as well as an AC source. Interrupter VI 1 was built in the circuit, outlined in fig. 3.4.
The AC source is realized with one or more $L_oR_oC_o$ blocs with a resultant resonance frequency of 50 Hz. Capacitor C_o is charged to a voltage U_o (U_o from 1 - 15 kV). After closing of back-up circuit breaker S, a sinusoidal current flows through the breaker. The amplitude of this current is regulated with U_o. By using more than one $L_oR_oC_o$ bloc, a suitable range (between 60 and 500 A) of amplitudes could be assured. Capacitor C_k (7.71 μF) effects the high frequency shunting of the

source. Resistor R (6.6 Ω) has such a value that at the moment of current chopping the effective source voltage U_{ck} is considerably higher than the arcing voltage U_a: $U_{ck} = I_c R + U_a$. The parasitic inductance L_p of the loop circuit formed by VI 1, R and C_k was determined by resonance measurements: L_p = 4 μH.

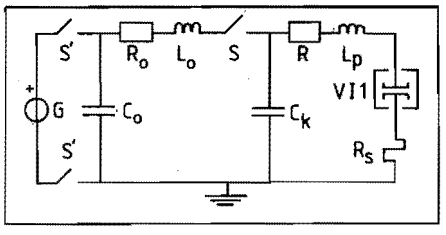

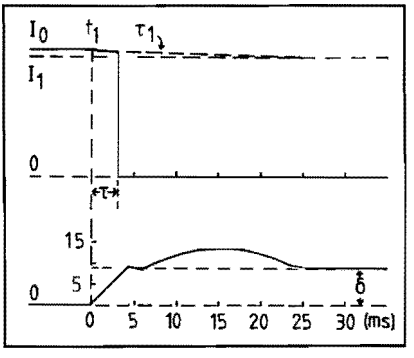

Fig. 3.4: AC-DC circuit for VI 1. G: DC generator (100 kVA, 60-500 V); S', S: switches; C_o, C_k: capacitors (112 μF, 7.7 μF); L_o, L_p: inductances (90 mH, 4 μH); R_o, R: resistors (1.7 Ω, 6.6 Ω); R_s: measuring shunt (11.6 mΩ).

Fig. 3.5: Current through interrupter (top) and contact travel (in mm; bottom). τ: arc lifetime; δ: final distance; t_1 moment of contact separation. I_o, I_1, τ_1: see text.

The moment of the contact separation was chosen such, that contacts had reached their final distance of 8 mm approx. 1 ms before the natural zero of the circuit current.

The DC source consisted of a regulable 100 kVA generator (60 - 500 V). In the DC experiment, switch S remains closed and the circuit is powered by switch S'. The behaviour of arc current i_a at DC operation of this circuit is visualized in the drawing of fig. 3.5 together with the contact travel. At the moment t_1 (approx. 30 ms following closing of S') the contacts of the vacuum interrupter are separated. Arc current (i_a) vs. time is then given by (neglecting a short transient through C_k):

$$i_a(t) = (I_o - I_1) \exp\left[-\frac{(R_o + R)}{L_o} t\right] + I_1,$$

with $I_o = \frac{U_c}{R_o + R}$ and $I_1 = \frac{U_c - U_a}{R_o + R}$; U_c the generator voltage.

Because average arc lifetimes can be expected that are smaller than $L_o/(R_o + R)$, it is important to use a generator voltage much higher than arc voltage: $U_c >> U_a$. Only when this is true, arc current can be considered as a constant during arc lifetime.

For the measurements involving interrupter VI 2, the circuit of fig. 3.4 is modified. This is because the contact distance of a near current zero AC arc should be kept equal to the contact distance of a DC arc during its entire lifetime. Capacitor C_k is replaced by a resistor R_k (7.3 Ω) and a series thyristor Th (fig. 3.6).

In DC experiments, contacts were separated at t_1, and after their standstill at t_2, thyristor Th was triggered at t_3. Arc current is given in fig. 3.7, together with contact travel. Currents and time constants of exponential variations are expressed in circuit parameters as follows (I_o, I_1 as above):

$$I_2 = \frac{R_k U_c - R_k U_a - R_o U_a}{R_o R_k + R_o R + R_k R}$$

$$I_3 = \frac{(U_c - U_a)R_k - U_a(R_o + R)}{(R_o + R)(R_k + R)}$$

$$\tau_1 = \frac{L_o}{R_o + R} \approx 10 \text{ ms} ;$$

$$\tau_2 = \frac{L_o(R_k + R)}{R_o(R_k + R) + R_k R} \approx 20 \text{ ms} , \qquad \tau_3 = \frac{L_p}{R_k + R} \approx 0.3 \ \mu\text{s} ,$$

τ_1, τ_2, τ_3 are the time constants that determine the fall (or rise) of current to the values I_1, I_2, I_3 respectively.

DC lifetime at a constant contact distance is then expressed as the time between thyristor firing t_3 and spontaneous extinction t_4:

$\bar{\tau}_r(I_3) = t_4 - t_3$, and will be called residual lifetime.

The circuit and timing was dimensioned to fulfil a number of demands:

$t_3 > t_2$ (lifetime measurement must start when contacts have stopped moving),

$\tau_3 < 1\ \mu s$ (lifetimes of microseconds must have a well defined start),

$\tau_2 >> \bar{\tau}_r(I_3)$ (arc current must be approximately constant during lifetime),

$\bar{\tau}(I_1) >> t_2 - t_1$ (the arc must not extinguish before completion of contact motion).

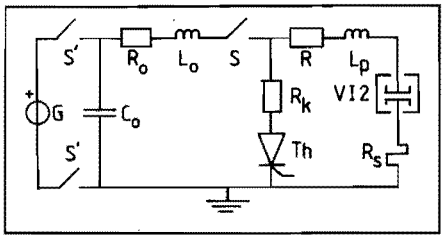

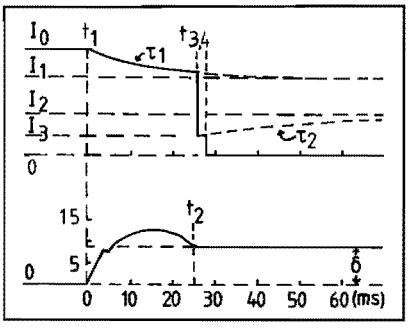

Fig. 3.6: AC-DC circuit for VI 2. G, S, S', C_o, L_o, L_p, R_o, R, R_s: as in fig. 3.4. R_k: resistor (7.3 Ω); Th: thyristor.

Fig. 3.7: Current through interrupter (top) and contact travel (in mm; bottom). t_1: moment of contact separation; t_2: contact standstill; t_3: thyristor firing; t_4: spontaneous extinction; δ: final contact distance. I_o, I_1, I_2, I_3, τ_1, τ_2: see text.

In AC experiments, thyristor Th was short circuited. Resistor R_k was not removed because the impedance of the circuit as seen from the interrupter, should be equal for AC and DC arcing.

Currents were measured with a low-inductance shunt R_s, the signals of which were recorded by means of a digital oscilloscope having a sampling frequency of 2 MHz and with 75 MHz analogue storage oscilloscopes.

d. Comparison of experimental AC and DC data

In this section, chopping currents, obtained directly from AC measurements, will be compared to chopping currents, calculated from

eq. (3.11) using DC data as input parameters. The comparison will be performed for the two interrupters VI 1 (Cu contacts, test breaker) and VI 2 (CuCr contacts, commercial breaker) because of the different range of chopping currents.

VI 1 is investigated with contacts at a standstill on final distance when current chops, and contacts moving while obtaining DC lifetimes (cf. fig. 3.5).

Using VI 2, contact distance is kept the same during chopping current measurement and DC lifetime determination (cf. fig. 3.7).

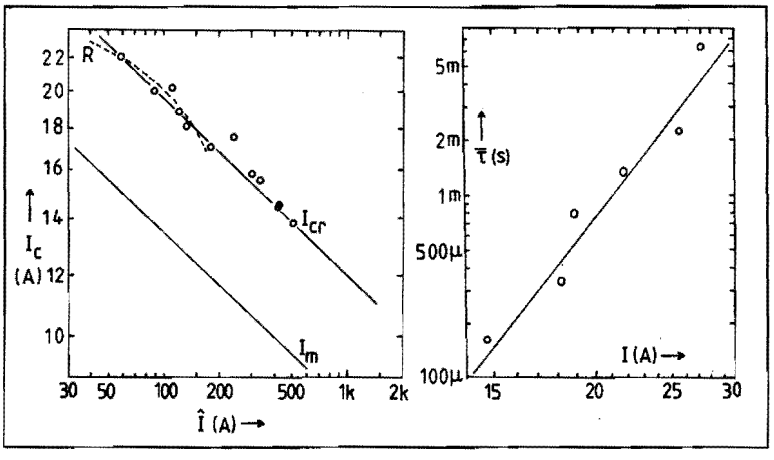

Fig. 3.8a: Measured chopping currents (circles) (I_c) as a function of AC amplitude ($\hat{i}$) in VI 1. Also entered is DC lifetime-based critical current (I_{cr}) and maximum prospective current (I_m). R: measurements by Reininghaus (83).

Fig. 3.8b: DC lifetime ($\bar{\tau}$) as a function of current (I) in VI 1.

Experimental results of both AC and DC measurements for the Cu-arc (VI 1) in the circuit of fig. 3.4 are shown in fig. 3.8. First, in fig. 3.8a measured chopping currents (I_c) as a function of amplitude ($\hat{i}$) in a range $60 < \hat{i} < 500$ A are plotted on a double logarithmic scale. The results can be approximated by $\log I_c' = 1.7 - 0.21 \log \hat{i}'$. They can be compared to earlier results from Reininghaus (83). He gives an empirical expression for chopping current as a function of amplitude ($45 < \hat{i} < 70$ A) and surge impedance ($60 < Z_0 < 20$ kΩ). This relation is entered in fig. 3.8a too, and is denoted by "R". It can be seen that there exists a good agreement in the overlapping range of $\hat{i}$.

In fig. 3.8b lifetime $\bar{\tau}$ is given as a function of arc current. These lifetimes are somewhat higher than those, given in sect. 2c, due to different parameters of the actual circuit.

The presented lifetimes are the average over 50 measurements per current value; relative inaccuracy is 8 - 11%. The best description of the function, assuming an exponential relationship is: $\bar{\tau} = \alpha\ (I')^{\beta}$

With the aid of the lifetime parameters $\alpha = 3.39\ 10^{-11}$ s and $\beta = 5.62$, the two functions $I_{cr}(\hat{\imath})$ and $I_m(\hat{\imath})$ [eqs.(3.10) and (3.11) respectively] are plotted in fig. 3.8a. According to the model, outlined in sect. b, chopping currents, predicted by the DC lifetime parameters, should lie close to $I_m(\hat{\imath})$ and below $I_{cr}(\hat{\imath})$. Comparison of these theoretically predicted values with the directly measured ones makes clear immediately that $I_m(\hat{\imath})$ cannot be taken here as a measure for real chopping currents $I_c(\hat{\imath})$. Although the slope of the $I_m(\hat{\imath})$ is in good agreement with that of the (measured) course of $I_c(\hat{\imath})$, absolute values of predicted chopping currents are about 30 - 35% below the measured ones.

Apparently, measured arc lifetimes are too long in order to get even an approximate equality of calculated and measured chopping currents.

The reason for this discrepancy is the contact motion. When obtaining AC chopping currents, contacts were on their final position a sufficient time before current zero, whereas the DC lifetimes were measured with contacts moving. It was demonstrated in sect. 2g to what an extent a variable contact distance affects DC arc lifetime. Therefore it seems necessary to acquire AC as well as DC data under the same (and constant) contact distance conditions.

These measurement could be performed in the circuit of fig. 3.4 (cf. sect. c), now taking residual lifetime $\bar{\tau}_r$ as the important quantity. In this case, interrupter VI 2 was used.

Fig. 3.9 shows the results. The first one, fig. 3.9a gives the directly measured chopping currents as a function of amplitude ($\hat{\imath}$), as well as the functions $I_{cr}(\hat{\imath})$ and $I_m(\hat{\imath})$, calculated with the DC parameters ($\alpha = 6.2\ 10^{-16}$ s and $\beta = 14.3$).

These parameters were determined on the basis of the residual lifetime vs. current relation, given in fig. 3.9b. It can be noticed, that a much better agreement between measured and calculated values is established now AC and DC data are obtained under similar contact distance conditions. Measured chopping currents I_c are in the interval

$I_m < I_c < I_{cr}$ as predicted by the model and deviate less than 15% from

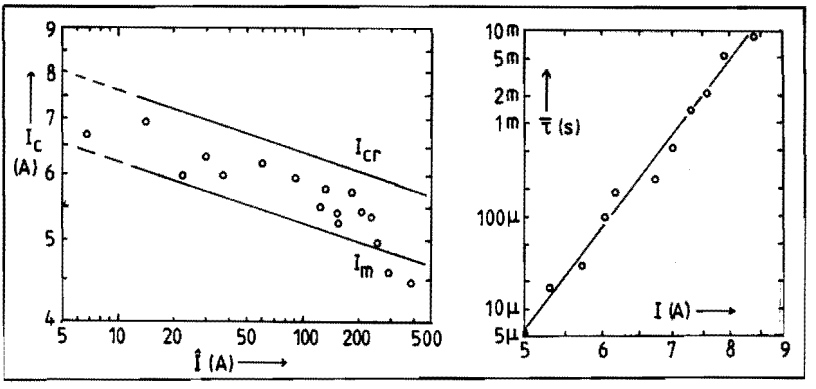

Fig. 3.9a: Measured chopping currents (circles) (I_c) as a function of AC amplitude ($\hat{i}$) in VI 2. Also entered are DC lifetime-based critical current (I_{cr}) and maximum prospective current (I_m).
Fig. 3.9b: DC lifetime ($\bar{\tau}$) as a funtion of current (I) in VI 2.

$I_m(\hat{i})$ in a wide range of amplitudes. Besides, dependence on $\hat{i}$ is congruent with the DC based calculations. Hence it is assumed, that a reasonable approximation of chopping currents can be calculated from relatively simple DC lifetime measurements, as outlined in sect. b and c. It must be stressed again however, that chopping levels, estimated in such a way, are only valid in a similar circuit under similar contact distance conditions.

e. Circuit effects

There is unanimous agreement on the fact that the interaction between an arc discharge and the circuit in which it operates is important. When considering current chopping, the influence of circuit parameters on chopping current and resulting (practically relevant) overvoltages is relatively well understood for high pressure arcs in conventional (air-, oil-, or SF_6-) breakers. Of all the circuit parameters, the effect of capacitance parallel to a breaker, is studied most intensively.

From Mayr's model (Mayr 43) it was derived that for a high pressure arc the chopping current is proportional to the square root of this capacitance (C) (Kopplin 59):

$$I_c = \kappa \sqrt{C} \qquad (3.13)$$

with $\kappa = \sqrt{(P/\theta_a)}$; P represents the power loss in the arc, θ_a is the arc time constant.
Relation (3.13) was verified experimentally a number of times (e.g. by Damstra 64). Combining eq. (3.13) with (3.1), it would result from theory, that overvoltage is not dependent on parallel capacitance. In practice however, an increase of overvoltage with increasing capacitance is often found. Reignitions due to a still hot arc residu will naturally limit the peak value of overvoltages. This limiting mechanism is impaired by parallel capacitance. Its presence lowers the rate of rise of the recovery voltage so reducing the reignition probability but increasing the overvoltage.

A different situation again is encountered in a vacuum breaker. A comparative study of circuit effects on chopping current and overvoltages in gas- as well as in vacuum breakers (Murano 77) showed that the increase of chopping current with capacitance in vacuum breakers is much less than proportional to $\sqrt{C}$. Due to this, adding of parallel capacitance increases chopping current and at the same time reduces overvoltages. A similar finding was reported by Holmes (74).
The increase of chopping current with parallel capacitance is a subject often studied (Yano 70, Damstra 76, Reif 80, Froncek 85). These authors also noted a decrease of chopping current when increasing the circuit's series inductance.
Keeping in mind the shortening of DC lifetime by a parallel capacitance, and the lengthening by series inductance, discussed in sect. 2e, it is logical now to assume that a long DC lifetime gives low chopping currents and short lifetimes cause high chopping levels. Stated otherwise, DC lifetime parameters α, β are functions of circuit parameters (among others).

Probably, the parameter α alone can incorporate dependence on capacitance:

$$\frac{1}{\alpha} \left| \frac{\partial \alpha}{\partial C} \right| >> \frac{1}{\beta} \left| \frac{\partial \beta}{\partial C} \right| \qquad (3.14)$$

Inequality (3.14) is suggested by an experiment by Cobine (60) who found a relative lifetime shortening (due to a capacitance) roughly independent on arc current (cf. sect. 2e). Further, the combined effect of capacitance and inductance may be summarized by putting:

$$\frac{1}{\alpha} \left| \frac{\partial \alpha}{\partial Z_o} \right| >> \frac{1}{\beta} \left| \frac{\partial \beta}{\partial Z_o} \right| , \qquad \text{with } Z_o = \sqrt{(L/C)} \text{ as usual.}$$

As stated earlier, the current $I'_m = (\alpha\ \beta\ \omega\ \hat{\imath}')^q$ [with $q = (1-\beta)^{-1}$] can serve as an estimation for the chopping current I_c:

$$I_c \approx I_m .$$

Then the following expression can be obtained:

$$\log I'_c \approx q \log \alpha' + q \log (\beta\ \omega\ \hat{\imath}'). \qquad q < 0,\ \alpha > 0,\ \beta > 0 \qquad (3.15)$$

From extensive measurements by Holmes (74) empirical expressions for measured chopping current were derived of the form:

$$\log I_c \approx q_H \log Z'_o + \log (A - B\hat{\imath}') \quad q_H < 0,\ A > 0,\ B > 0. \qquad (3.16)$$

with q_H, A, B constants for a given material.
Comparing eq. (3.15) with eq. (3.16) it seems reasonable to associate α (more than β) with the circuit dependent DC parameter.
Parameter β is probably a strong function of contact distance, as the different slope in the $\bar{\tau}$ vs. I curves for different distances in fig. 2.14 indicates.
Both parameters α and β are undoubtebly strongly dependent on the choice of contact material.

f. Concluding remarks

Characteristic parameters α and β, derived from measurements of the DC arc lifetime $\bar{\tau}$ as a function of arc current I are used to predict AC chopping currents I_c for a given amplitude $\hat{\imath}$ and frequency ω:

$$\bar{\tau} = \alpha\ (I')^{\beta} \rightarrow I_c \approx (\omega\ \alpha\ \beta\ \hat{\imath}')^{1/(1-\beta)},\ \alpha = \alpha(Z_o) \text{ and } \beta = \beta(\delta) \qquad (3.17)$$

Herein, δ represents contact distance and Z_o surge impedance. It was shown in sect. d that the DC → AC transformation (3.17) only holds if DC values are obtained from an arc having the same length (throughout its entire lifetime) as the AC arc near current zero.
In the derivation of eq. (3.17) the motion of the contacts in the AC case is not included. As DC lifetime is a function of current and contact distance (for a given circuit and contact metal), chopping current might be influenced by the contact motion.
The variation of arc lifetime with time remaining before current zero is given by :

$$\frac{d\bar{\tau}}{dt} = \frac{\partial\bar{\tau}}{\partial I}\frac{dI}{dt} + \frac{\partial\bar{\tau}}{\partial\delta}\frac{d\delta}{dt} = \alpha\ \beta\ (I')^{\beta-1}\ \omega\ \hat{\imath}' + v_o\frac{\partial\bar{\tau}}{\partial\delta} \approx (I/I_c)^{\beta-1} + v_o\frac{\partial\bar{\tau}}{\partial\delta} \qquad (3.18)$$

Herein, v_o is the opening speed of the contacts. From fig. 2.14 it can be estimated that the factor $(\partial\bar{\tau}/\partial\delta) \ll 1$ s/m for currents near the chopping level. Also for higher currents the factor $(I/I_c)^{\beta-1}$ is always preponderating in eq. (3.18) for opening speeds in the range of some m/s. Hence it is expected that chopping currents will not be influenced seriously by the motion of the contacts: current decline deteriorates survival conditions on a much faster time scale than arc lengthening.

The fact that $\partial\bar{\tau}/\partial\delta$ is small for currents near the chopping level has an important practical bearing. It is expected that chopping currents will not depend strongly on the moment of the contact separation relative to the natural sine zero once a distance of some mm is reached, after which a further increase no longer seriously affects lifetime. This is in agreement with experiments by Holmes (74). He finds no apparent differences in chopping currents between a fixed opening moment and a

randomly chosen moment of contact separation. Similar findings are reported by Dobrogowski (72), Kuffel (74) and Froncek (85). This is an important conclusion for practical application, because any interrupter will always open at an arbitrary moment in the current sine.
Only when the contacts are separated very shortly before current zero, multiple reignitions are possible, due to a very small (up to some hundreds of μm) gap and a subsequent interruption of high frequency currents (Czarnecki 84).

Central in the derivation of the DC → AC transformation is the assumption that the physical processes in the arc proceed on a much faster time scale than AC current decays. For an arc in the diffuse mode (i.e. the state of the arc in which a number of independent cathode spots are spread evenly over the cathode surface) it was shown by Paulus (72) that below current rates of approx. 100 A/μs the discharge is able to follow the changing current quasi-stationary. For a practical interrupter, AC decline is always much slower, so that the DC → AC conversion is permitted in this respect.
However, when large scale anode melting occurs, which is (without precautive measures) at some kA AC currents, cooling time constants in the order of 1 ms are involved. Whenever this happens, the history of the arc is important at current zero and the model no longer holds.

It was demonstrated in this chapter, that it is possible to replace direct measurements of chopping currents by reasonable predictions based on DC measurements. These lifetime measurements are easy to perform and do not involve large high-voltage circuits, commonly used for chopping measurements. This clear simplification has an advantage in practical testing, but also reduces the study of the complicated phenomenon of current chopping to an essentially time independent problem. This advantage in methodological respect will be exploited in the next chapters.

References:

- Baltensperger P., CIGRÉ Report 116 (1950)
- Burrage L.M. and Guertin J.P., Holm Conf. on Elec. Cont. Phen. (1973) 180-7
- Cobine J.D. and Farrall G.A., J. Appl. Phys., vol. 31 (1960) 2296-304
- Czarnecki L. and Lindmayer M., XIth Int. Symp. on Disch. and Elec. Ins. in Vac., Berlin DDR, (1984) 253-60
- Czarnecki L., Ph.D.Thesis, Technical University of Braunschweig (1986)
- Damstra G.C., CIGRÉ Report 120 (1964)
- Damstra G.C., CIGRÉ Report, commitee 13.08 (1976)
- Dobrogowski J., Vth Int. Symp. on Disch. and Elec. Ins. in Vac., Poznan (1972) 355-9
- Farrall G.A., GEC Report no. 62-RL-3068G, General Electric Company (1962) 1-20 (unpublished)
- Farrall G.A., Lafferty J.M. and Cobine J.D., IEEE Trans. Comm. Elec. 114 (1963) 253-8
- Farrall G.A., GEC Report no. 71-C-133, General Electric Company (1971) 1-6 (unpublished)
- Filip G., Ph.D. Thesis, Technical University of Vienna (1984)
- Frey P., Klink N. and Säger K.E., Metall 38 (1984) 647-51
- Froncek F., Wróblewski Z. and Schmidt H., etz Archiv Bd 7 (1985) 233-9
- Hammann J.F., Kippenberg H., Häßler H., and Schreiner H., Siemens Forsch. u. Entwickl. Ber. Bd. 9 (1980) 210-6
- Heuvel vd W.M.C.,Ph.D. Thesis, Eindhoven University of Technology (1966)
- Heuvel vd W.M.C., IEEE Trans. on Plasma Sci., PS - 8 (1980) 326-31
- Holmes F.A., IEEE Winter Meeting PES # C74 088-1 (1974) 1-9
- Kopplin H. and Schmidt E., ETZ - A 80 (1959) 805
- Kuffel E. and Dobrogowski J., VIth Int. Symp. on Disch. and Elec. Ins. in Vac., Swansea (1974) 236-40
- Kurosawa Y., Iwasita K., Wanatabe R., Andoh H., Takasuna T. and Wanatabe H., IEEE Trans. Pow. App. Syst., PAS-104 (1985) 3634-42

- Mayr O., Arch. für Elektrotechnik 37 (1943) 588
- Murano M., Yanabu S., Ohashi H., Ishizuka H. and Okazaki T., IEEE Trans. Pow. App. Syst., PAS - 96 (1977) 143-9
- Néveri I., Polgar T. and Szauter F., Int. Conf. on Cont. Phen., Budapest (1980) 161-74
- Paulus I., Holmes R. and Edels H., J. Phys. D: Appl. Phys., vol. 5 (1972) 119-32
- Reece M.P., Proc. IEE, vol. 110 (1963) 793-802
- Reif W., Appl. Phys., vol. 21 (1980) 169-71
- Reininghaus U., Ph.D. Thesis, Technical University of Braunschweig (1983)
- Rizk F.A.M., CIGRÉ Report 107 (1964)
- Rondeel W.G.J., J. Phys D: Appl. Phys., vol. 8 (1975) 934-42
- Sämann D., Ph.D. Thesis, Technical University of Braunschweig (1984)
- Slade P.G., Holm Conf. on Elec. Cont. Phen. (1973) 194-200
- Yano M., Ozaki Y., Morimiya O. and Nakano Y., Elec. Eng. in Japan, vol. 90 (1970) 73-83

4. LOW-CURRENT VACUUM ARC INSTABILITIES AND EXTINCTION

a. Introduction

In chapter 2, it was noticed that after a certain lifetime, a DC vacuum arc extinguishes spontaneously. This finiteness of DC arc lifetime has been shown in the chapter 3 to result in AC current chopping. The question why a DC arc extinguishes spontaneously thus stands central in a fundamental approach of the current chopping phenomenon. It might seem strange that an arc ceases spontaneously, inspite of the constancy of all parameters involved. The continued survival of a vacuum arc however, seems strongly coupled to the repetitive nature of the emission process. From intensive study of the cathode surface, eroded by arcing activity, it is well known that typical patterns are left behind (Daalder 78, Lafferty 80). These "post mortem" studies reveal tracks of individual crater-like structures, apparently formed in a random motion of the cathode spot. The mass, necessary to sustain a continued emission is liberated from the cathode leaving emptied, half-spherical structures, commonly referred to as "cathode craters". These craters have dimensions in the order of some micrometres, and formation times between some nanoseconds and several microseconds, depending on the author cited.
It is thus clear that a very large number of cyclic processes occur in one arc lifetime. Statistical analysis of these repetitive processes, all within the life of one single arc can give additional and important information concerning the arc's instability behaviour.

While in previous chapters only arc lifetime was used to characterize arc stability at a certain current, this chapter focusses on the high frequency behaviour of arc current and voltage. The (long term) aim is to get insight in the fundamental emission processes. After a discussion of the measuring set-up (sect. b), suitable for recording fast transient events in the arc, the existence of typical "instabilities" will be demonstrated (sect. c). Then, a statistical treatment of these instabilities is used to explain spontaneous arc extinction (sect. d).

In sect. e, f an electrical model is presented that is able to explain the phenomena dealt with. Finally, conclusive section g will exploit further some of the features, embodied in the model.

b. Experimental set-up

For the measurement of transients in arc current and voltage, the low inductive DC circuit of fig. 2.2, described in sect. 2b is used. A low inductance and capacitance is necessary to study the arc in its most pure form. In this way, circuit responses on arc transients, caused by physical processes in the arc, are reduced to a minimum. However, arc transients are so rapid - as shall be demonstrated - that even very small parasitic reactances in the immediate vicinity of the interrupter are noticable.
Therefore, parasitic capacitance and inductance of the (demountable) housing was determined using a high-frequency resonance technique. This yielded an equivalent electrical circuit diagram of the breaker housing as given in fig. 4.1.

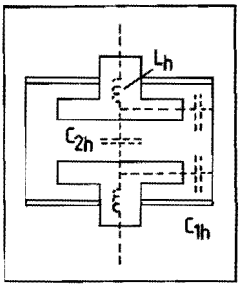

Fig. 4.1: Parasitic capacitances (C_{1h}, C_{2h}) and inductances (L_h), pertinent to the geometry of a vacuum interrupter.

Capacitance of the contacts to the housing (C_{1h}) is 13 pF, contact-to-contact capacitance (C_{2h}) is between 20 pF for 0.3 mm distance and 4 pF for 5 mm (measured values). The inductance of the contact supports (L_h) is found to be about 200 nH each (at a length of 12 cm).
Apart from the determination of the interrupter housing parasitics, it was necessary to specify the circuit of fig. 2.2 more realistically with respect to high-frequency responses on rapid changes in arcing conditions. Detailed measurements of the circuit's frequency characteristic learned that (for HF purposes only) a good approximation of reality requires a split-up of the lumped components L_v, C_p both into

two: $L_{v1} \approx 4.5$ µH located in the power source and $L_{v2} \approx 1.5$ µH in the shielding box; $C_{p1} \approx 100$ pF is the capacitance of the power source and $C_{p2} \approx 300$ pF the capacitance of the (unmatched) coaxial cable to the shielding box. Now, a HF equivalent circuit for the feeding circuit and the interrupter housing emerges as outlined in fig. 4.2.

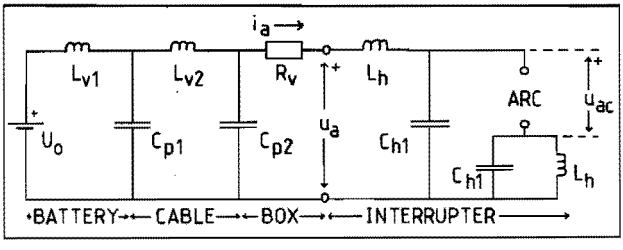

Fig. 4.2: HF-equivalent diagram of the feeding circuit. U_o: battery (72 V); L_{v1}, L_{v2}, L_h: parasitic inductance (4.5 µH, 1.5 µH, 200 nH); C_{p1}, C_{p2}, C_{h1}: par. capacitances (100 pF, 300 pF, 13 pF); R_v: resistance (≈2 Ω). i_a, u_a: measured current and voltage; u_{ac}: interelectr. voltage.

Transients in arc currents were measured with HF current transformers Pearson 411 and 110 (fixed round the cathode lead) having a rise time of 10 and 20 ns respectively. DC currents were monitored with a 102.7 mΩ shunt having a risetime of 100 ns.

The measurement of arc voltage is a problem in itself. When dealing with high di/dt in arc current, a difference should be made between the actual interelectrode voltage (u_{ac}) and the apparent arc voltage measured over the interrupter terminals (u_a):

$$u_a = u_{ac} + 2L_h \, di_a/dt \qquad (4.1)$$

Inspite of the seemingly insignificant L_h, current transients can be so severe, that the measured voltage largely exceeds the interelectrode voltage. In order to minimize induced voltages, an interrupter was constructed equal to the one described in sect. 2b, with voltage measuring leads connected just "below" the electrode surfaces and fed out through hollow electrode supports, illustrated in fig. 4.3.

Residual inductance was estimated by applying a di/dt = 500 A/µs with contacts in closed position, and measuring the induced voltage differentially. Mutual inductance with the current path could so be reduced to 50 nH. This special interrupter was applied when dealing with extremely high di/dt (> 50 A/µs) and will be referred to as "low

inductance interrupter". Preparation and conditioning of the contacts took place as described in sect. 2b.
Voltages were measured with 75 MHz 1:10 and 1:1000 conventional voltage dividers.

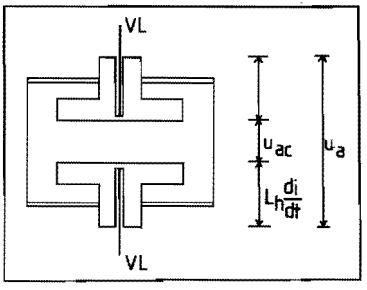

Fig. 4.3: Low inductance interrupter. u_{ac}: interelectrode voltage; u_a: (outside) measured voltage; $L_h di/dt$: induced voltage over support inductance; VL: voltage measuring leads.

The recording equipment consisted of two 75 MHz storage oscilloscopes (Tektronix 7623) arranged in a master-slave set-up for simultaneous monitoring of arc current and -voltage. Synchronicity was better than 10 ns. In a later phase, one single digital oscilloscope having two channels, sampling at a maximum rate of 100 MHz was added (Le Croy 9400). Vertical resolution is 8 bit, horizontal memory is 32 k words per channel. This recorder was coupled to a micro computer system, allowing numerical evaluation of the recorded data. A penplotter was applied to plot directly the contents of the recorder's memory.

c. Vacuum arc instabilities

A short glance at fig. 2.5 makes clear immediately that both arc current and voltage have a noisy character. To study the structure of this noise in detail, numerous recordings of arc current and voltage were made, employing fast sampling and storage techniques. These revealed a behaviour of current and voltage that is far from being stable: during an arc's life, a (large) number of transient momentary current reductions characterizes the instable arc. Typical oscillograms are given in fig. 4.4 for some arc currents at different levels.
Strictly speaking, such arcs can hardly be called DC arcs. Nevertheless, the term "DC arc" will remain in use, indicating an arc, the current of which is limited to a value $I = (U_o - U_a)/R_v$ with U_o, U_a source- and (time-averaged) DC arc voltage respectively.

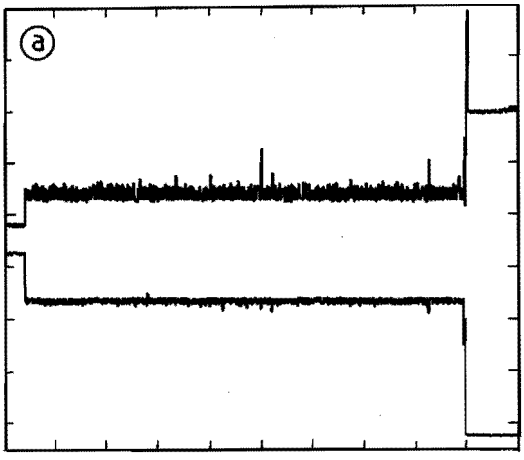

Fig. 4.4: Instable arc voltage (upper trace) and currrent (lower trace). a: I = 36.2 A, 14 A/div, 32 V/div, 5 ms/div; b: I = 17.0 A, 4 A/div, 32 V/div, 100 µs/div; c: I = 9.4 A, 4 A/div, 32 V/div, 5 µs/div. Arc currents were monitored with a shunt having a limited (3 MHz) bandwidth.

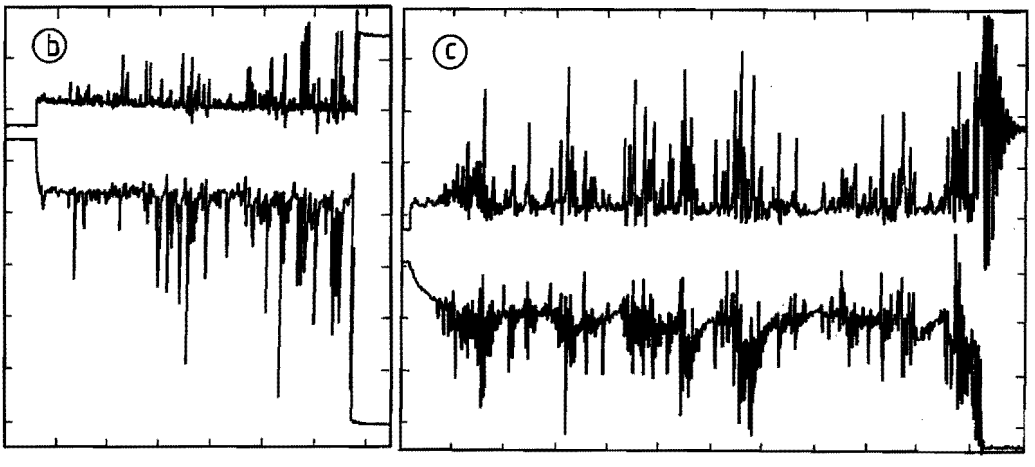

The momentary current reductions of fig. 4.4 can be interpreted as tendencies to extinguish, thus endangering arc stability. In the following, the transient momentary current reductions will therefore be called "instabilities".

Detailed observation of a large number of such instabilities has revealed a more or less uniform shape, apart from inevitably accompanying high-frequency circuit oscillations. Two characteristic phases are discernible in each instability:

1. Decay phase: Within a time Δt (of some hundreds of ns) a current reduction ΔI occurs ($0 < \Delta I \leq I$). The associated di/dt is in the order of 100 A/µs. Simultaneously, the arc voltage u_a rises to a value much higher than the steady state DC voltage U_a, and then returns to U_a.

2. Recovery phase: Starting from a current value $I - \Delta I$ exponential recovery of the current is achieved:

$$i_a(t) = I - \Delta I \exp(-t/\theta_r), \qquad (4.2)$$

with θ_r the recovery time constant. During this phase the arc voltage is essentially equal to its steady state value: $u_a(t) \approx U_a$.

In fig. 4.5, oscillograms of two such instabilities (current i_a and voltage u_a recorded simultaneously) and a fast recording of the decay phase of a third instability, illustrate this behaviour.

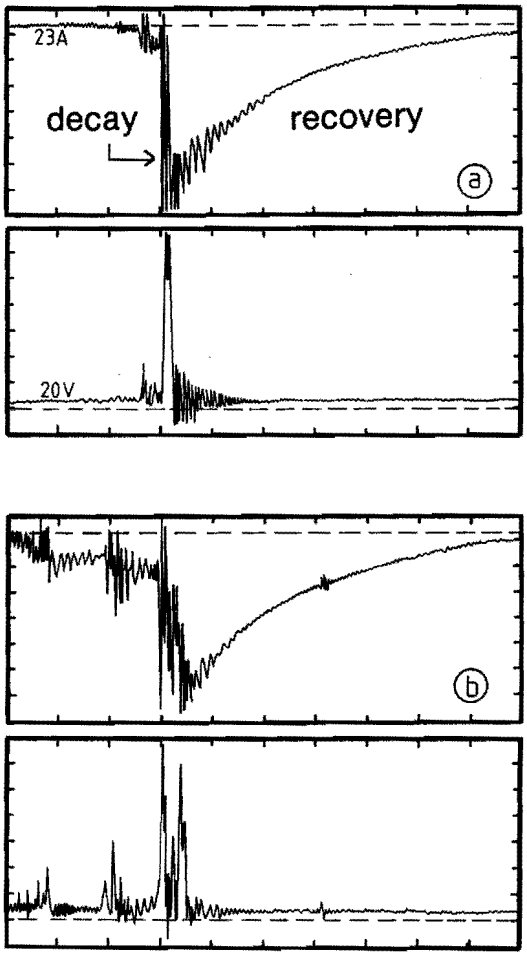

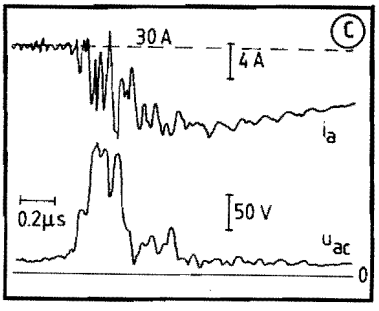

Fig. 4.5: Arc instabilities. a,b: upper traces: current 2 A/div; lower traces: voltage 50 V/div, time: 1 µs/div (digitally sampled at 100 MHz); c: analogue oscillogram of decay phase; upper trace: current; lower trace: voltage.

The exact share of the arc's contribution to the depicted phenomena is hidden by high-frequency oscillations originating from the circuit.

In the decay phase, high frequencies are observed, attributed to the housing reactances. In the recovery phase, a damped oscillation with a frequency in the order of 10 MHz is recognized.
Variation of the circuit resistance R_v and addition of inductance to the parasitic $L_v = L_{v1} + L_{v2}$, has taught that recovery time constant θ_r is circuit dependent: $\theta_r = L_v/R_v$. (4.3)
The observed instabilities reflect a very abrupt and drastic change in arcing conditions, unquestionably related to spontaneous arc extinction.

d. Statistical analysis of arc instability; arc extinction

Since one arc consists of a large number of individual instabilities, the consequences for the arc lifetime can only be understood by taking into account the cooperative action of the instabilities.
After recording several hundreds of arcs at a certain current (I), a numerical procedure was used to count the total number of times $N(\Delta I, I)$ that arc current was reduced more than a given amount ΔI. The sum of all arc lifetimes ($\Sigma \tau$) was divided by this number, resulting in a quantity called "average instability repetition time" $[\bar{\theta}(d,I)]$:
$\bar{\theta}(d,I) = [\Sigma \tau(I)] / N(\Delta I/I, I)$.
Herein, d is used for the relative current reduction: $d = (\Delta I/I)\times 100\%$.
The quantity $[\bar{\theta}(d,I)]^{-1}$ can be interpreted as an (unnormalized) probability for an instability to occur.
The results of such an analysis for a number of currents in the range $20 < I < 30$ A are summarized in fig. 4.6.
It is clearly seen that the average repetition time strongly decreases with arc current, and that "small" instabilities occur much more often than larger ones.
The average lifetime $\bar{\tau}(I)$ pertinent to the circuit, is also entered in fig. 4.6. Below the studied current range ($I < 18$ A) too severe an accumulation of instabilities takes place; above it ($I > 30$ A), large instabilities become so rare that measuring time is unacceptably long.

From oscillograms of the arc current (fig. 4.4b,c), the impression is created that arc instabilities can be held responsible for spontaneous arc extinction.

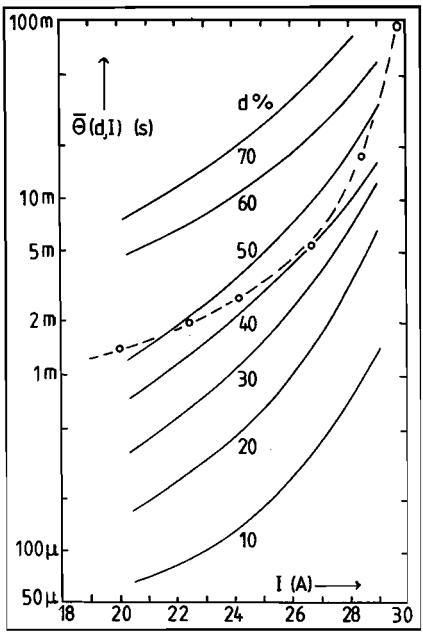

Fig. 4.6: Average repetition time $[\bar{\theta}(d,I)]$ *of instabilities leading to a relative current reduction* $(\Delta I/I)$ *greater than d %. Open circles (o): average lifetime* $(\bar{\tau})$ *obtained in the same circuit. The two are given as a function of arc current* (I).

By interpretation of numerous oscillograms having sufficient time resolution, it was made clear that spontaneous arc extinction can in principle occur according to two mechanisms:

1. By a rapid succession of instabilities with a depth $\Delta I < I$, and a succession time shorter than the recovery duration (of approx. $3\theta_r$) of the previous instability ("step wise extinction").
2. By one single instability having a depth $\Delta I \approx I$.

Mechanism 1. is much more frequent, as ascertained by inspection of a large number of recordings of arc extinctions. Some of these are brought together in fig, 4.7.

Here, 33 A arcs, shunted by a 0.95 Ω resistor in order to damp HF oscillations reach current zero in a number of steps, each identified by a rapid decay of current (instability-decay phase) and only partial recovery. A special illustrative example of step wise extinction is the oscillogram in fig. 4.8 that shows the last 9 µs of a 19 A vacuum arc.

Apart from these oscillograms, a more quantitative argument emerges at closer inspection of fig. 4.6. It can be seen, that instabilities with a relative depth of more than (say) 70% have a much longer average repetition time than the average arc lifetime.

This means, that such "deep" instabilities on the average occur less than once per arc lifetime. Only at higher currents ($I > 30$ A)

extinction by 100% instabilities does take place more frequently.

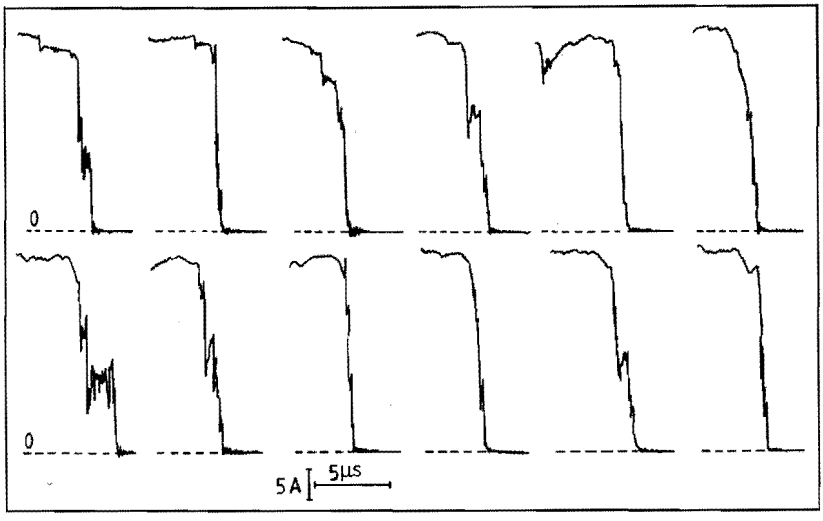

Fig. 4.7: Current at spontaneous extinctions of 33 A vacuum arcs.

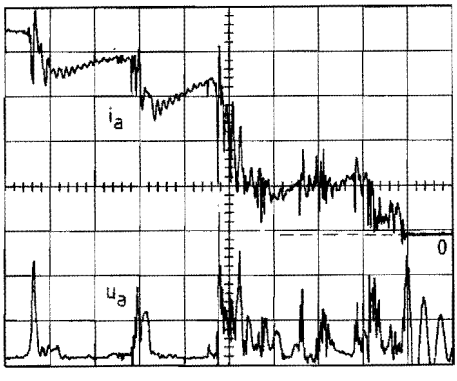

Fig. 4.8: Current (upper trace, 4 A/div) and voltage (lower trace, 40 V/div) in a step wise extinction. Time: 1 µs/div.

After the experimental observation that extinction predominantly results from a succession of instabilities, spaced less than a recovery duration, the question arises why instabilities accumulate to such an extent.

In the following it is made plausible purely on statistical grounds that the described mechanism of arc extinction is feasible. Assuming a random distribution of instabilities over the arc lifetime, clustering of instabilities predominantly occurs as a result of reduced current in the recovery phase of a previous instability. According to fig. 4.6, a momentarily reduced current in the recovery phase should enhance the probability of a subsequent instability.

In order to test the above hypothesis, a semi-empirical model has been constructed, the experiment being incorporated in this model by fig. 4.6. From the average instability repetition time $\overline{\theta}(d,I)$ observed, a dimensionless expression $\theta'(d,I')$ is derived that fits the experiments:

$$\log \theta'(d,I') = \exp [0.057\ I' + 0.91 - \exp (0.25 - 0.05\ d)] \qquad (4.4)$$

Herein d is restricted to the discrete values d = 5, 15...., 95 only; the time $\theta(I,d)$ associated with $\theta'(I,d)$ is in μs. $[\theta(d,I)]^{-1}$ is interpreted as the average number of instabilities per μs that lead to a current reduction ΔI given by: $d - 5 < 100(\Delta I/I) < d + 5$.
Using $\theta(d,I)$, artifical arc current shapes were generated with the aid of a Monte Carlo-like computer program. These simulated arc currents had a distribution of instabilities that differed not more than 15% from the experimental distribution of fig. 4.6 and its extrapolation to lower currents. In the range $15 \leq I \leq 23$ A a hundred of such arcs were constructed per current value. The resultant average lifetime is shown in fig. 4.9 by the triangular symbols.

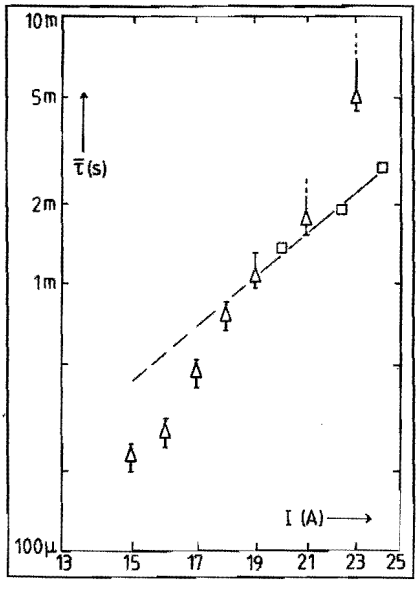

Fig. 4.9: Average lifetime ($\overline{\tau}$) measured in the circuit of fig 4.2 (□) and calculated with a Monte-Carlo program (Δ) as a function of current (I). 100 arcs per indicated point were averaged over.

Owing to an unacceptably long calculation time, currents higher than 23 A could not be evaluated. Also plotted are values of lifetimes (squares) obtained from measurements in the same circuit.

Bearing in mind the simplicity of the model, the agreement between calculated and experimental lifetimes is satisfactory, at least when considering orders of magnitude. There are at least two reasons why discrepancy can be expected:

1. Extrapolation to currents far below the measured range is inevitable.
2. It is assumed that instabilities are distributed evenly over the arc lifetime. Because of a larger contact distance in a later period of the arc, it is expected (and observed) that here deeper instabilities are more frequent.

The latter assumption is thought to cause the discrepancy in slope that is expressed in fig. 4.9.

From the above, it seems reasonable now to assume that typical arc instabilities like in fig. 4.5, can be held responsible for arc extinction. The current dependence of their probability of occurrence together with a circuit determined recovery are of primary importance in this respect.

e. An equivalent electrical diagram for the instable arc

For purposes of modelling, it is useful to design an equivalent electrical diagram of the arc that can describe the behaviour of current and voltage during an arc instability. Besides, such a model must be capable of expressing the dependence on a number of parameters the same way as do the experimental results.

A very simple and yet satisfactory arc model is constituted by a resistor R_a, parallelled by an ideal switch S, and an ideal voltage source U_a in series (fig. 4.10).

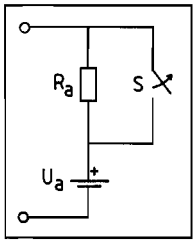

Fig. 4.10: Electrical model of a vacuum arc for simulation of instabilities. R_a: transient arc resistance, switched in/out by opening/closing ideal switch S; U_a: ideal DC voltage source.

The arc resistance (R_a) however, should at this moment be interpreted as a model representation for calculation purposes only. The question about the physical meaning of this R_a will be postponed to chapter 7.

Opening of the switch (S) causes a sudden transient arc resistance (R_a), leading to a circuit determined decay of current. Closing of S will restore the stationary situation after some (circuit determined) time. The time that the switch is in open position is in the model be equal to the duration of the instability decay phase.

This transient arc resistance model was first substituted in the diagram of the measuring circuit of fig. 4.2 containing a number of parasites. In a computer simulation, the thus resulting circuit was excited by the opening of the switch at t = 100 ns, and subsequent closing at t = 400 ns; model parameters U_a = 20 V and R_a = 10 Ω. Resistor R_v was chosen R_v = 2 Ω, so that before the switch opens the DC current is 26 A.

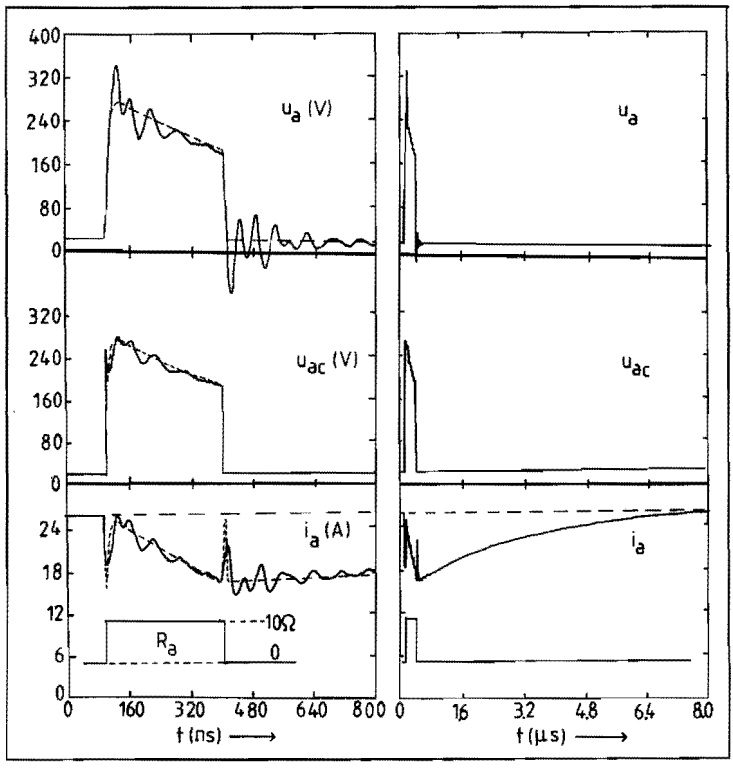

Fig. 4.11: Computer simulations of response of voltage (u_a, u_{ac} see fig. 4.2) and current (i_a) upon the indicated step in arc resistance. Hereby the diagram of fig. 4.10 is inserted between "ARC" in fig. 4.2. Dashed curves: response on the same excitation but now in the simplified circuit of fig. 4.12.

The calculated responses of arc voltage i_a, measured voltage u_a and interelectrode voltage u_{ac} are presented in fig. 4.11 on a timescale (800 ns) giving details of the decay phase, as well as on a timescale (8 µs) covering the entire instability.
Comparing the theoretical $i_a(t)$ and $u_a(t)$ with their measured equivalences in fig. 4.5, the model of both circuit and transient arc resistance seems to describe reality reasonably.

Further numerical analysis has shown, that the measuring circuit model can be simplified without loss of its significant characteristics. The recovery-phase course of $i_a(t)$ is determined by the largest time constant $(L_{v1} + L_{v2})/R_v$ of the circuit in fig. 4.2, while the other impedances only contribute to the HF behaviour. From analogue reasoning, it follows that the time constant $(C_{p1} + C_{p2})R_v$ is essential for $u_a(t)$.

Now a simplified circuit is obtained, describing the arc as a voltage source U_a in series with a time dependent resistor R_a in a feeding circuit having one R_v, $L_v = L_{v1} + L_{v2}$ and $C_p = C_{p1} + C_{p2}$ (fig. 4.12).

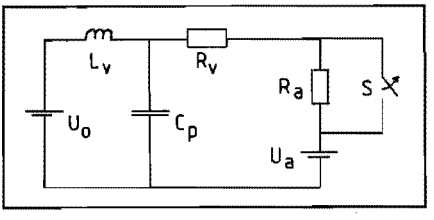

Fig. 4.12: Simplified model of circuit and instable arc comprising essential features for current- and voltage response. Symbols see text.

The response of this circuit on a step wise change of R_a to 10Ω and back to 0 Ω after 300 ns is entered in fig. 4.11 as dashed curves, showing agreement with the complicated circuit response on the essential points.

As long as $R_v + R_a \ll (L_v/C_p)^{1/2}$, which holds in this case, the relative current reduction attained at a time Δt after opening of the switch S is given by:

$$\frac{\Delta I}{I} = \frac{R_a}{R_v + R_a}\left[1 - \exp\left[-\frac{R_v + R_a}{L_v}\Delta t\right]\right] \quad \text{, with } I = \frac{U_o - U_a}{R_v} \qquad (4.5)$$

The maximum voltage, associated with current decay is then:

$$\hat{u}_{ac} = \hat{u}_a = U_a + IR_a \qquad (4.6)$$

After closing of S, current and voltage is given by:

$$i_a(t) = I - \Delta I \exp\,[-(R_v/L_v)t] \qquad (4.7)$$

$$u_a(t) = U_a \qquad (4.8)$$

Concluding, it can be summarized that a sudden insertion of a short lasting resistance in the arc path leads to a current decay with a time constant $L_v/(R_a + R_v)$ and a slower recovery with time constant L_v/R_v. Arc voltage reaches high values only during the decay of current.

f. Experimental check of the transient arc resistance model

The important features of the transient arc resistance model are expressed by the circuit parameters U_o, L_v, R_v and the internal (or arc model) parameters U_a, R_a, Δt.
As mentioned in sect.e, eq.(4.5) through (4.8) describe well the overall appearance of an instability. Now, the influence of circuit parameters and contact distance is discussed.

Inspection of (4.5) and (4.6) makes clear, that adding extra inductance to L_v should not influence the maximum voltage $\hat{u}_a$, accompanying an instability but should reduce the relative depth (with constant internal parameters).
The first model implication has been subjected to an experimental verification:
In a way, analogue to the method outlined in sect. d, average repetition times $\bar{\theta}_1(\hat{u}_a, I)$ of transient arc voltages, higher than a predetermined value $\hat{u}_a$ ($\hat{u}_a$ = 100, 200, 300, 400, 500 V) were measured for 3 currents (I = 11.2, 22.7, 30.4 A). The results are presented in fig. 4.13 (drawn lines). Next, an inductance of 60 µH was added to L_v, and measurements were repeated for currents I = 9.0, 19.2, 25 A.
It can be noted, that the repetition times of the overvoltages in the 66 µH circuit fit well between those in the 6 µH circuit. Hence, an effect of extra inductance on frequency of instabilities and on amplitude distribution seems unlikely. A similar finding is reported by Masnari (70), who observed that addition of up to 2.5 mH inductance

caused no measurable change in (voltage) noise power.

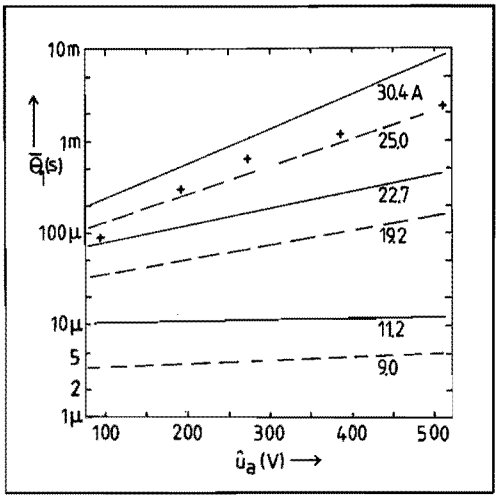

Fig. 4.13: Measured average repetition time ($\bar{\theta}_1$) of transient arc voltages greater than $\hat{u}_a$, at a number of arc currents. Drawn lines: circuit inductance 6 µH; dashed lines: inductance 66 µH. +: points calculated from model prediction at I = 22.7 A.

When combining eqs. (4.5) and (4.6), R_a can be eliminated and a direct relation can be established between $\Delta I/I$ and $\hat{u}_a$ for a given circuit:

$$\frac{\Delta I}{I} = \frac{\hat{u}_a - U_a}{IR_v + \hat{u}_a - U_a}\left[1 - \exp\left[\frac{IR_v + \hat{u}_a - U_a}{IL_v}\Delta t\right]\right] = f(\hat{u}_a) \qquad (4.9)$$

Eq. (4.9) makes it possible to confront the repetition time measurements of instabilities deeper than d% (fig. 4.6) with the repetition times of maximum voltages higher than $\hat{u}_a$ (fig. 4.13) at a given current.
For I = 22.7 A repetition times $\bar{\theta}$ (d,I) for d = 10, 20, 30, 40, 50% were read from fig. 4.6. Values for $\hat{u}_a$, corresponding to $\Delta I/I$ = 0.1, 0.2, 0.3, 0.4, 0.5 were solved from eq. (4.9), with U_a = 20 V; Δt = 200 ns. Thus obtained points $\bar{\theta}_1[f^{-1}(\Delta I/I), 22.7] = \bar{\theta}(\hat{u}_a, 22.7)$ are entered in fig. 4.13, denoted by "+". A certain discrepancy between these points and the direct overvoltage measurements is clear. This may be caused by the way voltage is measured.
As stated in sect. e the simple model is only employed in the case $R_v + R_a \ll Z_o$. Adding extra parallel capacitance to C_p, has the following effect on a typical voltage response during the decay phase: The rate of rising of the voltage $u_a(t)$ is inverse proportional to the parallel capacitance. When a fast rising overvoltage must be seen as an agent to overcome the instability phase - a point pursued in chapter 7 - it is clear that parallel capacitance impairs this restoring mechanism. This effect has a negative influence on arc stability and is reflected

in a reduction of arc lifetime, when adding parallel capacitance to the arc as observed and discussed in sect. 2e.
The opposite is true for adding series inductance: from eq. (4.5) it can be understood that reduction of instability depth is a consequence of the model. It is therefore thought, that the observed increase of arc lifetime with larger inductance (sect. 2e) is based on this effect.

Of the arc model parameters U_a, R_a and Δt, the maximum overvoltage (in a given circuit is determined by R_a, whereas current reduction is a function of R_a and Δt [eq. (4.5)].
It is demonstrated now, that the instability duration Δt in its turn, is a function of the momentary contact distance (δ). This was proved by studying some hundreds of instabilities at four different distances. All of the instabilities were recorded in drawn arcs (current of 38 A) at least 15 ms after contact separation, in order to assure constant and reproducible values of δ (cf. fig. 2.3). The arc was shunted by a resistor of 1.1 Ω in order to damp HF oscillations. Typical oscillograms of voltage and current at various values of δ are given in fig. 4.14.

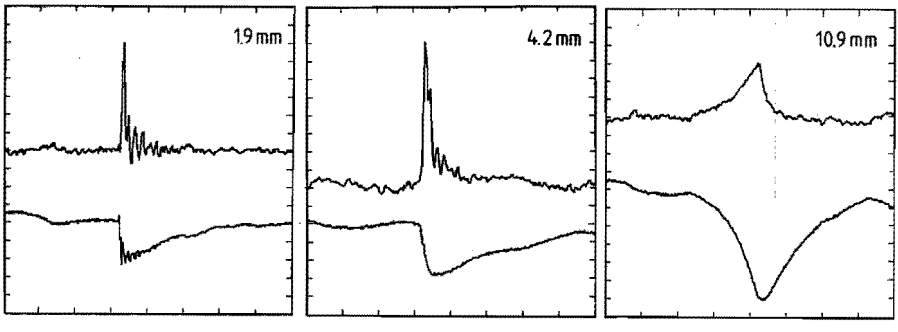

Fig. 4.14: Oscillograms of voltage (upper; 8 V/div) and current (lower; 2 A/div) of instabilities at 3 contact distances. Time: 500 ns/div.

It can be seen that the duration of the overvoltage is longer at larger contact distance. This finding is quantified in fig. 4.15. Herein, about 10 instabilities causing an overvoltage of ($\hat{u}_a \pm 5$) V are averaged to each of the indicated points, which have an abscissa of $R_a = (\hat{u}_a - U_a)/I$ and ordinates of ΔI and $\Delta I/\Delta t$. This was done for four different values of δ. It can be noted (1) that a similar value of R_a results in larger current reductions at larger distances and (2) that a dependence of $\Delta I/\Delta t$ on R_a, and hardly on δ exists.

From this, it is inferred that Δt is a function of δ alone, also expressed directly by measurement of Δt in fig. 4.16.

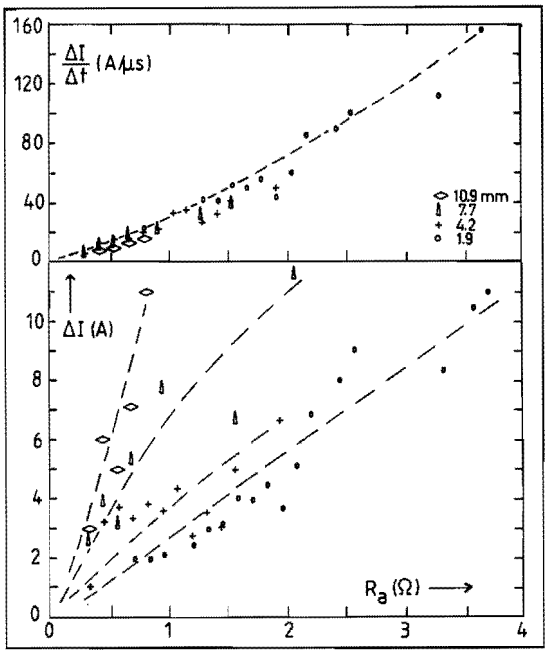

Fig. 4.15: *Dependence of current reduction (ΔI) and decay rate ($\Delta I/\Delta t$) on arc resistance (R_a) for four contact distances.*

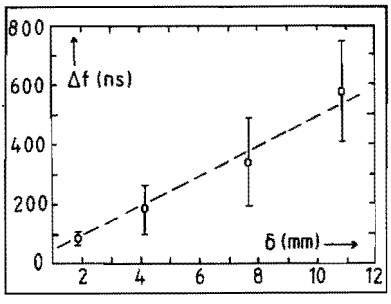

Fig. 4.16: Dependence of the instability duration (Δt) on contact distance (δ)

The relationship can be approximated by a straight line, having a slope of 2.10^4 m/s. In chapter 7 the observed dependence will be explained.

g. Concluding remarks

The observed phenomena can be described by representing the interacting system of arc and circuit by a cyclic dynamical process. At the start of the cycle, a sudden increase of arc resistance causes a circuit determined decay of current. At the same time, voltage rises with a rate, determined by the parallel capacitance. Owing to this overvoltage, arc resistance is eliminated after a certain time, and current is restored at a circuit determined rate. Voltage is then returned to its steady state value. After a certain time, the cycle sets in again, and arc existence is endangered once more.

This repetition time can be approximated from the measuring results of repetition time of instabilities deeper than a certain depth (fig. 4.6) and of overvoltages higher than a certain value (fig. 4.13).

An average repetition time of instabilities, irrespective of their depth can be obtained from eq. (4.4) by summation over all the possible values of d. By substitution of d = 10j - 5 in eq. (4.4), an integrated average instability repetition time ($T_i[I]$) as a function of current can be defined:

$$T_i(I) = \left[\sum_{j=1}^{10} [\theta(j, I)]^{-1} \right]^{-1} \qquad (4.10)$$

Alternatively, from the measurements presented in fig. 4.13, an empirical expression can be derived for the average repetition time of transient arc voltages higher than $\hat{u}_a$ for a given current: (θ_1 in μs)

$$\theta_1'(\hat{u}_a', I') = \exp\left[(3.9\ 10^{-4} I' - 3.7\ 10^{-3})\hat{u}_a' + 0.15\ I' + 0.30\right] \qquad (4.11)$$

From this expression, an average repetition time ($T_u[I]$) of voltages irrespective of their height (but higher than a normal fluctuation of approx. 3 V) can be derived:

$$T_u(I) = \theta_1(23, I) \qquad (4.12)$$

Both $T_i(I)$ and $T_u(I)$ should serve as an approximation of "how often" an instability can be expected for a given arc current. In fig. 4.17 $T_u(I)$ and $T_i(I)$ are plotted. The discrepancy between the two is not too bad, in view of the necessary extrapolations beyond the measuring range of voltage and current.

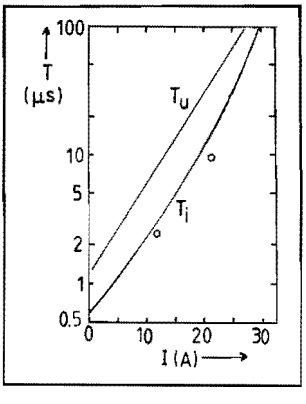

Fig. 4.17: Integrated average instability repetition times $T_i(I)$ and $T_u(I)$. For explanation see text. Circles: inverse voltage noise spectrum peaks as obtained by Nazarov (84).

The time-current relations (4.10) and (4.11) reflect the shift to higher

frequencies of the arc voltage noise spectrum when lowering arc current. Nazarov (84) studied this shift quantitatively under conditions comparable to ours (Cu contacts, 5 μH circuit inductance). At 20 A arc current, an average repetition time of 7.5 μs was found for voltage peaks $\hat{u}_a > 50$ V. At 12 A this time drops to 2.5 μs. These data are represented in fig. 4.17 by circles, and agreement with the semi - empirical model is reasonable.

A possible relation of arc stability with arc voltage noise was suggested for the first time by Cobine (61). Farrall (71) was the first to observe a synchronicity of transient arc overvoltage and arc current decay. He assumed (partial) extinction and reignition by a rapidly rising voltage and subsequent breakdown. In the present work however, moments of current zero before definite arc extinction were never observed. Besides, breakdown voltage higher than 1 kV were measured as short as 50 ns after current zero (Smeets 86), making breakdown of the gap after several hundreds of ns irreconcillable with the relatively low overvoltages measured. Like Farrall (71) did, a partial extinction-breakdown sequence was supposed by Fröhlich (80), who recorded currents of AC arcs just before current zero with a high time resolution. He estimated breakdown voltages of 500 - 1000 V from the observed decay time of current during an instability (10 ns) and the calculated voltage rate of rise. Unfortunately, his measurements do not yield voltage data.
Froncek (84) studied the response of a parallel LRC branch on transient current reductions during "intervals of unbalance arc stability", that last for approx. 1 μs. Owing to the parallel branch, various oscillations can arise depending on the value of R, L and C.

The experimental evidence, collected in this chapter leads to the following conclusions: periods of arc instability can be distinguished; the duration of these periods seem to depend on the distance between the contacts. An arc induced instability appears at random moments during the arc lifetime, but the more often the lower the DC current is. The instable arcing condition can be described by a transient arc resistance. A simultaneously rising arc voltage may overcome arc instability. Thereafter, circuit induced continuation of reduced current

makes the arc susceptible for a repeated instability, although the arc proper is in a stable condition. Only after a circuit determined time, the initial condition is regained. Extinction is then a result of an accumulation of instabilities. The behaviour of DC arc lifetime (and thus of chopping currents) as a function of the circuit can be explained qualitatively by its effects on the signal shape of one individual instability.

The question that inevitably arises next is what physical phenomena cause the arc resistance to increase, so provoking an instability. In the next chapters, it will be tried to clarify some aspects of this crucial point.

References:

- Cobine J.D. and Farrall G.A., Proc. Int. Res. Symp. on Electric Contact Phen., Univ. of Maine (1961) 263-83
- Daalder J.E., Ph.D. Thesis, Eindhoven University of Technology (1978)
- Farrall G.A., J. Appl. Phys., vol. 42 (1971) 3084-8
- Fröhlich K., IEEE Trans. on Plasma Sci., PS-8, (1980) 319-25
- Froncek F.R., IEEE Trans. on Elec. Ins., EI-20 (1985) 751-4
- Lafferty J.M., "Vacuum arcs, theory and application", Wiley & Sons, New York (1980)
- Masnari N., GEC Report no. 70-C-183 General Electric Company (1970) (unpublished)
- Nazarov S.N., Rakhovskii V.I. and Zhurbenko V.G., XIth Int. Symp. on Disch. and Elec. Ins. in Vac., Berlin DDR (1984) 179-82
- Smeets R.P.P., J. Phys. D: Appl. Phys., vol. 19 (1986) 2401-13

5. HF FLUCTUATIONS OF CATHODE SPOT EMISSION PRODUCTS

a. Introduction

In the preceeding chapter, the term "arc instability" was introduced to nominate a specific circuit response on a certain irregularity of the discharge [1]) condition, hitherto called "stable". The term "stable arc" or "stable discharge", however, merely expresses the absence of large scale and externally observable irregularities; it does not imply any constancy of the fundamental cathodic processes, characterizing the vacuum discharge. At a time scale, much shorter than the average repetition time of instabilities, cyclic formation and subsequent extinction of electrically active areas on the cathode (cathode spots) cause extremely rapid changes of a number of relevant parameters. This means, that instabilities occur only "once in a while" during the pseudo-continuous process of emission site displacement.

Cathode spot physics is a controversial field of research. Information, gathered from literature is often contradictory and conclusions are far from unanimous. This is in the first place due to the complexity of the physical principles that govern the cathode processes. Secondly, the cathode spot is very inaccessible to direct measurement, due to its inherent small dimensions and a rapid motion over the surface.
Above all, time resolved analyses of externally measurable discharge parameters are scarce. For the study of instabilities, occuring at random in an otherwise stable discharge - as looked upon from the outside - it is necessary to gain at least a qualitative insight in the time dependent discharge behaviour. Stated otherwise, it is hard to understand instable behaviour without relevant knowledge of the undisturbed discharge.

In this chapter, a study will be discussed of the rapidly fluctuating components of the following emission products: ion current, electron-

---

[1]) Now, entering into the physical phenomena, the word "arc" will more appropriately be replaced by "discharge", and "contact" by "electrode".

(arc) current and (visible) light. Time resolved measurements will be presented of ion currents, that can be drawn from the discharge plasma by a current collecting probe (sect. b), and the relation of these currents to the rapidly fluctuating component of the voltage over the discharge (sect. c). Further information is collected from time resolved (and time integrated) measurement of the light intensity, coming from the cathode spot. In sect. d, these measurements are presented. From these results, certain conclusions can be drawn after an analysis concerning the origin of light intensity fluctuations (sect. e). A general summary of the nature of HF fluctuations of ion current, voltage, light intensity and arc current in a vacuum discharge, for stable and instable situations, is given in sect. f.

b. Natural fluctuations of ion current

The central point that distinguishes a vacuum discharge from all other discharge types is the need to supply its own conducting material from the cathode. It is therefore without doubt, that the ability to vapourize a sufficient amount of mass is an essential prerequisite to maintain a discharge.

It is widely accepted that a high electrical field in front of the cathode, in combination with a high temperature enables thermal-field electron emission to take place (Lee 59). The electrons so emitted are accelerated in the cathode voltage drop, and ionize metal neutrals, that are abundantly evaporating, due to the very high metal temperature (Lee 61). Further, it is generally assumed that this region - the cathode spot - is the only source of charged particles in a vacuum discharge (Kimblin 73).

At this point, the mechanism of ion production will not be treated in detail and a quantitative treatment is postponed to chapter 7.

The electron emission is located in a current constriction zone, not larger than several μm, where an extremely high current density must maintain all relevant processes. It will be clear that very high plasma densities are encountered here, giving rise to expansion of the plasma into the entire interelectrode gap. In a steady state, the voltage drop over the plasma body outside the cathode spot is small, implying a quasi

zero net charge density here.

It was shown by Kimblin (71) for the first time that a conducting cilinder around the discharge (commonly called "shield") can be considered as a third electrode immersed in the discharge plasma. When this shield is held at cathode potential, an ion current of 8-10% of the arc current can be drawn by the shield. In fact it is more accurate to speak about time integrated current: in a given time, a fixed portion of the net charge transported between the electrodes is transferred to a shield at cathode potential.

A different situation is encountered when the fluctuating components of arc- and shield currents are considered. These arise due to natural variations in the discharge.

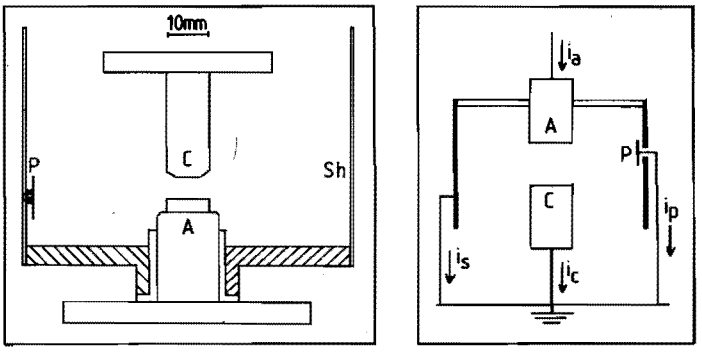

Fig. 5.1: Geometry of the electrodes. P: probe; Sh: shield; C: cathode; A: anode. Shaded: insulating material.

Fig. 5.2: Definition of positive currents. i_a: anode current; i_c: cathode current; i_s: shield current; i_p: probe current. A: anode; C: cathode.

In order to study time dependent currents, the electrode configuration of fig. 5.1 is employed. As always, cathode material is OFHC copper. The discharge volume is surrounded by a cylindrical stainless steel shield (Sh), 37 mm in diameter. Electrically insulated from it, a circular current probe (P) (10 mm in diameter) is attached to the shield. Seen from the cathode center a solid angle $\Omega_p = 0.05$ sr is subtended by the probe; the linear distance from cathode centre to probe is $r_p = 36$ mm. The cathode diameter is reduced to 10 mm, so that due to spot motion over the surface, an inaccuracy in r_p can arise of 5 mm.

The advantage of using a small probe instead of the whole shield as an

ion current collector is a better defined distance r_p and thus a better time resolution. A drawback is a lower current yield, owing to a smaller surface (effective shield surface 10700 mm^2; probe surface 78 mm^2).
The notion of "arc current" is no longer meaningful here, as radial currents come into play. Therefore, currents are redefined (positive in the arrow-direction) by fig. 5.2 introducing i_a (anode current), i_c (cathode current), i_s (shield current) and i_p (probe current). Note that a positive i_s, i_p means a flow of ions in the plasma directed from the cathode region. Currents i_c, i_a, i_s could be monitored with Pearson 411 HF current transformers (risetime 10 ns, sensitivity 50 mV/A) positioned as close as possible to the outside of the vacuum housing. Current i_p was measured with a highly sensitive high-frequency (risetime 5 ns) active current monitor type Philips PM 9355. Absolute current values were obtained with appropriate measuring shunts (risetime < 70 ns), taking care not to create a voltage drop over the shunt larger than 1 V. The feeding circuit is the one, specified in fig. 2.2. The discharges were initiated by electrode separation, anode current is approx. 40 A, guaranteeing a lifetime longer than 10 ms.

After 10 ms, with electrodes at their final distance, fast recordings (sampling frequency 100 MHz) were made of the currents involved, resulting in the oscillograms of fig. 5.3.
Simultaneous recording of the ion currents i_s, i_p (fig. 5.3a) shows severe fluctuations around an average level, defined by:

$$\bar{I}_{s;p;a} = T^{-1} \int_o^T i_{s;p;a}(t)dt \qquad (5.1)$$

Numerical integration over a time $T = 200\ \mu s$ yielded $\bar{I}_s = 3.1$ A and $\bar{I}_p = 17.3$ mA. From that, the ratio of the average currents: $\bar{I}_s/\bar{I}_a \approx 0.08$ in good agreement with Kimblin (71). For the average probe current, an empirical expression was derived by Jüttner (86), accounting for an anisotropy in ion flux:

$$\bar{I}_p = 4.10^{-2} A_p \bar{I}_a r_p^{-2} \cos \vartheta \qquad (5.2)$$

Herein, A_p is the probe's area, and ϑ the angle between the discharge axis and the position vector. Within the reported uncertainty of the numerical constant in eq. (5.2), a good agreement exists.

Fig. 5.3b is a ten times horizontal expansion of the section "EXP", illustrating a peak-wise behaviour of ion deposition on both shield and probe. Having averaged over 25 peaks, a mean peak value of shield current $\hat{i}_s = (6.7 \pm 0.5)$ A was measured, whereas in probe current $\hat{i}_p = (77 \pm 16)$ mA was observed. In order to detect possible prevailing frequency components in the two signals, fast Fourier-transforms were computed, and plotted in fig. 5.3c. It can be seen, that such an analysis yields a 1/f character for i_s, but concerning i_p, the frequency spectrum shows more a "white noise" character.

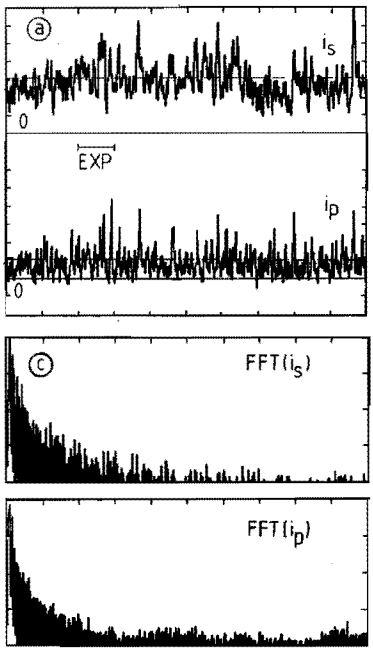

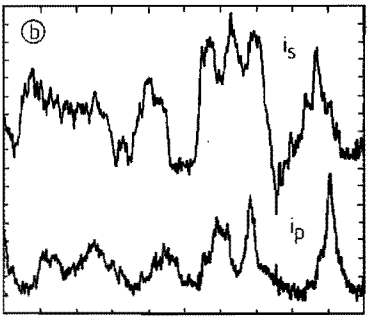

Fig. 5.3a: Shield current i_s (1 A/div) and probe current i_p (20 mA/div); Time: 20 µs/div.

Fig. 5.3b: Expansion (EXP) of fig. 5.3a. i_s: 0.4 A/div; i_p: 12 mA/div; 2 µs/div.

Fig. 5.3c: Fast Fourier Transform of i_s and i_p. Hor: 5 MHz/div; vert: 5 dBm/div. Frequency from 0 - 50 MHz.

A striking oscillogram can be obtained, when the fluctuating components Δi_s, Δi_c, Δi_a of the corresponding currents are monitored simultaneously (fig. 5.4). Presented on the same scale, it is immediately clear that the fluctuations in shield current are only present in the circuit formed by cathode and shield. It was found that the small variations in i_a are circuit induced, caused by variations in arc voltage. The fluctuations in i_s (and thus in i_c) however, are of a fundamental nature as they were found to be circuit independent and seem to be a manifestation of a strongly time dependent abundance of ions in the gap.

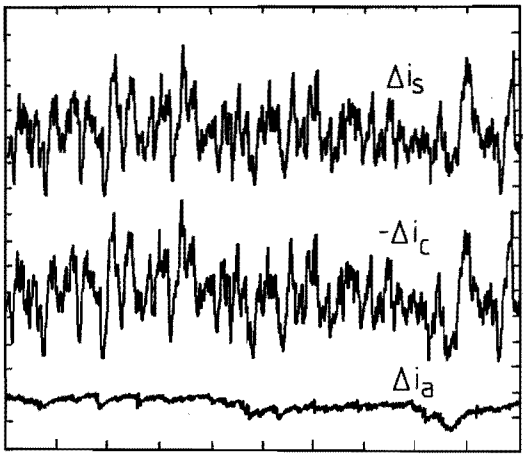

Fig. 5.4: HF components of shield current ΔI_s (1 A/div), inverted cathode current $-\Delta I_c$ (1 A/div), and anode current ΔI_a (1 A/div); time: 20µs/div.

The saturated ion current, drawn by a probe having a potential well below the plasma potential is usually given by:

$$i_p = A_p \, z_i \, n_i(r_p) \, v_i \, e \qquad (5.3)$$

with: A_p: probe area,
z_i: average ion charge in units of the elementary charge,
$n_i(r_p)$: ion density in front of the probe,
v_i: mean ion velocity-component perpendicular to the probe,
e: elementary charge.

Fluctuations in i_p can thus arise as a result of a changing ion density or velocity (direction as well as magnitude). An experiment was carried out in which the current i_a - and thus the number of ions, produced in the cathode spot - was increased step wise (risetime 400 ns) by a factor of two. This was accomplished by the discharge of a capacitor of 10 µF charged to 700 V. The probe current response hereupon was recorded simultaneously with the current, yielding oscillograms like fig. 5.5.

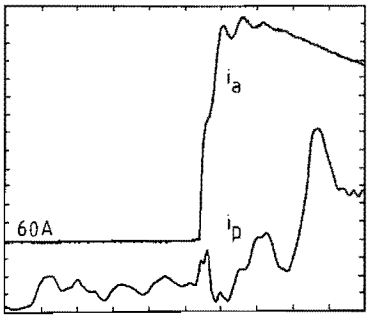

Fig. 5.5: Probe current response i_p (8 mA/div) upon stepwise anode current increase i_a (10 A/div); time: 1 µs/div.

This and many more oscillograms showed, that after a certain delay time δt, a new average probe current level is established approximately twice as high as before the arc current step. From this, it may be inferred that the increased ion current is the result of an increase in ion production at its source - the cathode spot - and subsequent motion of a high density front (consisting of ions and electrons) to the probe. This front will arrive at the probe after a delay time being the ratio of probe-to-source distance and mean directed ion velocity.
Quasi-neutrality of the front prevents a current to flow in the cathode-probe circuit before it reaches the probe.

The relation of the source particle production rate $\Gamma(t)$ (in s^{-1}) and the density (n_i) at a certain distance (r) and time (t) can be expressed (Molmud 60, Lins 86) as follows:

$$n_i(r,t) = \int_0^t g(r,t-\tau)\,\Gamma(\tau)\,d\tau \qquad (5.4)$$

$$g(r,t) = \left[\frac{m_i}{2\pi k T_i}\right]^{3/2} \frac{1}{t^3} \exp\left[\frac{m_i}{2kT_i}\frac{r^2}{t^2}\right] \qquad (5.5)$$

With m_i the ionic mass; k the Boltzmann constant.
In the derivation of eq. (5.4) it is assumed that the particles have a Maxwellian velocity distribution with a mean velocity v_i and a temperature T_i coupled by:

$$\frac{1}{2} m_i v_i^2 = \frac{3}{2} k T_i \qquad (5.6)$$

The expression (5.4) is derived for a collisionless expansion of a number of atoms in vacuum, but may be valid too in this case, provided that the particle mean free path is sufficiently large.

A sudden release by the source at t = 0 of a number of ions (ΔN_i) is described by the Dirac-function $\delta(t)$:

$$\Gamma(t) = \Delta N_i\,\delta(t), \qquad (5.7)$$

in which case [with eq. (5.3)] the probe current that arises as a result

of the sudden release is easily expressible in the source term ΔN_i:

$$i_p(t) = A_p\ z_i\ e\ v_i\ \Delta N_i\ g(r_p,t). \qquad (5.8)$$

A first order estimation of v_i can be gained from fig. 5.5:
$\delta t = r_p/v_i \approx 3.3\ \mu s$, giving an average ion velocity of $v_i \approx 1.1\ 10^4$ m/s, corresponding to values found by other researchers employing different methods (Plyutto 65, Davis 69, Rondeel 74). From Davis (69) an average ion charge number $z_i = 1.8$ is taken. With these parameters, $i_p(t)$ as a result of a "charge pulse" $z_i e \Delta N_i$ at $t = 0$ is calculated and plotted in fig. 5.6.

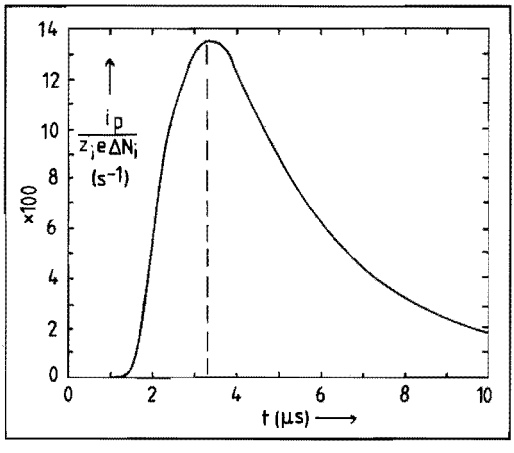

Fig. 5.6: Calculated probe current response upon sudden charge release ($z_i e \Delta N_i$) at the cathode.

This figure expresses the fact that a sudden release of charge is "smeared out" in time due to the velocity distribution of its individual constituents. In order to describe a realistic situation in a vacuum discharge, where the flow of ions is non-isotropic (Daalder 76), in eq. (5.8) a term proportional to $\cos \vartheta$ should be added.
From the reasoning above, it is qualitatively clear, that charge releases, (possibly) induced by crater formation processes at a repetition time in the order of the crater formation time (less than 1 μs) can never be detected by probe current measurements well away from the source. By analogeous reasoning it is conceivable, that the peaks in probe (and shield-) current are manifestations of unusually large "charge bursts", every 2 μs or so (cf. fig. 5.3b).
An order of magnitude estimation gives from fig. 5.3 a source charge burst $z_i e \Delta N_i \approx 60\ \mu C$ resulting in the (measured) maximum probe current

$\hat{i}_p$ = 77 mA, whereas a "normal" cathode spot operation yields only about 5 μC of ionic charge per μs, using a mass loss (in ionic form) of 4.10^{-8} kg per coulomb transferred between the electrodes (Daalder 75).

The observations made above only hold for a discharge condition where instabilities are absent. Due to their high di/dt, an inductive shift of plasma potential relative to a (grounded) probe or shield causes an electron flux to arise. A detailed treatment is postponed to chapter 6.

c. The correlation between voltage and ion current

It is not surprising, that HF fluctuations are also present in the voltage over the discharge. A typical example of the extremely "noisy" behaviour of arc voltage is the oscillogram of fig. 5.7. This voltage is

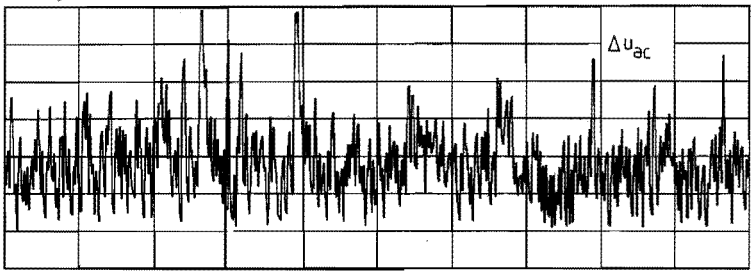

Fig. 5.7: Spontaneous fluctuations of interelectrode voltage Δu_{ac} *(2 V/div); time 10 µs/div. Arc current: I = 50 A.*

the interelectrode voltage u_{ac}, measured, as described in sect. 4b. As is obvious from fig. 5.7, very high frequencies are present; Fourier analysis indicates a broadband spectrum of up to 50 MHz, without peaks. The overall appearance of the voltage, recorded during a 100 μs observation window , shows no change when circuit inductance is brought to a 10 times higher value. As for the current dependence of the fluctuation amplitude, it is observed that in the range 40 to 280 A, the average amplitude is reduced roughly by a factor of two. Below 40 A, the overvoltages accompanying instabilities, as treated in chapter 4, are orders of magnitude higher than the natural voltage fluctuations.

Because the voltage u_{ac} is a quantity, integrated over the discharge plasma, it is difficult to relate the variations of u_{ac} to localized processes, such as particle emission in the cathode spot. In the preceeding section, it was assumed that probe current can be related to the localized process of charge production.

It is now interesting to search for an experimental correlation between this probe current and discharge voltage. Therefore, probe current $i_p(t)$ and voltage $u_{ac}(t)$ were recorded simultaneously (sampled at 50 MHz), and their correlation function $\psi_{iu}(t)$ was computed:

$$\psi_{iu}(t) = T^{-1} \int_0^T i_p(\tau - t)\, u_{ac}(\tau)\, d\tau, \qquad (5.9)$$

for T = 400 μs and $0 \leq t \leq 10$ μs, involving 25k data points per signal.

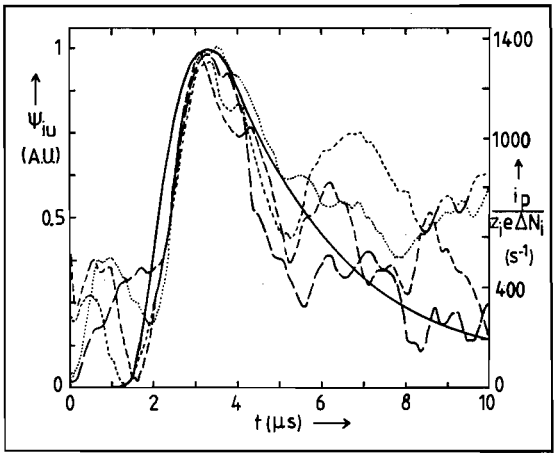

Fig. 5.8: Correlation functions ψ_{iu} (dashed) of probe current and arc voltage (arbitrary units). Also plotted is the calculated probe current caused by charge release $z_i e \Delta N_i$ (drawn).

The procedure was repeated four times, yielding correlation functions as plotted in fig. 5.8 (dashed lines). The function ψ_{iu} reaches a clear maximum at t = 3.2 μs, indicating an unambiguous correlation between a maximum in interelectrode voltage and a maximum in probe current 3.2 μs later. This implies a mean ion velocity of $v_i = 1.1\ 10^4$ m/s.

A similar experiment (de Cock 76) with much less data points resulted in a comparable outcome.

Again, as in the previous section, it is thought that a quasi-neutral enhanced ion density front reaches the probe, a time-of-flight of 3.2 μs after a pulse-wise charge production in the cathode spot.

Also plotted in fig. 5.8 (drawn line) is the function $i_p(t)$ - already shown in fig. 5.6 - calculated with eq. (5.8). A remarkable similarity

in shape is found between $\psi_{iu}(t)$ from measurement, and $i_p(t)/z_i eAN_i$ calculated as a response on a pulsed source term active at $t = 0$.
The convolution integral (5.9) can only be equal to one of the two factors of its integrand if the other factor is proportional to a Dirac-function. Algebraically:

$$\int_0^T i_p(\tau - t)\, u_{ac}(\tau)\, d\tau \approx \eta\, i_p(t), \qquad \text{(from fig. 5.8)} \tag{5.10}$$

which implies (η is a proportionality constant):

$$u_{ac}(t) = \eta\, \delta(t). \tag{5.11}$$

The function $\delta(t)$ here has the physical meaning of a rate of charge-production [cf. eq. (5.7)], so that it is reasonable to state at this point that the observed pulse-like behaviour of arc voltage coincides with a pulse-like ion production in the cathode spot.
Following this reasoning, it is plausible that the fluctuations in voltage over a stable discharge have their origin in the cathode spot zone, rather than in the plasma away from the source.

d. Measurements of light intensity

The cathode spot takes its name from its appearance to the eye as a point source of high luminosity. The size of this luminescent area is hard to define, and photographic techniques to determine it must be handled with extreme care (Rakhovskii 76). At present, experimental estimates of a characteristic size (for copper spots) range over nearly 2 decades, from a few to a few hundred micrometres.
From visual observation, as well as from literature (e.g. Djakov 74, Rakhovskii 76) it is well known that for a low-current arc, the cathode spot is the only relevant source of light. The body of the plasma surrounding the cathode spot is assumed to be optically thin, so that light, intercepted outside, may reflect certain cathodic processes synchronously. Only at higher current values, or at high axial magnetical fields, the luminosity of a discharge channel between cathode and anode becomes considerable (Rondeel 75).

Measurements of the light intensity were carried out in an experimental set-up, the heart of which is formed by a triggered vacuum gap (TVG) - its principle of operation is described in sect. 2b - that permits observation of the cathode spot in a direction, normal to the cathode. The anode, opposing the cathode at a distance of 3 mm, consisted in these experiments of a small-mesh wire netting, leaving 80% of its area open to a head-on view of the cathode. Approx. 10 cm farther on, a sapphire observation port (transparent from 200-5000 nm) was situated. Due to copper vapour deposition, a gradual decrease of transparency of the observation window made cleaning necessary a number of times in the course of the work.

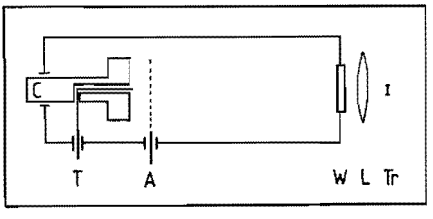

Fig. 5.9: Triggered vacuum gap set-up, suitable for light intensity measurements, C: cathode; T: trigger pin; A: anode; L: lens; Tr: light transducer, W: window.

Fig. 5.9 is a sketch of the TVG set-up. A circuit, similar to the one outlined in fig 2.4 could establish and maintain a discharge, the duration of which is regulable with the DC circuit current.

In order to obtain insight in the spectral composition of the light, emitted by the cathode spot, time-integrated spectroscopy was applied. A quartz spectrograph, (Hilger and Watts) with an opening angle of 3.6° and a dispersion ranging from 0.4 nm/mm at 200 nm to 15 nm/mm at 700 nm was used. (The width of the entrance slit was adjusted to 0.05 mm). In the focal plane, a high speed (5000 ISO) recording film (type Kodak 2485), (non uniformly) sensitive for a spectral range from 300 to 670 nm, was placed. This film was exposed during 100 ms by the light of several consecutive discharges of 30 A. After development of the film (during 15 min. at 25 °C in Neofin Rot), the spectrogram came out, printed in fig. 5.10.

This spectrum clearly consists of a large number of lines belonging to transitions in the Cu I (neutral copper), Cu II (singly ionized) and Cu III (doubly ionized) system. Especially the Cu I lines, having a transition probability of more than 20% of the (325, 327 nm) resonant

lines are evident. This does not necessarily mean that the density of neutrals is larger than the charged particle density, because Cu II and Cu III lines have a much lower transition probability than Cu I lines.

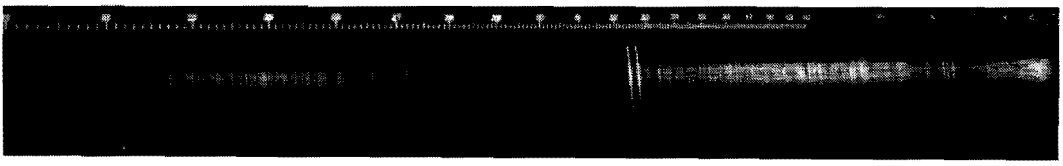

Fig. 5.10: Spectrogram (from 220 - 700 nm) of the light emitted by a Cu cathode spot (scale is in tens of nm).

The intensity of the continuum was too small to be detected by the photographic method. Therefore, it will be assumed, that light intensity is mainly due to line radiation.

Time resolved measurement of the light intensity, integrated over a certain wavelength interval, can give additional information.
A HF light intensity transducer was constructed featuring a silicon PIN photodiode (type Siemens BPW 34) and integrated amplifiers. The spectral sensitivity of the diode is sketched in fig. 5.11. Linearity of output

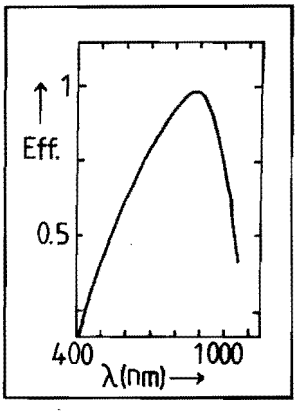

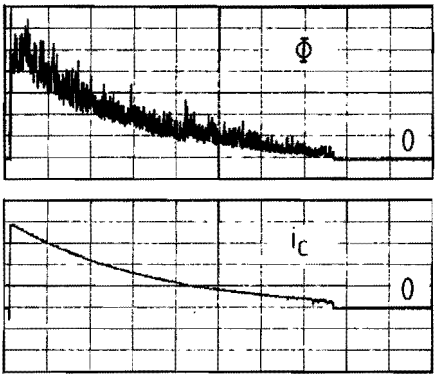

Fig. 5.11: Spectral efficiency of the PIN diode vs. wavelenght (λ).
Fig. 5.12: Response of light intensity Φ and cathode current i_c (50 A/div) upon a capacitor discharge. Time: 100 μs/div.

signal vs. light intensity is excellent over a wide range. Special attention was paid to the shielding of the transducer against

electromagnetic interference originating from the instable discharge. With the optically sensitive surface screened off against all optical radiation, a pick-up noise level less than 5% of the signal output could so be realized. The frequency characteristic of the transducer appeared to be flat up to 2 MHz, its -3dB point was at 5 MHz. The sensitive surface (area 4 mm^2) was placed in the focus of a lens (f = 20 mm).

The output signal of the transducer, proportional to the intercepted light intensity (Φ), is recorded simultaneously with current starting at 200 A resulting from a capacitor (100 μF) discharge through the arc path. A typical oscillogram, presented in fig. 5.12 shows an approximate proportionality between current and a certain minimum level of light intensity. Besides, severe fluctuations, ranging from 50% (at high currents) to > 100% (near current zero) of this minimum level are found. The behaviour at higher currents (I > 100 A) qualitatively seems not to differ much from the near current zero course. Therefore, attention is focussed to the latter region, with the hope that additional information concerning the nature of instabilities can be gained.

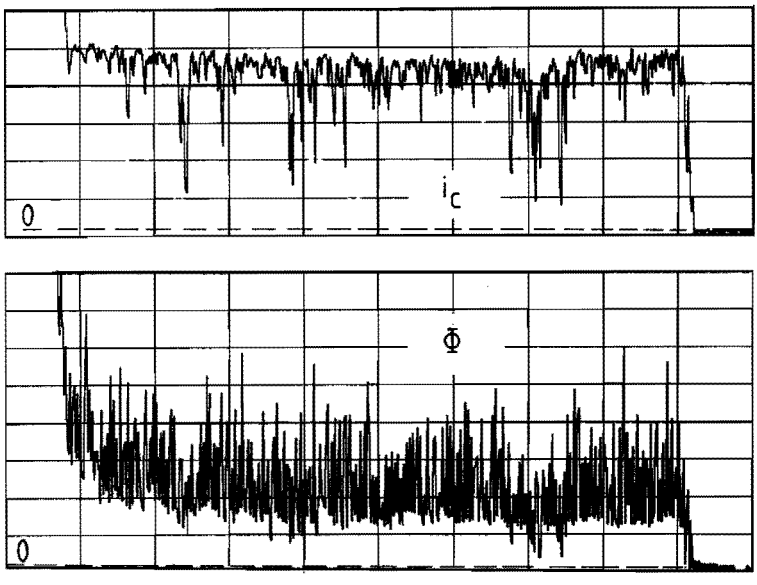

Fig. 5.13: Cathode current i_c (4 A/div) and light intensity after the initial pulse. Arc lifetime: 81 µs. Time: 10 µs/div.

A more detailed oscillogram representing a low-current (18 A) discharge

is shown in fig. 5.13. A number of remarkable features can be observed and summarized as follows:

i. Spontaneous extinction is not associated with an enhanced emission of light. This contradicts an increase in "local brightness" (evaluated from spot-photography) preceeding such an extinction, as found by Jüttner (79). An oscillogram of a typical extinction is fig. 5.14. There is no sign of light emission after current zero.

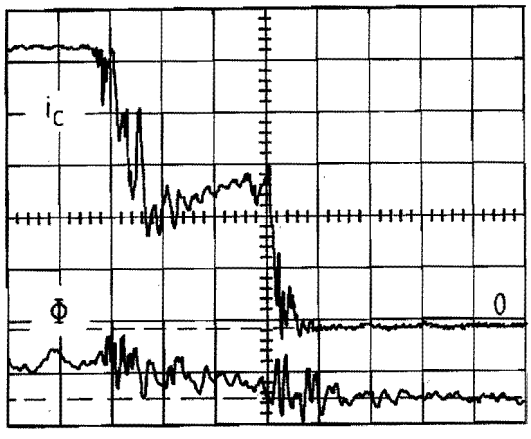

Fig. 5.14: Current zero of cathode current i_c (4 A/div) and light intensity Φ. Time: 0.5 µs/div.

ii. The minimum light intensity level follows arc current instantaneously. A (direct) proportionality of light intensity to current can be assumed up to high frequencies. This is verified by deliberately applying a momentary change in current. Fig. 5.15 comprises the response of the light signal upon forced current decrease and increase.

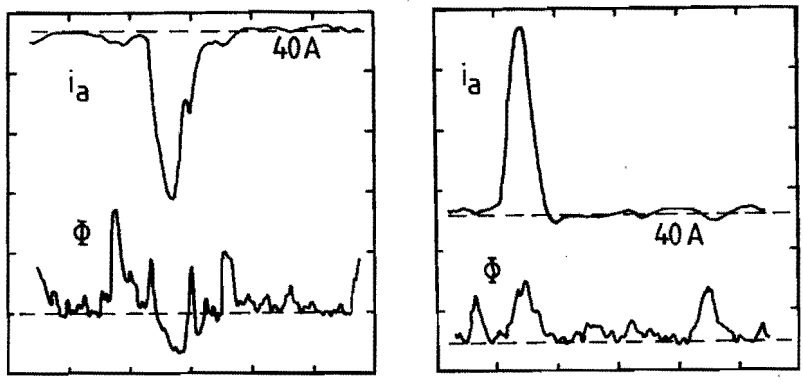

Fig. 5.15: Decremental (left) and incremental (right) pulse in current i_a (4 A/div) and light response Φ; Time: 1 µs/div.

iii. Fluctuations having amplitudes exceeding the average level seem to be natural constituents of the phenomenon. As fig. 5.15 indicates, a spontaneous rise of light intensity can be as high as one, caused by a 70% increase in current. The Fourier spectrum of a signal like that of fig. 5.13 did not reveal any preferred frequency.

Further analysis has demonstrated a strong correlation between the fluctuations in light intensity ($\Delta\Phi$) and those in the voltage over the discharge (Δu_{ac}) (cf. sect. c). The synchronicity of the two is immediately clear from the oscillogram in fig. 5.16. This synchronicity

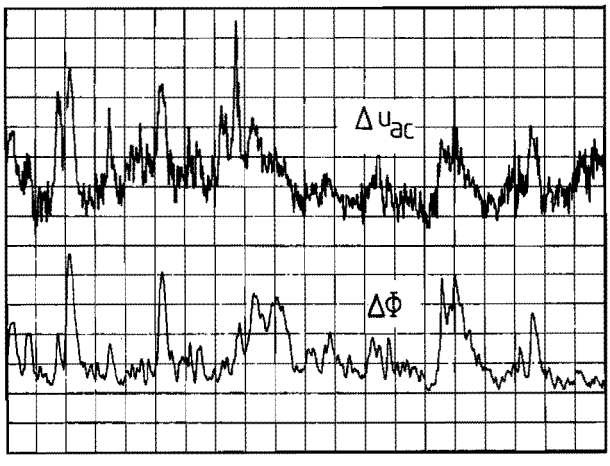

Fig. 5.16: Interelectrode voltage fluctuations Δu_{ac} (1 V/div) and light signal fluctuations $\Delta\Phi$; time 1 µs/div; I = 40 A.

is quantitatively corroborated by computing the correlation function:

$$\psi_{\Phi u}(t) = T^{-1} \int_0^T \Delta\Phi\ (\tau - t)\ \Delta u_{ac}(\tau)\ d\tau$$

This function is shown in fig. 5.17 (T = 400 µs, 25k data points per signal). Looking at the relative amplitudes however, it must be stressed that $\Delta\Phi/\Phi$ is about an order of magnitude larger than $\Delta u_{ac}/u_{ac}$.

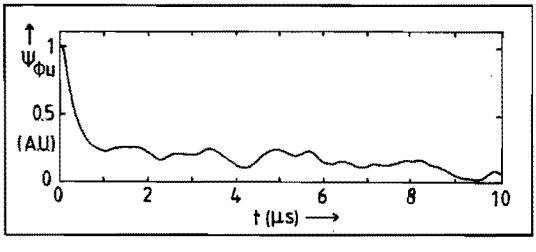

Fig. 5.17: Correlation function $\psi_{\Phi u}(t)$ of light intensity and voltage (arbitrary units).

e. Analysis of light intensity measurements

Due to the integration of the light intensity over a range of wavelengths, the described measurements do not allow a quantitative spectroscopical interpretation. Within a few (not unreasonable) assumptions however, a certain amount of information can be deduced.
The most important assumptions are:

i. The intensity of light is mainly due to line emission (cf. fig. 5.10) with wavelengths < 700 nm. The latter was checked by placing a Wratten filter (type 89B, transmission only above approx. 700 nm) in the optical path, leaving only 15% of the signal from the diode in spite of its high infra-red sensitivity (cf. fig. 5.11).

ii. The electron density (n_e) in the cathode spot is sufficiently high to assure local thermal equilibrium (LTE). This is further supported by a criterium for optically thin plasmas (Griem 63) satisfied in this case, and by experiments by Kock (68).

iii. The electron temperature (T_e) within the spot is proportional to the cathode voltage drop (u_c). A model will be presented in chapter 7, in which the emitted electrons are accelerated in the cathode voltage drop, giving satisfactory results. Hence:

$$k\,T_e \approx e\,u_c \tag{5.12}$$

From sect. c, it is taken that fluctuations (Δu_{ac}) in the interelectrode voltage are located in the cathode spot so that:

$$\Delta u_{ac} \approx \Delta u_c \approx \frac{k}{e}\,\Delta T_e \tag{5.13}$$

The intensity ($\Phi_{pq,z}$) of a spectral line emitted at an optical transition from level p to level q within the atomic system with charge z is proportional to the upper state density ($n_{p,z}$):

$$\Phi_{pq,z} = \frac{1}{4\pi}\,n_{p,z}\,A_{pq}\,h\nu_{pq} \tag{5.14}$$

Herein, A_{pq} (transition probability) and $h\nu_{pq}$ (photon energy) are constant for a given line.
In the case of LTE, the excited state density ($n_{p,z}$) of level p in the atomic system with charge z is coupled to the density of the ground

level in this system ($n_{o,z}$) through the Boltzmann distribution function:

$$n_{p,z} = n_{o,z} \frac{g_{p,z}}{g_{o,z}} \exp\left(-E_{po,z}/kT_e\right), \tag{5.15}$$

and to the ground level density ($n_{o,z-1}$) of the atomic system with charge z-1 through the modified Saha-equation:

$$n_{p,z} = n_{o,z-1} \frac{g_{p,z}}{g_{o,z-1}} \frac{2}{n_e} \left[\frac{2\pi m_e kT_e}{h^2}\right]^{3/2} \exp\left[\frac{-\epsilon_z - E_{po,z}}{kT_e}\right] \tag{5.16}$$

Herein, $g_{i,z}$ equals the statistical weight of level i in system z; m_e is the electron mass; h is Planck's constant; ϵ_z is the ionization energy and $E_{po,z}$ the energy of level p to the ground level in the system z.
When dealing with Cu I and Cu II transitions exclusively, the intensity of a given line ($p \rightarrow q$) can be expressed as follows:

$$\begin{aligned} &\text{Cu I:} \quad \Phi_{pq,o} = \xi_{pq,o}\, n_{o,o} \exp\left[-E_{po,o}/kT_e\right] \\ &\text{Cu II:} \quad \Phi_{pq,1} = \zeta_{pq,1} \frac{n_{o,o}}{n_e} T_e^{3/2} \exp\left[-(\epsilon_1 + E_{po,1})/kT_e\right], \end{aligned} \tag{5.17}$$

with $\xi_{pq,o} = \dfrac{A_{pq} h\nu_{pq} g_{p,o}}{4\pi g_{o,o}}$, and $\zeta_{pq,1} = \dfrac{2A_{pq} h\nu_{pq} g_{p,1}}{4\pi g_{o,o}} \left[\dfrac{2\pi m_e k}{h^2}\right]^{3/2}$ constants

for a given transition. From eq. (5.17) it is clear that the intensity of a given line is a function of $n_{o,o}$, T_e and n_e. Only taking into account Cu I and Cu II radiation (z = 1, 2), n_e can be expressed as:

$$n_e = \sum_p n_{p,1}(n_{o,o}, T_e, n_e) \tag{5.18}$$

With eqs. (5.16) and (5.18) n_e can be given explicitely in $n_{o,o}$ and T_e, so that light fluctuations $\Delta\Phi_{pq,z}$ can be expressed in variations of T_e and $n_{o,o}$:

$$\Delta\Phi_{pq,z} = \left[\frac{\partial\Phi_{pq,z}}{\partial n_{o,o}} + \frac{\partial\Phi_{pq,z}}{\partial n_e}\frac{\partial n_e}{\partial n_{o,o}}\right] \Delta n_{o,o} + \left[\frac{\partial\Phi_{pq,z}}{\partial T_e} + \frac{\partial\Phi_{pq,z}}{\partial n_e}\frac{\partial n_e}{\partial T_e}\right] \Delta T_e \tag{5.19}$$

This yields an expression for the relative light intensity fluctuations:

$$\frac{\Delta\Phi_{pq,z}}{\Phi_{pq,z}} = \left[1 - \frac{1}{2}\delta_{1z}\right]\frac{\Delta n_{o,o}}{n_{o,o}} + \left[\frac{3}{4}\delta_{1z} + \frac{E_{po,z} + \delta_{1z}(\epsilon_1 - 0.5\langle E_1\rangle)}{kT_e}\right]\frac{\Delta T_e}{T_e}, \tag{5.20}$$

$$\langle E_1\rangle = \sum_p g_{p,1}(\epsilon_1+E_{po,1})\exp[-(\epsilon_1+E_{po,1})/kT_e]/\sum_p g_{p,1}\exp[-(\epsilon_1+E_{po,1})/kT_e],$$

the expectation value of the energy and δ_{1z} the Kronecker delta. A summation over all the transitions that contribute to a total light intensity (Φ) (partly) measurable with the photodiode is necessary:

$$\Phi = \sum_{z=o}^{1}\sum_{p,q}\Phi_{pq,z} \tag{5.21}$$

An increase in measured intensity can be caused by an increase in T_e or in $n_{o,o}$. In order to determine, which of the two causes the observed large (> 100%) fluctuations in light intensity (cf. fig. 5.13), eq. (5.20) can be of use. Assuming that the electron energy is gained in the cathode drop, eq. (5.12) can be substituted in eq. (5.20). Evaluation of the energy dependent term between brackets shows a maximum value not higher than approx. 2. From the experiment it is clear, that the voltage fluctuations $\Delta u_{ac}/u_{ac} \approx 0.1$ (cf. fig. 5.7) so that the high value of $\Delta\Phi/\Phi$ is most probably due to large fluctuations in $n_{o,o}$.
In other words, an increased light intensity is not the result of a shift of spectral distribution towards smaller wavelengths (higher T_e) but it is caused by a higher particle density at the cathode spot.
Another indication for this is the correlation of peaks in light intensity with peaks in cathode spot ion production, as suggested (indirectly) when combining fig. 5.8 with fig. 5.17.

The analysis given above, is pertinent to a stable discharge. In fig. 5.18 a typical light signal response on an instability shows a decrease, directly proportional to current, as expected. From the observations, reported in sect. 4c, such an instability is always accompanied by a very high arc voltage transient (cf. fig. 4.5). From this, it follows that coincidence of light intensity and voltage does not apply in the case of such an instability transient. Were this transient (for its

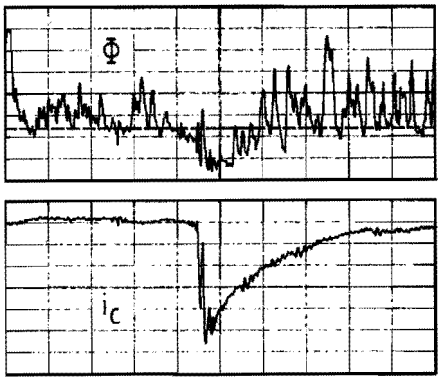

Fig. 5.18: Response of light signal Φ upon spontaneous instability in cathode current i_c (2 A/div); time 2 μs/div. Arc current: I = 18 A.

whole duration) located in the cathode spot region, a strong outburst of light would have been a logical consequence. The absence of such an outburst justifies the important conclusion that the voltage transient, accompanying an instability in the discharge, arises from processes located outside the cathode spot region.

f. Concluding remarks

Study of the HF fluctuations in current, voltage and light intensity can give information on the time dependent particle emission in the cathode spot zone. The above mentioned quantities can be expressed as:

anode current	$i_a(t) = \bar{I}_a + \Delta i_a(t)$	
cathode current	$i_c(t) = \bar{I}_c + \Delta i_c(t)$	
shield current	$i_s(t) = \bar{I}_s + \Delta i_s(t)$	(5.22)
voltage	$u_{ac}(t) = U_a + \Delta u_{ac}(t)$	
light intensity	$\Phi(t) = \Phi_o + \Delta\Phi(t)$	

A number of (approximate) relations between different quantities can be expressed, provided that instabilities in the discharge are absent:

$$\Delta i_a(t)/\overline{i_a(t)} \approx 0; \quad \Delta i_s(t) \approx -\Delta i_c(t); \quad \bar{I}_s \approx 0.1\ \bar{I}_a; \quad \bar{I}_a = \bar{I}_s + \bar{I}_c \qquad (5.23)$$

$$\overline{\Delta i_s(t)}/\bar{I}_s \approx 1; \qquad \overline{\Delta u_{ac}(t)}/U_a \approx 0.1; \qquad \overline{\Delta\Phi(t)}/\Phi_o \approx 1 \qquad (5.24)$$

$$\text{Proportionalities:} \qquad \Phi_o \sim \bar{I}_a; \qquad \Delta\Phi(t) \sim \Delta u_{ac}(t) \qquad (5.25)$$

From the analysis of the measuring results formulated in eqs. (5.21) - (5.23) it was deduced that voltage fluctuations occur simultaneously with an excess of mass production at the cathode spot causing a synchronous increase in light intensity and an increase in shield (or probe) current a time-of-flight later. The repetition time of this event is larger than the largest estimation of the crater formation time, so that these "explosive" events seem to be an exception in the pseudo-continuous formation-extinction process.

It was made plausible, that all the observed fluctuations are caused by processes in the cathode spot. There is only one important exception: at an instability in the discharge an overvoltage is generated in a region of the plasma that does not contribute to externally measurable light intensity. It is therefore assumed, that a large voltage peak arises in the plasma outside the cathode spot.
In the literature, high resolution measurements of the quantities in eq. (5.22) are hard to find. A study under comparable conditions as in this thesis, was reported by Hoyaux (69). A voltage "hash" is investigated together with the light, emitted from the cathode spot. Fluctuations of light intensity recurring at a frequency of about 500 kHz were observed at a small electrode spacing. However, no correlation between voltage and light could be detected, probably due to a difficult synchronization of light intensity recording (streak photography) and voltage. The fluctuations in light are attributed to a time variant cathode evaporation mechanism thus in agreement with the (better experimentally supported) findings in sect. c and e.
Another study is carried out by Jüttner (79), resulting in open shutter photographs of a Cu cathode spot, driven by a magnetic field. The photometrically determined "spot brightness" shows large variations in time, but these could not be compared to other quantities.

In this chapter, measurements of some HF-features of important discharge quantities are presented. It is clear, that large variations in one of the most important quantities, involved in the discharge process, namely the mass produced by it, are inherent to a "normal" cathode spot operation.

References:

- Cock, de W.M. and Daalder J.E., VIIth Int. Symp. on Disch. and Elec. Ins. in Vac., Novosibirsk (1976) 288-92
- Daalder J.E., J. Phys. D: Appl. Phys., vol. 8 (1975) 1647-59
- Daalder J.E., J. Phys. D: Appl. Phys., vol. 9 (1976) 2379-95
- Davis W.D. and Miller H.C., J. Appl. Phys., vol. 40 (1969) 2212-21
- Djakov B.E. and Holmes R., J. Phys. D: Appl. Phys., vol. 7 (1974) 569-80
- Griem H.R., Phys. Rev., vol. 131 (1963) 1170-6
- Hoyaux M.F. and Kimblin C.W., Holm Conf. on Elec. Cont. Phen. (1969) 217-23
- Jüttner B., preprint 79-9, Zentralinst. für Elektronenphys. (1979) 1-9
- Jüttner B., XIIth Int. Symp. on Disch. and Elec. Ins. in Vac., Shoreh (1986) 90-8
- Kimblin C.W., Proc. IEEE, vol. 59 (1971) 546-55
- Kimblin C.W., J. Appl. Phys., vol. 44 (1973) 3074-81
- Kock M. and Richter J., Z. Astrophysik, vol. 69 (1968) 180-7
- Lee T.H., J. Appl. Phys., vol. 30 (1959) 166-71
- Lee T.H. and Greenwood A., J. Appl. Phys., vol. 32 (1961) 916-23
- Lins G., XIIth Int. Symp. on Disch. and Elec. Ins. in Vac., Shoresh (1986) 219-23
- Molmud P., Phys. Fluids, vol. 3 (1960) 362-6
- Plyutto A.A., Ryzhkov V.N. and Kapin A.T., Sov. Phys.-JETP, vol. 20 (1965) 328-37
- Rakhovskii V.I., IEEE Trans. on Plasma Sci., PS-4 (1976) 81-102
- Rondeel W.G.J., J. Phys. D: Appl. Phys., vol. 7 (1974) 629-34
- Rondeel W.G.J., J. Phys. D: Appl. Phys., vol. 8 (1975) 934-42

6. TRANSIENT ELECTRON SHIELD CURRENTS AND POST-ZERO PHENOMENA

a. Introduction

A cylindrical shield, kept on a potential well below the plasma potential, can draw a saturated ion current of about 10% of the arc current. Electron currents will be obtained when the shield potential is a sufficient amount higher than the plasma potential. Shield current measurements are mostly described - as in the previous chapter - in steady state situations with stable vacuum discharges.
In this chapter, shield current measurements are described under conditions of a rapidly changing arc current. The time scale of the current transients applied, is in the order of that of spontaneously occurring instabilities. Since these instabilities are the cause of spontaneous extinction and of current chopping, it is expected that important information can be deduced concerning the behaviour of the discharge, fractions of microseconds before and after current zero. It is this very short time interval, that is decisive for the success of current interruption by a vacuum interrupter.

In sect. 6c (after an introduction into the experimental set-up in sect. 6b), it will be demonstrated that under certain conditions cathode spot emission can continue after circuit current zero.
The transitional process of the interelectrode volume returning from highly conductive into completely insulating is commonly called "recovery". The rapidity of recovery is of primary importance in current interruption, and gives the vacuum interrupter its prevailing advantages over high-pressure breakers. In sect. 6d, measurements are presented that - for the first time - picture the first (essential) microsecond of recovery, and the consequences of an (unwanted) post-zero cathode spot emission. The relation of transient shield currents with spontaneous instabilities will be discussed in sect. 6e. Some conclusions of the work, important for the application of vacuum interrupters, are contained in sect. 6f.

b. Experimental set-up

The measuring circuit is shown in fig. 6.1a,b, basically the one already described in sect. 2b.

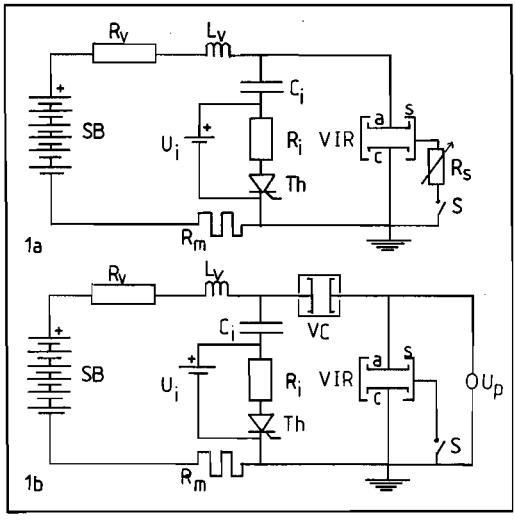

Fig. 6.1: Exp. circuits. 1a: Injection circuit. SB: battery (72 V); R_v: resistor (≃ 1 Ω); L_v: par. inductance (6 μH); C_i: cap. (20 nF); R_i: res. (5 Ω); Th: thyristor; VIR: vacuum interrupter ; R_m: shunt (3.53 mΩ); U_i: charging voltage (1 kV); R_s: shield resistor; S: switch. 1b: Circuit for recovery measurements. Added: VC: vacuum contactor; U_p: HV pulse unit.

In order to perform the measurements described further on, a current injection branch was added. This branch C_i-R_i (fig. 6.1a) could generate a 200 ns (halfwidth) current pulse, the amplitude of which was determined by the charging voltage U_i (max. 1 kV) on the capacitor C_i (20 nF) and by the resistor R_i (5 Ω). The maximum amplitude was 100 A. The inductance of the loop formed by the injection branch and the interrupter was such (0.5 μH) that this current pulse mainly passed through the interrupter and hardly through the feeding circuit. The injection pulse is actuated by a fast switching high surge-current thyristor.

Furthermore, in order to measure the dielectric strength of the vacuum gap after current zero, the principle of "synthetic testing" is adopted (fig. 6.1b). To that purpose, an insulating vacuum contactor (VC) was inserted in series with the test interrupter. The test gap could so be stressed with a high-voltage pulse from the (high-impedance) source U_p. The HV-pulse has a fixed half-width of about 50 ns and a variable polarity as well as amplitude. Maximum amplitude was 14 kV, maximum slope was 300 kV/μs. The interrupter is the one, described earlier in sect. 2b. The total arcing volume was surrounded by a stainless steel cylindrical shield, 63 mm in diameter, connected to an outside terminal.

c. Current zero experiments

In these experiments the circuit in fig. 6.1a was used. When dealing with high di/dt in arc current, a difference should be made between the interelectrode voltage (u_{ac}) and the voltage over the interrupter's terminals (u_a), cf. sect. 4b:

$$u_a = u_{ac} + u_{an} + u_{ca}, \quad \text{with} \quad u_{an} = L_a \, di_a/dt \quad \text{and} \quad u_{ca} = L_c \, di_c/dt.$$

The currents i_a (anode current), i_c (cathode current) and i_s (shield current) are defined positive in the arrow direction in fig. 6.2. Also indicated are the inductances L_a, L_c and L_s, the values of which are minimized to 100, 220 and 250 nH respectively.

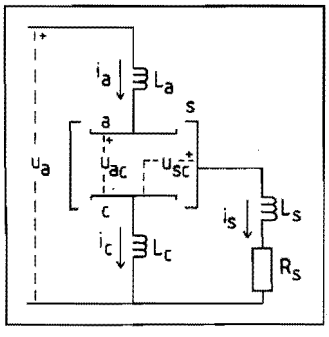

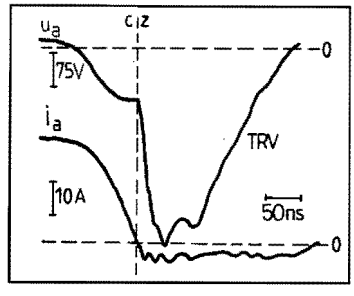

Fig. 6.2: Detailed circuit of the test breaker's vicinity. For symbols see text.

Fig. 6.3: Measured voltage u_a and anode current i_a during a 500 A/μs current ramp (floating shield). CZ: current zero.

To obtain extremely rapidly declining arc currents, current injection is used (fig. 6.1a). In this way, arc currents of up to 100 A are ramped to zero with a rate $di_a/dt \simeq 500$ A/μs. Using this as a typical value, it is clear that $|u_{an} + u_{ac}| \gg |u_{ac}|$.

Fig. 6.3 shows a typical oscillogram in the situation with the shield kept floating (open switch S in fig. 6.1a): $i_c = i_a$. The measured voltage (u_a) goes strongly negative, because the induced (negative) voltage in $L_a + L_c$ is much higher than the interelectrode voltage. Just after current zero, the remainder of the injection pulse commutates in

the main circuit, thereby inducing several hundreds of volts in L_v. This (negative) voltage appears across the recovering gap, so stopping the electrons and allowing a positive ion sheath to develop (Childs 80).
After some 100 ns, the recovery voltage (TRV) starts to rise with a rate of approx. 3 kV/µs, determined by the capacitance of the injection branch (≃ 10 nF). Meanwhile, a post-arc ion current of a few amperes is being collected at the former anode.
When repeating such current injection experiments after grounding of the shield (closed switch S in fig. 6.1a and $R_s = 0$), an interesting phenomenon can be observed. Simultaneous recording of anode- (i_a) and cathode current (i_c) yields a considerable difference. As the oscillogram of fig. 6.4 indicates, current zero in the cathode current is reached several hundreds of ns after current zero of the anode current. Necessarily, the difference between i_c and i_a must manifest itself as a shield current (i_s). This is verified by oscillograms of which fig. 6.5 is a typical example: before the onset of current injection a saturated ion current of approx. 1 A is drawn by the shield.

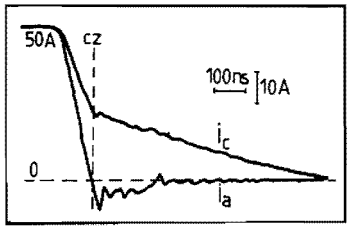

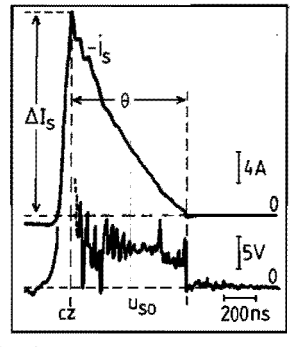

Fig. 6.4: Cathode current (i_c) and anode current (i_a) before and after current zero (CZ).

Fig. 6.5: Inverted shield current $-i_s$ (max. value ΔI_s and post-zero duration θ) and measured shield-to-ground voltage u_{so}.

During the decline of arc current the shield current reverses sign and rises rapidly to a top value ΔI_s, reached at anode current zero. During a time θ a considerable current persists in the circuit $L_c - L_s$.
Meanwhile, a strong oscillatory voltage of 5 - 10 V is measured between shield and ground, indicating a voltage between shield and cathode (u_{sc}) of 14 - 19 V.

The reported post-zero shield current must consist of electrons, emitted by a cathode spot still active after anode (circuit) current zero.
Hence we assume that during this post-zero current, the shield is temporarily acting as an anode.
The question of how partial arc commutation to the shield occurs, can be explained by treating the electrode configuration of fig. 6.2 as a double probe system (Johnson 50). In a stationary situation both cathode and (grounded) shield are on ground potential. In a preparative experiment, in which the inductance between the voltage measuring terminals is reduced from 320 nH to 55 nH, by using the "low inductance interrupter" (cf. sect. 4b), it was established that interelectrode voltage remains essentially constant during current decline. This is corroborated by a report of arc voltage collapse not before the very moment of current zero (Krynytzky 75). Because of the presence of L_c, the cathode potential drops the amount $L_c|di_c/dt|$ under ground potential; anode potential is also lowered that amount.

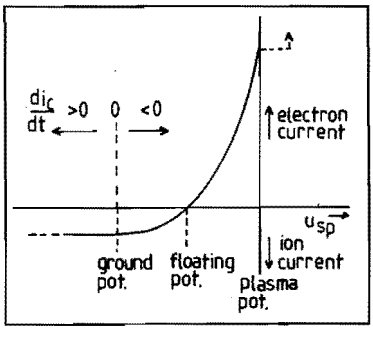

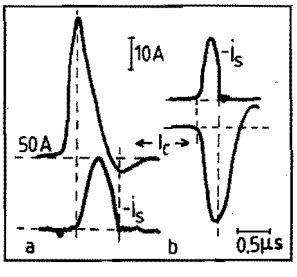

Fig. 6.6: Plasma probe characteristic applied to the present situation. Horizontal: u_{sp}: shield potential relative to plasma potential; vertical: shield current (from Cobine 80).
Fig. 6.7: a) Inverted shield current ($-i_s$) during the negative slope of an incremental cathode current pulse i_c. b) Idem, during a decremental pulse in the cathode current.

Since the plasma potential is (almost) equal to the anode potential, a situation now arises in which the potential difference between plasma and shield is changed from about 20 V to 20 + L_c di_c/dt.
In other words, the steady state situation of a shield "biased negative" with respect to the plasma potential changes into "less negative or even

positive biasing" during current decay. In fig. 6.6 this is explained qualitatively: depending on the shield potential relative to plasma potential u_{sp}, a net ion- or electron current can be drawn (Cobine 80). This reasoning can be verified by applying a fast current pulse to a stable arc current of about 50 A. The oscillogram in fig. 6.7 clearly demonstrates that an electron shield current only arises as a result of a negative di_c/dt in incremental (fig. 6.7a) as well as decremental (fig. 6.7b) pulses.

After having reached current zero, cathodic emission will be sustained a time θ by the magnetic energy stored in the circuit $L_c - L_s$. This energy - estimated at 0.14 mJ -, must match the energy supplied to the arc:

$$\frac{1}{2}(L_c + L_s)(\Delta I_s)^2 = u_{sc}\left[\int_0^{\theta} |i_s(t)|\, dt\right] \qquad (6.1)$$

The maximum electron current ΔI_s (occurring at current zero of anode current) and its post-zero duration θ (fig. 6.5) is strongly determined by the circuit parameters. An electrical model is used, including a resistor R_s in the shield-to-ground lead. Further, a constant voltage u_{sc} is assumed between cathode and shield during the post-zero time θ. Based on the circuit of fig. 6.2, current ΔI_s and time θ is given by:

$$\Delta I_s = \frac{1}{R_s}\left[u_{sc} + L_c\frac{di_a}{dt}\right]\left\{\exp\left[\frac{-R_s I}{L_c + L_s}\left|\frac{di_a}{dt}\right|^{-1}\right] - 1\right\} \qquad (6.2)$$

$$\theta = \frac{L_c + L_s}{R_s}\log\left[\frac{\Delta I_s R_s}{u_{sc}} + 1\right], \qquad (6.3)$$

with I the anode current prior to the current decay. These equations are derived in the appendix to this chapter.
As $di_a/dt < 0$ in the definition of fig. 6.2, a critical relationship between L_c and di_a/dt can be obtained from eq. (6.2):

$$\left|\frac{di_a}{dt}\right| > \frac{u_{sc}}{L_c} \simeq 75\ A/\mu s, \text{ when } u_{sc} = 16\ V. \qquad (6.4)$$

Relations (6.2) and (6.3) where experimentally checked by varying R_s.

In fig. 6.8 measured values of currents (ΔI_s) are indicated with closed circles, measured times (θ) with open circles. Expressions (6.2) and (6.3) are represented by drawn curves. It can be seen that there is a good agreement between theory and experiment.
The magnetic energy stored in $L_s + L_c$ at anode current zero must now be shared by arc and resistor:

$$\frac{1}{2}(L_c + L_s)(\Delta I_s)^2 = u_{sc}\left[\int_0^{\theta} |i_s|\,dt\right] + R_s\left[\int_0^{\theta} i_s^2\,dt\right] \qquad (6.5)$$

The ratio of arc energy input and resistor dissipated energy drops from 10 at $R_s = 0.1\ \Omega$ to 0.5 at $R_s = 3\ \Omega$.

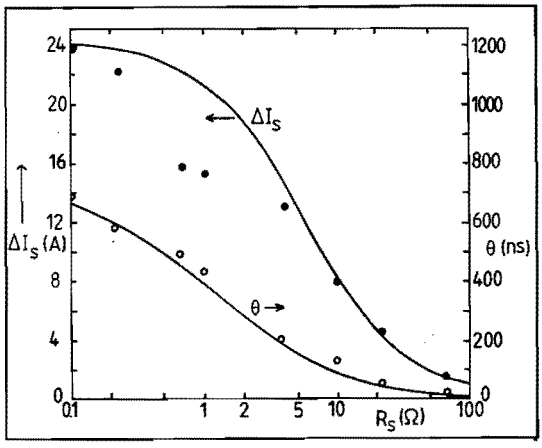

Fig. 6.8: Comparison of measured- (circles) and calculated (curves) values of maximum shield current ΔI_s (closed) and post-zero emission time θ (open) as a function of the shield resistor R_s. u_{sc} = 16 V; di_a/dt = -500 A/µs; I = 60 A.

d. Recovery experiments

In these experiments, a 55 A stable DC current was forced to zero as described in sect. 6b. An insulating vacuum contactor was used to disconnect the test interrupter from the feeding circuit following extinction of the two arcs in series (cf. fig. 6.1b). Next, a high-voltage pulse (300 kV/µs slope) could be applied at the test interrupter's anode at a predetermined time t following anode current zero. By studying the behaviour of the voltage U_b at which the recovering gap breaks down, insight can be gained in the diffusion of residual particles in the gap (Rich 64, Kimblin 71, Farrall 78). These particles reduce the dielectric strength of the gap, thus impairing the ability of a breaker to withstand a fast rising TRV after interruption.

The aim of this section is to study the influence of the reported post-zero cathode-to-shield emission on the recovery behaviour, as well as to assess the role of the residual particles in the first microsecond of recovery. Therefore, measurements were carried out with floating and grounded shield and positive and negative polarity pulses on the interrupter's anode.

In fig. 6.9, a typical oscillogram is given of a pulsing and breakdown sequence in the case that a negative pulse is applied (shield floating).

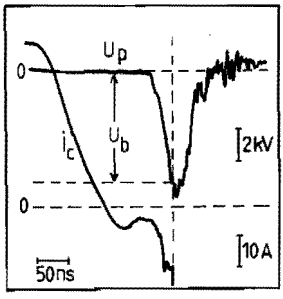

Fig. 6.9: Typical pulsing and breakdown sequence when applying a high voltage pulse U_p, to the gap after forced extinction of a 50 A arc (shield floating); U_b: breakdown voltage.

Fig. 6.10 shows the breakdown voltage U_b as a function of time t of pulse application after anode current zero. All the indicated points were averaged over 15 measured values.

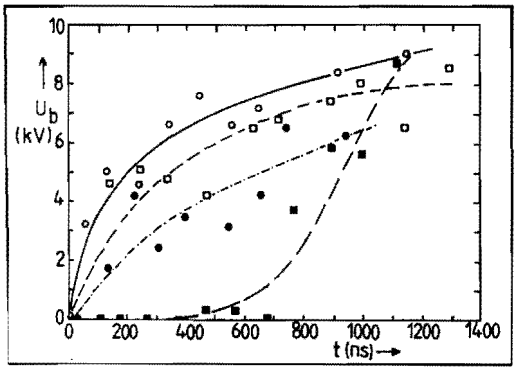

Fig. 6.10: Average breakdown voltage U_b as a function of post-zero application time t of a HV pulse. Circles: floating shield; squares: grounded shield; closed symbols: same polarity as arcing voltage; open symbols: reversed polarity relative to arcing voltage.

Although there is a large scatter in points in fig. 6.10, some trends are clearly visible. When using a floating shield (circular symbols) positive pulsing (with respect to arcing polarity) yields a slower recovery than negative pulsing. This is also observed by Załucki (68) and Kimblin (71), and can be understood by realizing that due to the presence of a (decaying) plasma the entire voltage pulse is essentially applied over a thin space charge sheath at the most negative electrode.

In this view, a positive voltage pulse stresses the ex-cathode with a high electrical field whereas a negative pulse stresses the ex-anode. The first situation may result in lower breakdown voltages for at least two reasons. First, an asymmetry is introduced by the higher density of ions in the vicinity of the ex-cathode, whereas in the ex-anode region the ion density is much lower. The cathodic ions may facilitate breakdown after acceleration in the field caused by the applied voltage. Secondly, remnants of cathode spots retain an elevated temperature a certain time after current zero. The time of solidification of the still hot residue of a crater, no longer emitting, is calculated by Prock (86) and was found to be some tens of nanoseconds at the most. Hence we conclude that this effect may only play a role during a negligible short time following current zero.

A different situation is created when the vapour shield is grounded (square symbols). When stressing the gap with a positive pulse, the onset of recovery is delayed by a time of about 700 ns. This is due to the post-zero emission during a time θ, reported in sect. 6c, as can be understood easily. Recovery after a negative pulse does not show such a delay. It will be clear that applying such a voltage immediately halts the emission of a cathode spot.

In estimating the contribution of neutral and charged particle decay to final (full vacuum) recovery, Farrall (78) suggests a neutral dominated recovery when comparing the ion decay time with the neutral decay time. Ions in a stationary arc have velocities in the order of $v_i = 10^4$ m/s (cf. sect. 5b) thus traversing the gap in about 0.5 - 1 μs.
The time scale of neutral decay is reported to be much longer. Recently, Lins (85) obtained from laser fluorescence measurements a copper vapour density decay that can be written as:
$n(t) = n_o \exp(-t/40)$ $\quad (-50 < t < 50\ \mu s,\ t = 0$ at current zero),
with $n_o \simeq 4.10^{16}$ m^{-3} and di/dt $\simeq$ 0.22 A/μs.
A model by Rich (64) predicts a similar time dependence in a time interval of 100 μs around current zero for a given current zero density. Kimblin (71) relates the reduction in the total number of particles in the gap volume to the particle speed and the gap dimensions, and also arrives at an exponential decay. Inserting our gap dimensions and a

particle temperature of 2000 K, yields a decay time constant of 9 μs, opposed to the much longer one found by Lins (40 μs). Nevertheless, it seems reasonable to assume a constant neutral density during the first microsecond following current zero.
Hence it may be concluded, that the sharp rise of breakdown voltage during this period, must be attributed to the disappearing space charge in the gap. The neutral decay is decisive in a later stadium and determines the time after which maximum dielectric strength is reached.

The exact breakdown mechanism during this initial (1 μs) recovery is hard to assess. Oscillogram 6.9 suggests that a high-energy ion flux causes a considerable energy input into the electrode, thus initiating breakdown. This type of "space charge dominated dielectric breakdown" might be related to the "thermal reignition" due to high post arc currents as observed by Yanabu (85). In his findings, this reignition is different from a later occurring "dielectric reignition".

It is difficult to compare the breakdown voltages vs. time, here obtained with experiments using a different geometry, as gaplength and electrode diameter are relevant parameters (Rich 64). The interesting aspect of this work therefore, lies more in the comparison of recovery behaviour under the four conditions of fig. 6.10 than in obtaining absolute breakdown voltages.

e. Experiments in an instable arc

In this section, electron shield currents following spontaneous arc instabilities are analyzed. In order to study transient shield currents simultaneously with arc instabilities, the circuit of fig. 6.11 is used.

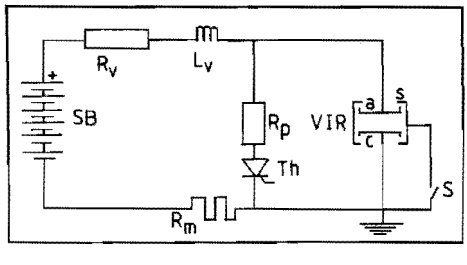

Fig. 6.11: Measuring circuit: SB, R_v, L_v, R_m, VIR: see fig. 6.1. Added: R_p: parallel resistor (1.7 Ω); Th: thyristor; a,c,s: anode, cathode, shield.

The injection branch was replaced by a 1.7 Ω resistor in series with a thyristor. Resistor R_v was regulated to a value, resulting in a sufficiently high arc current (50 A), so that the DC arc did not extinguish spontaneously before 10 ms following initiation.
After about 7 ms, when the cathode's center was subtended by a maximum shield solid angle of 2.0 sr, current was reduced to about 30 A by triggering the parallel-thyristor. From this moment on, oscilloscopes were armed for triggering by an arc voltage transient, exceeding an adjustable level. Because such a transient always accompanies a current instability, suitable oscillograms could be produced. A typical example of an oscillogram so obtained is fig. 6.12. A large number of such oscillograms show that a "natural" di/dt can be the cause of a short electron flux to the (grounded) shield.

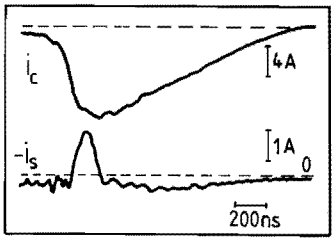

Fig. 6.12: Typical spontaneous instability in cathode current i_c and the inverted shield current $(-i_s)$. L_c = 250 nH.

It can easily be checked that the above mentioned electron flux can be explained using the same arguments as in sect. 6c, where current transients were applied deliberately. Spontaneous current reduction is now an amount $\Delta I \leq I$, so that in eq. (6.2) the current I must be replaced by ΔI. The values of di_c/dt, di_s/dt and ΔI (-80 A/μs, -20 A/μs, 10 A respectively) and the circuit parameters ($R_s = 0$, u_{sc} = 16 V) give after substitution in eqs. (6.2) and (6.3) a maximum electron current ΔI_s = 1.3 A and a time θ = 40 ns. The former value is in accordance with the measurements, whereas the latter one has lost its meaning of post-emission time, now anode current has not reached zero.
In a case like in fig. 6.12 the present (circuit) parameters bring about an electron shield current ΔI_s that is small with respect to the total fall of the anode current (ΔI). Inspection of eq. (6.2) shows that for $R_s = 0$ the maximum shield current (ΔI_s) approximates the anode current reduction ΔI when $L_c \gg L_s$ (cf. fig. 6.2):

$$\lim_{L_s/L_c \to 0} \Delta I_s = \Delta I \left[1 - \left[\frac{u_{sc} \left| \frac{di_a}{dt} \right|^{-1}}{L_s + L_c} \right] \right] \simeq \Delta I \quad \text{when} \quad L_c \gg L_s \qquad (6.6)$$

This means that under this condition the entire anode current fall can be commutated through the shield, thus avoiding a reduction of current through the cathode spot. To check this, an extra inductance of 3.5 μH was placed in series with the (parasitic) L_c. L_s was maintained at its minimum value of 0.25 μH. Further, a third 75 MHz recording channel was added to record i_a, i_c and i_s simultaneously. Fig. 6.13 shows such a typical oscillogram of an instable arc current: the extra inductance leads to a "smoother" i_c than i_a, due to the presence of the grounded shield.

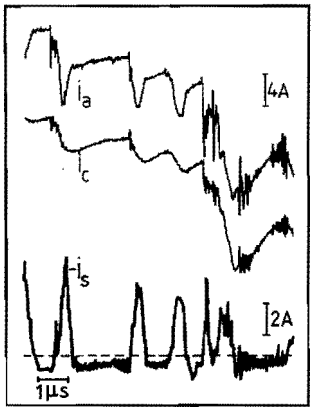

Fig. 6.13: Typical instable part of an arc prior to spontaneous extinction. Simultaneously recorded anode-, cathode-, and inverted shield current i_a, i_c and $-i_s$. L_c = 3.8 μH, L_s = 250 nH. Sampling frequency 100 MHz.

It was described in chapter 4 how the (arc determined) frequency of occurrence and the (circuit determined) depth of individual instabilities affect arc stability as a whole.

Arc stability can be quantified as the average lifetime. A possible influence of shield potential on arc lifetime was studied by reducing a 50 A stable arc current some 10 ms after initiation to about 30 A and measuring from this moment on the residual average lifetime ($\bar{\tau}_r$) at the reduced current level. The results are summarized in the following table (L_c = 3.7 μH, 20 measurements per value; fl. = floating; gr = grounded).

Arc current (A)	33.1		31.2		28.0	
Shield potential	fl.	gr.	fl.	gr.	fl.	gr.
residual lifetime (ms)	1.67	1.55	1.00	1.01	0.49	0.48
standard deviation (ms)	0.29	0.23	0.15	0.30	0.12	0.07

It can be seen that grounding of the shield does not seem to affect the arc stability in the studied current range. Hence it might be concluded that the distribution of depths of individual instabilities is not altered, since this distribution determines the average lifetime.

f. Concluding remarks

It is demonstrated that the presence of a grounded shield can postpone cathode spot current zero with respect to circuit current zero. This is due to an inductive shift of the plasma potential relative to the shield potential, causing the shield to act temporarily as an auxiliary anode. The magnetic energy stored in the cathode-shield circuit can maintain the emission a certain time after circuit current zero.
In this view, the extra cathode-shield circuit forms an energy reservoir the energy of which is released after circuit current zero. If the instable arc is characterized by a succession of extinctions and reignitions (Farrall 71), one would expect the presence of this post-zero energy to facilitate reignition thus extending the average arc lifetime. However, such an effect is not observed. This corroborates the earlier assumption that instabilities are current reductions, rather than arc extinctions.

The initial voltage that appears across the gap following a chopped current, has arcing polarity (cf. fig. 3.1). A grounded shield drastically reduces the breakdown voltage of arcing polarity with respect to a floating shield situation (closed squares vs. closed

circles in fig. 6.10), for a sufficiently rapid current chop [condition (6.4)]. For this reason it might be expected that grounding of the shield makes high overvoltages due to a chopped current less probable. However, the breaking capacity of a vacuum interrupter that has its shield connected to either electrode, might be reduced with respect to a floating shield interrupter. This is indeed observed in practical interrupters (Schellekens 86). One might think that the inevitable capacitive coupling of a "floating" shield to ground in a usual interrupter allows certain effects, hitherto only ascribed to a grounded shield, to play a role. An oscillation can arise in the circuit, formed by parasitic capacitance of the shield and inductance of the cathode support. The HF impedance however of that circuit (for a usual interrupter) is such that shield currents are estimated to be too small to interfere with the current interruption process.

At first sight, the high values of di/dt and du/dt applied in our experiments, seem somewhat unrealistic for a circuit interrupter in an existing power network. Again, however, it is important to realize that the extremely rapid vacuum arc processes provoke considerable circuit responses by the very small parasitics in the arc's vicinity. Arc extinction times in the order of 300 ns are met (sect. 4d), with an associated di/dt corresponding to the experimental values applied in this study. Typically, every 100 nH can then give induced voltages higher than the stationary arc voltage. Analogue reasoning illustrates that a chop of some amperes through a typical parallel capacitance of 10 pF causes initial voltage rates of rise of hundreds of kV/μs. Although these severe transients do not penetrate into a practical network, their existence can influence important quantities like breaking capacity and chopping level.

Appendix

Herein, eqs. (6.2) and (6.3) are derived. It is assumed that the anode current i_a is ramped down linearily from I to zero in a time t_o:

$\frac{di_a}{dt} = -\frac{I}{t_o}$ (cf. fig. 6.14).

The circuit equations for this case are (def. in fig. 6.2):

$$L_c \frac{di_c}{dt} - L_s \frac{di_s}{dt} - i_s R_s + u_{sc} = 0 \quad \text{and} \quad i_c = i_a - i_s \tag{A1}$$

Two time intervals can be distinguished: (see fig. 6.14)

1. $0 \leq t \leq t_o$. For this interval the set (A1) can be rewritten as:

$$(L_s + L_c) \frac{di_s}{dt} + R_s i_s = u_{sc} + L_c \frac{di_a}{dt}$$

The right hand side is treated as a constant. With $i_s(0) = 0$ the solution is:

$$i_s(t) = -\frac{1}{R_s}\left[u_{sc} + L_c \frac{di_a}{dt}\right]\left\{\exp\left[-\frac{R_s}{L_s + L_c} t\right] - 1\right\} \tag{A2}$$

Defining the maximum shield current as $\Delta I_s = -i_s(t_o)$, eq. (6.2) is easily obtained.

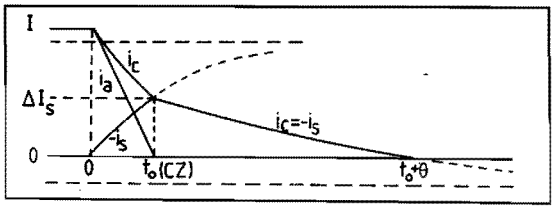

Fig. 6.14: Modelling of currents i_a, i_c, $-i_s$ for calculation purposes. For symbols see text.

2. $t_o \leq t \leq t_o + \theta$: ($t_o$ is defined as the exact current zero of i_a).

$i_a' \frac{di_a}{dt} = 0$ so that the set (A1) simplifies to:

$$(L_s + L_c) \frac{di_s}{dt} + R_s i_s = u_{sc} \quad \text{and} \quad i_s = -i_c$$

With the initial value $-i_s(t_o) = \Delta I_s$, the solution is:

$$i_s(t) = -\left[\Delta I_s + \frac{u_{sc}}{R_s}\right] \exp\left[-\frac{R_s}{L_c + L_s}(t - t_o)\right] + \frac{u_{sc}}{R_s} \tag{A3}$$

Defining the post-zero duration (θ) as $i_s(t_o + \theta) = 0$, θ can be explicitely expressed as is given in eq. (6.3).

References:

- Childs S.E. and Greenwood A.N., IEEE Trans. on Plasma Sci., PS-8 (1980) 289-94
- Cobine J.D., Chapt. 1 in "Vacuum arcs, theory and application" by Lafferty J.M., Wiley and sons, New York (1980)
- Farrall G.A., J. Appl. Phys., vol. 42 (1971) 3084-8
- Farrall G.A., IEEE Trans. on Plasma Sci., PS-6 (1978) 360-9
- Johnson E.O. and Malter L., Phys. Rev., vol. 80 (1950) 58-68
- Kimblin C.W., IEEE Trans. Pow. App. Syst., PAS-90 (1971) 1261-70
- Krynytzky B.S., Proc. IEEE, vol. 63 (1975) 331-2
- Lins G., IEEE Trans. on Plasma Sci., PS-13 (1985) 577-81
- Prock J., J. Phys. D: Appl. Phys., vol. 19 (1986) 1917-24
- Rich J.A. and Farrall G.A., Proc. IEEE, vol. 52 (1964) 1293-301
- Schellekens H., Lenstra K., Hilderink J., ter Hennepe J., and Kamans J., XIIth Int. Symp. on Disch. and Elec. Ins. in Vac., Shoresh (1986) 241-4
- Yanabu S., Homma M., Kaneko E. and Tamagawa T., IEEE Trans. Pow. App. Syst., PAS-104, (1985) 166-72
- Załucki Z., Seidel S. and Kutzner J., Proc. IIIrd Int. Symp. on Disch and Elec. Ins. in Vac., Paris (1968) 358-63

7. MODELLING OF INSTABILITIES IN LOW-CURRENT VACUUM DISCHARGES

a. Introduction

In a vacuum discharge, three prevailing regions can be distinguished. First, and most important is the cathode spot. In a low-current discharge, the cathode spot alone is responsible for a sufficient supply of "conducting medium" in order to sustain the discharge. From the work, reported in chapter 5, it is clear that this supply comes in large fluctuations on a microsecond time scale, although a very constant current through the discharge can be guaranteed. Apparently, above a certain current level, a minimum supply is established firmly.

The cathode spot region in its turn consists of three relevant zones:

- A liquid metal layer, that penetrates as a hemispherical shell into the cathode metal. This zone is called "emission crater".
- A transition sheath between the liquid metal and the discharge plasma.
- An ionization- or space charge zone, that may have a larger lateral expansion than the crater area.

In general, the cathode spot is distinguished from the rest of the discharge by its high electric field. The large number of interrelated phenomena, an impression of which can be gained from fig. 7.1, makes a theoretical approach of the cathode spot region exceptionally difficult.

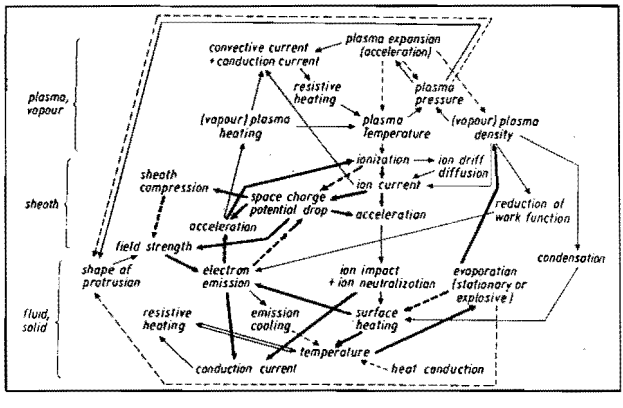

Fig. 7.1: Scheme of the cathode spot (feedback) processes. Solid lines: causal connections with intensification or increase; broken lines: with weakening or decrease (after Hantzsche 83). Thick lines: interactions taken into account in the calculations of sect. d..

Secondly, the interelectrode plasma provides a conducting "path" to realize the current transport from the cathode spot to the anode. In the literature on vacuum discharges, this region has attracted only little attention. Its importance in low-current studies is evident: in a high pressure discharge, it is this region that is responsible for instabilities at low currents.
Thirdly, the anode region. In low current discharges, the anode is just a passive collector of charge and a considerable space charge (adjacent to the anode) may only build up under "abnormal" conditions. At high currents, a large power input gives rise to phenomena, intensively studied, owing to their importance in short circuit interruption.

The aim of this chapter is to get a more quantitative impression of some relevant parameters in the three regions, paying special attention to the conditions, that must be fulfilled in order to maintain a vacuum discharge.
It was found necessary, in the framework of this experimentally inclined thesis, to include measuring results as additional conditions in a theoretical treatment. Such an ad hoc approach has the advantage (from the experimentalist's point of view) of a relatively direct access to the relevant processes, so avoiding esoteric physical theories. The danger of such a semi-empirical approach, however, is the inclination to simplify the physics to such an extent that consistency may be sacrificed to an easy manageability of a certain model.

In sect. b a global review will be given of present cathode spot theory. A survey of theoretical treatment of the current chopping phenomenon follows next in sect. c. In order to investigate, whether instability of the discharge originates from the emission mechanism proper or from its repetitive character, a calculation of various cathode spot parameters as a function of arc current is undertaken in sect. d. In sect. e, the time-dependent mass flow into the discharge plasma will be analyzed. Based on the results from sect. d and e, a possible explanation of vacuum arc instability will be given in sect. f. Concluding remarks on the proposed model will be made in sect. g.

b. Review of cathode spot theory

In the past 25 years, a number of different cathode spot models were developed. The differences often lie in the ability to explain the phenomena, each observed by the various model designers. Therefore, this can hardly be considered as a sufficient proof that a given theoretical model is universally applicable. Material parameters and important initial- and boundary conditions are only inexactly known, thus impairing the credibility of many theories.

In literature, a given cathode spot theory mostly consists of a set of equations, describing relevant physical processes. The first of such is to be found in the work of Lee (61). Solution of these sets of equations then results in modes of stable and stationary operation of the cathode spot. Such a treatment has most recently been pursued by Andanson (84), who derives a number of internal spot parameters as a function of arc current.

An important contribution to cathode spot theory stems from Ecker (a survey of his work is given in Lafferty [80] ch. 7), who uses inequalities rather than equations to derive areas of possible cathode spot existence in the temperature - current density plane.

Recent reviews of the state of theoretical progress are given by Hantzsche (83) and Ecker (83).

From experiments, it is abundantly clear, that the cathode spot is subjected to an erratic motion over the surface. This means, that a time dependent behaviour of all parameters should be incorporated in any model. This was first performed by Ecker (73) using the concept of the "Moving Smooth Surface Spot" as a refinement of the "Smooth Surface Spot" theory. Again, an existence diagram was calculated showing now two modes of existence (against only one for the immobile spot).

A further development towards reality was the recognition of the role of surface irregularities, acting through their E(lectrical)-field intensification as strong electron emitters. A sufficiently high current density in such micro-protrusions causes them to explode on a sub-nanosecond time scale (Mesyats 85), associated with a pulse-like plasma release and a subsequent cathode spot formation. This explosive emission seems to be of importance; Mesyats (85) and the group of Mitterauer (86) consider this mechanism as prevailing, while Hantzsche

(81) takes it only as an additional effect. Ecker (in Lafferty [80] ch. 7) incorporates the surface condition as an average effect, with a large number of irregularities inside the spot zone or as an individual structure effect. Existence diagrams arise, very strongly determined by the dimension and shape of "the average micro-protrusion".
All the available theories pronounce upon a number of internal cathode spot parameters that are difficult - if not impossible - to measure.
One of the few possible exceptions herein is the current density, that can be estimated from crater tracks (Daalder 74) or from luminous zone-size measurements (Rakhovskii 84). Whereas the former method gives current densities (j_e) in the order of $j_e \approx 10^{12}$ A/m^2, the latter measurements yield $j_e < 10^9$ A/m^2. Notwithstanding a continued discussion on this matter, a growing acceptation of the high value is noticeable (Hantzsche 84), also influenced by a third way of measurement pointing towards high j_e (Jüttner 84). It seems thus reasonable to take such a high current density ($j_e > 10^{11}$ A/m^2) as a starting point in a pragmatically theoretical analysis.

The considerations above are specified for the region outside the metal. Much less attention is paid to the process of crater excavation. As the discharge "consumes" a certain amount of evaporated metal, a cathode crater is formed. The formation process, i.e. the crater radius as a function of time, can be calculated from suitable energy balances. This has been undertaken by Daalder (78) and in a more refined way by Prock (86). Both studies yield resistive heating, predominant over ion impact heating as a creative power source. Predicted crater radii and erosion rates are found, in good agreement with experimental values.

c. Review of the theoretical approach of current chopping

The only (substantially founded) theoretical analysis of the current chopping phenomenon in a vacuum discharge is worked out by Ecker (74). As remarked previously, his "Smooth Surface Theory" gives rise to an "existence area" in the $T_c - j_e$ plane (T_c cathode spot temperature) outside of which the cathode spot cannot operate. For a given cathode voltage drop (u_c), there is a certain threshold current (I_{th}), below

which the existence area vanishes. Cathode spot operation below this threshold current (I_{th} = 30 A at u_c = 15 V for Cu) is only possible at the cost of an increased cathode drop (u_c = 100 V at I_{th} = 5 A). This implies a negative current-voltage characteristic for low currents (I < 30 A). Current chopping can then (especially in inductive circuits) arise as a result of instability oscillations with an increasing amplitude, similar to high pressure arc chopping (cf. sect. 3a).
From Ecker's considerations, chopping currents in a practical circuit were calculated by Lippmann (76, 77) and a realistic qualitative dependence on AC amplitude current and parallel capacitance was found. Quantitatively, the calculated values are much too low (a factor of 3 at small parallel capacitances). A reduction of chopping current by resistively damping the instability oscillations, suggested by Ecker's theory was verified by Reif (80). Czarnecki (86) uses the "Smooth Surface Theory" as a basis to calculate a minimum current (4 A for Cu) below which the cathode spot energy balance can no longer be fulfilled, even at high cathode drop values. Comparison of chopping currents of arcs between a series of electrodes - each doped with an easily evaporating metal - with the minimum current belonging to the dope-metal, suggests a relationship between the two.

Commenting on this, the qualitative predicting value of the "minimum current concept" is subjected to little doubt. At the same time, however, a number of problems must be recognized. A negative u_{ac} - I characteristic for low-current vacuum discharges was never proved. On the contrary, current reduction experiments like in fig. 6.3 do not show a rising arc voltage very close to current zero. Even very low DC current Cu-discharges (5 A) have an arc voltage less than 20 V. Further, the use of the "Smooth Surface Theory" means the acceptance of low values of current density ($j_e < 10^{10}$ A/m^2). In the light of results of different experimentalists as well as theoreticians such a value seems about a 100 times too low.

A common outcome of many calculations is a minimum current that is about a factor 4 lower than the actual chopping current. This means, that another condition, necessary for the continued survival of the discharge, can not be fulfilled any more, long before (in a falling AC

current) Ecker's balancing of energy is violated. In this light, a stationary theory again seems to fail for chopping current estimations. As remarked earlier, a cathode crater must renew itself after a certain lifetime (5-500 ns). A necessary condition that seems to be a stronger prerequisite than the balancing of cathode spot processes, may lie in this ability of renewal. In other words, a cathode spot must be able to displace itself, and to excavate a new crater. The reason that renewal is necessary, may be because a crater becomes too large after some time, thus reducing the current density below a value required to ensure sufficient Ohmic heating (cooling criterium [Daalder 78]). Prock's analysis (86) shows that a lack of vapour production may end the crater excavation process before the cooling criterium has been reached.

In any case, the ease of cathode crater renewal seems to be strongly coupled to the stability of the discharge and thus to current chopping. Sub-micrometer size surface irregularities cause enhancement of an (existing) electrical field, thus favouring crater initiation at these locations. In this view, a large number of such field intensificators in the vicinity of an active emission crater means an easy take-over of the emission by one of them. There is indeed evidence of an enhanced stability of a discharge on a "rough" cathode, as is demonstrated by the experiments in sect. 2h.

d. Cathode-spot parameters in a stationary, high current density model

In this section, it is attempted to construct and solve a closed set of equations, describing the interfacial sheath of cathode and metal vapour plasma. Analogue to Ecker's "Smooth Surface Theory" a stationary spot is assumed. In contrast to his model, however, the set of equations presented below contains important experimental results as a starting point.

The aim of this semi-empirical model is to answer the following questions:

a. Do the equations, generally used in theoretical models of the cathode spot allow a solution in the case of a current density in the order of 10^{12} A/m^2?

b. Does the model predict instable behaviour at low currents ($I < 40$ A)?
c. What are the magnitudes of predicted ion flows in the cathode spot?

A set of equations [(7.1) through (7.9)], with the aid of which relevant cathode spot quantities are computed, is based on the following assumptions:

(1) Emission of electrons is localized in crater-shaped structures with a radius r_a; the entire emission electron current density is generated in this circular area.
(2) The emission mechanism is thermal-field emission. A high temperature (T_c) in the molten crater surface, combined with an intense electric field (E_c) in front of the cathode determines the electron current density (j_e).
(3) The intense field is a function of the ion current density directed towards the cathode, the electron current density (j_e) and a voltage drop (u_c) that accelerates ions towards the cathode and electrons in the opposite direction.
(4) All ions are formed by ionization of neutral vapour by emitted electrons having passed through u_c.
(5) The voltage drop is assumed to be present over a sheath with a thickness (δ_c) that is equal to the mean free path for ionization (λ_c) of a vaporized Cu atom.
(6) Neutrals are vaporized due to the high temperature (T_c) of the surface giving a mass flux (j_n) that - after ionization - supplies the necessary amount of ions.

Beside these, considerations based upon experimental results are incorporated in the model through the following assumptions:

(7) The net ion current, directed to the cathode ($I_{i,c}$) is 10% of the total arc current (Daalder 78*).
(8) Of all the ions formed, 50% returns to the cathode, whereas 50% does not so. This assumption is supported by the work of McClure (74), Harris (74) and Daalder (78*).
(9) The crater radius is a given function of the arc current (I) (Daalder 74).

A sketch of the flow of the various particles within the cathode spot region is given in fig. 7.2.
The assumptions (1) - (9) will next be quantified in a set of equations.

The median crater radius as a function of arc current is introduced as a measuring result. This function is specific for a certain cathode metal:

(9) → $r_a = g(I)$ (7.1)

A number of currents must now be defined (see fig. 7.3):

I: arc current;

I_e, I_e^x: electron currents to cathode and plasma respectively;

$I_{i,a}$: ion current from the cathode into the quasi neutral plasma;

$I_{i,c}$: ion current directed towards the cathode. This latter current is split up into two:

$$I_{i,c} = I_{i,c}^{\varepsilon} + I_{i,c}^{0} \quad (7.1a)$$

Herein, $I_{i,c}^{\varepsilon}$ is the ion current associated with the cathode field E_c, present in the emission area (πr_a^2), and $I_{i,c}^{0}$ the ion current hitting the cathode outside this area. $I_{i,c}^{\varepsilon}$ is assumed homogeneous, so that its current density ($j_{i,c}^{\varepsilon}$) is written as:

$$j_{i,c}^{\varepsilon} = I_{i,c}^{\varepsilon}/(\pi r_a^2) \quad (7.1b)$$

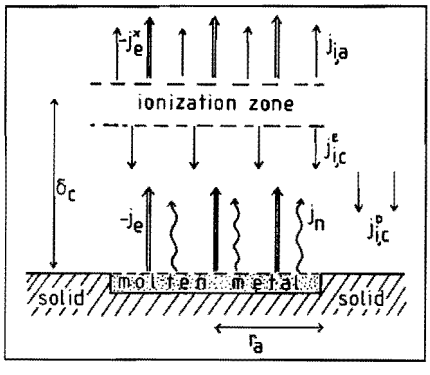

Fig. 7.2: *Modelled flow of particles in the sheath between plasma and cathode metal. Single straight arrows: ions; double arrows: electrons; curled arrows: neutrals. For symbols see text.*

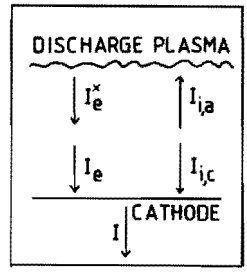

Fig. 7.3: Definitions of currents. For symbols see text.

From assumption (7) and (8) it follows:

(7) → $I_{i,c} = 0.1\ I$ (7.1c)

(8) → $I_{i,a} = I_{i,c}$ (7.1d)

So that (with the obvious relation $I = I_e + I_{i,c}$) it is clear that:

$$I_e = 0.9\ I \tag{7.1e}$$

Combining eq. (7.1e) and (7.1) yields an electron current density:

$$(1) \rightarrow \quad j_e = \frac{I_e}{\pi r_a^2} = \frac{0.9\ I}{\pi}\,[g(I)]^{-2} \tag{7.2}$$

Eqs. (7.1b), (7.1c) and (7.1e) substituted in eq. (7.1a) gives:

$$I^{\Box}_{i,c} = 0.1\ I - \pi\ r_a^2\ j^{\varepsilon}_{i,c} \tag{7.3}$$

For the emission mechanism, the thermal-field (TF) emission formalism of Murphy (1956) is assumed to apply. Herein, j_e is related to a cathode temperature (T_c) and an electric field (E_c) directly in front of the cathode:

$$(2) \rightarrow \quad j_e = \frac{4\pi e m_e k^2 T_c^2}{h^3}\,\frac{\pi\ D}{\sin \pi\ D}\,\exp\left[-\frac{e}{kT_c}\left\{\varphi_a - \left[\frac{eE_c}{4\pi\epsilon_o}\right]^{1/2}\right\}\right] \tag{7.4}$$

$$\pi\ D = \left[\frac{4\pi\epsilon_o}{e}\right]^{1/4}\ \frac{h}{2\pi e}\left[\frac{e}{m_e}\right]^{1/2}\ \frac{eE_c^{3/4}}{kT_c}\ ,$$

with φ_a the metallic work function (φ_a = 4.4 V for copper), m_e the electron mass and k, e, ϵ_o, h the usual constants.

The necessary field (E_c) is related to the current densities ($j^{\varepsilon}_{i,c}$, j_e) in front of the cathode crater, and the cathode drop (u_c). In the appendix, this relationship is derived with the following result:

$$(3) \rightarrow \quad E_c = \frac{2}{\sqrt{\epsilon_o}}\left[\frac{m_e u_c}{2e}\right]^{1/4}\left[\ j^{\varepsilon}_{i,c}\ \sqrt{(m_i/z_i m_e)} - j_e\right]^{1/2}\ , \tag{7.5}$$

with m_i the ion mass and z_i the average ion charge (in units of e).

A quasi-stationary treatment is justified here because the time scale of the cathode spot processes (10–1000 ns) is large compared to the inverse of the particle collision frequency.

Integration over E_c [eq. (7.5)] (see appendix) yields the sheath thickness (δ_c) over which the cathode drop falls:

$$\delta_c = \frac{\sqrt{\epsilon_o}}{2}\left[\frac{2e}{m_e}\right]^{1/4}\int_0^{u_c}\left\{j^{\varepsilon}_{i,c}\left[\frac{m_i(u_c-u)}{z_i m_e}\right]^{1/2} + j_e(\sqrt{u} - \sqrt{u_c})\right\}^{-1/2} du \tag{7.6}$$

Assumption (4) implies a balancing of neutral mass flux (j_n, in kg/m^{2}s) and ion currents (currents are added algebraically):

$$(4) \rightarrow \quad j_n \pi r_a^2 = \frac{m_i (I_{i,a} + I_{i,c})}{z_i e \alpha_i} \tag{7.7a}$$

The ionization process, located at an average distance δ_c from the surface, is incorporated through a parameter α_i ($0 < \alpha_i < 1$). With $\alpha_i = 1$ all neutrals are ionized (by electron collisions); $\alpha_i = 0$ means no ions are formed. Now, with (7.1c, d) a mass flux is related to arc current:

$$j_n = \frac{0.2\ I\ m_i}{\pi\ r_a^2\ z_i e \alpha_i} \tag{7.7}$$

The production of neutral atoms is performed by the local (high) temperature (T_c or dimensionless T_c') leading to a vapour pressure (p_n, p_n') according to the Clausius-Clapeyron law (Ecker 71):

$$(6) \rightarrow p_n' = \exp\ (a/T_c' + b + c\ \ln T_c') \quad \text{(a, b, c material constants)} \tag{7.8a}$$

The mass flux is approximated by the Hertz-Knudsen formula (Knudsen 52):

$$j_n = \frac{p_n}{4} \left[\frac{3 m_a}{k T_c} \right]^{1/2} \qquad (m_a \text{ the atomic mass; } m_a \approx m_i) \tag{7.8}$$

The neutral density (n_a) is related to the neutral pressure (p_n) by:

$$n_a = p_n\ (k T_c)^{-1} \tag{7.8b}$$

and with this the neutral mean free path (λ_n) becomes:

$$\lambda_n = (n_a \sigma_i)^{-1} = k T_c\ (\sigma_i p_n)^{-1} \tag{7.8c}$$

Herein, σ_i is the total ionization cross section, a material quantity that is a function of the energy of the ionizing electrons. Because this energy is gained by acceleration in the voltage drop, σ_i is considered here as a function of u_c.

With this, assumption (5) can be quantified as:

$$(5) \rightarrow \lambda_n(u_c) = \delta_c(u_c) \qquad (7.9)$$

Equations (7.1) through (7.9) define 9 independent relations between the unknown quantities r_a, j_e, T_c, E_c, $j^E_{i,c}$, $I^D_{i,c}$, δ_c, j_n and u_c. The independent variable is the current I; parameters in the model are z_i and α_i.

Until so far, the model is valid for all cathode metals, because the experimental evidence obtained by different researchers suggests that assumptions (1) - (9) are valid quite universally. In order to make a solution possible, specific material data must be added. These are for copper:

Vapour constants (Ecker 71):

$$a = -4.053\ 10^{4};\quad b = 35.77;\quad c = -1.28 \qquad (7.10)$$

Radius vs. current, fitted from Daalder's (74) results:

$$r_a = 4.10^{-10}\ I^2 + 2.10^{-6}\ m \qquad 5 \leq I \leq 100\ A \qquad (7.11)$$

Ionization cross section vs. cathode drop (Schroeer 73):

$$\sigma_i = (8.75\ 10^{-2}\ u_c + 0.38)\ 10^{-20}\ m^2 \qquad u_c < 80\ V \qquad (7.12)$$

This is a good approximation of the rising part of the measured $\sigma_i(u_c)$ curve, that reaches its maximum of $7.6\ 10^{-20}\ m^2$ at 100 V.

Further, an average ion charge $z_i = 2$ is taken, justified by a number of investigations (e.g. Davis 69). The ionization parameter (α_i) is taken $\alpha_i = 1$, prompted by resonance line absorption techniques that indicate an almost full ionization: $\alpha_i > 0.96$ (Tuma 78).

The set (7.1) - (7.9) was solved, including numerical integration of (7.9) for arc currents in the range I < 100 A. The results are plotted in fig. 7.4.

A number of conclusions asked for at the beginning of this section can be drawn on the basis of the model:

a. Electron emission is made possible by a thin boundary sheath between cathode and discharge plasma. The thickness of this sheath is much smaller that its lateral expansion: $\delta_c \ll r_a$. In the sheath, an electric field in the order $E_c \approx 2.10^9$ V/m, combined with a local temperature $T_c \approx 4000 - 8000$ K is associated with current densities in the order of $j_e \approx 10^{12}$ A/m^2.

b. A solution of the set is possible for all currents below 100 A. This means, that this model alone does not predict a minimum current, as long as a sufficiently high metal temperature can be guaranteed.

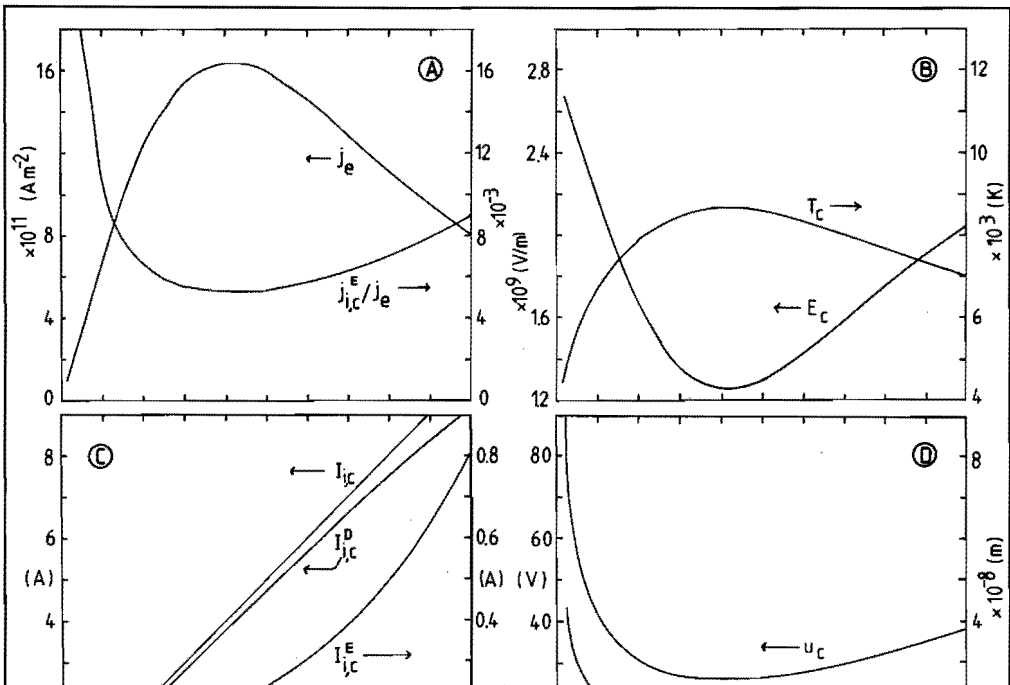

Fig. 7.4: Results of a stationary, high current density calculation.
A: crater electron- and ion current density (j_e, $j^E_{i,c}$);
B: cathode temperature and -field (T_c, E_c) in the emission crater;
C: ion currents, directed towards the cathode ($I_{i,c}$, $I^D_{i,c}$, $I^E_{i,c}$);
D: cathode drop and sheath thickness (u_c, δ_c). All quantities are given as a function of arc current.

From a thermodynamical analysis of Daalder (78), it is derived that this is the case: Joule heating in the metal is able to produce surface temperatures up to the critical temperature (8500 K for Cu). Thus it seems, that arc instability cannot be the result of reaching a current where the interacting processes can no longer support each other. This is partly due to the fact that at currents $I < 30$ A, the voltage drop is free to rise, at variance with measurement of the interelectrode voltage ($u_{ac} < 20$ V). This paradox can be solved by assuming a potential hump in front of the cathode leaving a lower interelectrode voltage intact. Contrary to Ecker's model (74) a negative u_{ac} - I characteristic can so be avoided.

c. The high electric field is accompanied by an ion current ($I^E_{i,c}$) that is smaller than 10% of the total ion current hitting the cathode ($I_{i,c}$). This implies, that almost the entire cathode-directed ion current ($I_{i,c} - I^E_{i,c} = I^D_{i,c}$) is available for the initiation of a new emission site.

A possible initiation mechanism is breakdown between plasma and the cathode (Fearn 69). The necessary high electrical field (outside an active crater) can be associated with a saturated ion current density $j^D_{i,c}$, that is drawn from the near-crater plasma by the cathode, negative with respect to the plasma.

Measurements by Jüttner (86) yield $j^D_{i,c}$ as a function of distance (x) in the cathode plane, and arc current:

$$j^D_{i,c} \approx 3.10^{-4}\ I\ x^{-2} \qquad x \geq 10^{-3}\ \text{m} \tag{7.13}$$

To illustrate merely a way of thinking, rather than to calculate exact results, eq. (7.13) is extrapolated to $x < 1$ mm. The surface field (E_s) outside - but close to - the crater area can then be estimated with eq. (7.5), substituting $j^D_{i,c}$ from eq. (7.13) for $j^E_{i,c}$ and $j_e = 0$ ($u_c = 20$ V). Field enhancement by microprotrusions or other surface irregularities is taken into account by writing the real surface field (E^x_s) as the product of the field (E_s) and a local field enhancement factor (β_s):

$$E^x_s = \beta_s E_s \tag{7.14}$$

From Bloomer (68) a breakdown field $E_b = 6.9\ 10^9$ V/m is taken to establish a maximum distance (x_m) between an actual emitting crater centre and a given microprotrusion (having a local field enhancement factor β_s) that explodes upon breakdown ($E_s^x > E_b$). With eq. (7.5) and eq. (7.13):

$$x_m = 7.10^{-8}\ \beta_s \sqrt{I} \qquad (x_m > r_a) \tag{7.15}$$

Again, it must be stressed that the numerical constant in eq. (7.15) contains a hazardous extrapolation of eq. (7.13).

Fig. 7.5 gives the course of the near crater field E_s^x, calculated for I = 60, 20 A. According to the reasoning above, protrusions located at 5 μm (β_s= 10) and 20 μm (β_s= 50) are candidates for emission take-over.

Qualitatively, eq. (7.15) underlines the idea that candidates for a new emission site must be located within a circle with radius x_m. This circle is larger for high currents and rough or otherwise "impure" surfaces, promoting an easier take-over of the emission.

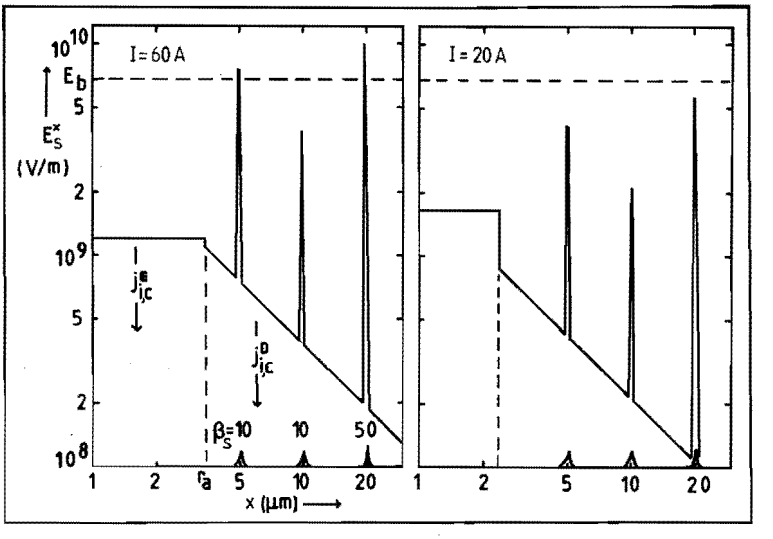

Fig. 7.5: Near cathode crater field (E_s^x) for currents I = 60, 20 A as a function of distance (x) along the cathode surface. Microprotrusions (not to scale) cause a local field enhancement (β_s), that can raise the local electric field to a value higher than the breakdown field (E_b).

From experiment (Daalder 78, Jüttner 84*), it is well known that the average distance between craters (after arcing) is much larger on rough or slightly oxidized surfaces than on clean ones. Also, the preference of a cathode spot to move over surface scratches and the tendency to cover a larger area on a rough surface, is verified by the experiments described in sect. 2h and by Daalder (73).

e. Time dependent mass flow from crater to plasma

In the previous section, values were derived for some physical quantities in a thin sheath covering the emission crater. For the crater radius, the median value (r_a) is taken, obtained from Daalder's study. It is clear, that during the formation process, the crater radius increases in time, making all the parameters time dependent.
In order to describe the crater excavation process, Daalder (78) considered the energy balance of a layer (thickness dr) at a distance r in the solid metal (fig. 7.6):

$$\frac{I_e^2 \rho_e(T) dr}{2\pi r^2} = 2\pi r^2 \, dr \, \rho_m c_p \frac{\partial T}{\partial t} \qquad (7.16)$$

Herein $\rho_e(T)$ is the electrical specific resistance as a function of temperature (T), ρ_m the specific mass, and c_p the specific heat of the solid metal.

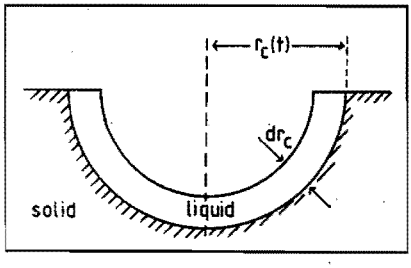

Fig. 7.6: Model of a cathode crater having radius $r_c(t)$. Thickness of the molten layer is dr_c.

Eq. (7.16) is the formulation of the fact that Joule heating entirely accounts for heating the layer; for small r, adiabatic heating is assumed thus neglecting heat conduction. From eq. (7.16) and using the Wiedemann-Franz relation (that couples ρ_e to the thermal conductivity λ_o), the position of a molten layer (r_c) as a function of time (t) can

be calculated (λ_o considered here as a constant) resulting in:

$$r_c(t) = \left[4\pi^2 \rho_m \lambda_o \left\{ \int_{T_o}^{T_m} c_p \frac{dT}{T} + \frac{P_m}{T_m} \right\}\right]^{-1/4} \left[I_e^2 L t\right]^{1/4} \qquad (7.17)$$

Herein, T_o, T_m: room-, melting temperature; P_m: heat of melting and L: Lorentz constant. For copper, substitution of the appropriate material constants, and making use of eq. (7.1e) yields:

$$r_c(t) = 2.04\ 10^{-5} \sqrt{I}\ (t)^{1/4} \qquad (7.17a)$$

After a time t, a molten layer dr_c is present at a distance $r_c(t)$. Due to the extremely high temperature, the molten material is evaporated. The mass of this layer, now available to the discharge is expressed as:

$$dm = 2\pi\ r_c^2\ \rho_m\ dr_c, \qquad (7.18)$$

so that the mass flow from the metal into the discharge (I_{md}) becomes:

$$I_{md} = \frac{dm}{dt} = 2\pi\ r_c^2\ \rho_m \frac{dr_c}{dt} = 1.2\ 10^{-10}\ I^{3/2}\ t^{-1/4} \quad \text{for copper.} \qquad (7.19)$$

The mass flow (I_n) needed by the discharge to produce an ion current to cathode ($I_{i,c}$) and plasma ($I_{i,a}$) is then given by eq. (7.7a) as:

$$I_n = j_n\ \pi\ r_c^2 = \frac{m_i(I_{i,a} + I_{i,c})}{z_i e\ \alpha_i} \qquad (7.20)$$

For a stable discharge, a proportionality between ion currents and arc current is assumed:

$$I_{i,a} + I_{i,c} = \gamma\ I$$

The fraction constant (γ) has been taken as $\gamma = 0.2$ in sect. d, based on experimental as well as on theoretical considerations, there leading to eq. (7.7). This value is certainly a time-averaged number. From measurements discussed in sect. 5b, it is clear that large fluctuations in ion production (up to 100% of the time averaged value) are present in the cathode spot region of a stable discharge. From this, it may be inferred that the minimum value (γ_{min}) must lie below the average value $\gamma = 0.2$.

The criterium, stating that mass production by crater excavation must exceed the minimum need of the discharge is then:

$$I_{md} > \frac{\tau_{min}\, m_i I}{z_i e \alpha_i} \qquad (7.21)$$

The function $I_{md}(t)$ is plotted in fig. 7.7 for several arc currents as a function of time. Denoted by "SEP", a separatrix is entered that divides the diagram into an area where (7.21) holds and an area where insufficient mass is released into the discharge. The position of the separatrix is dependent on τ; values of τ = 0.1, 0.13 and 0.2 are used.

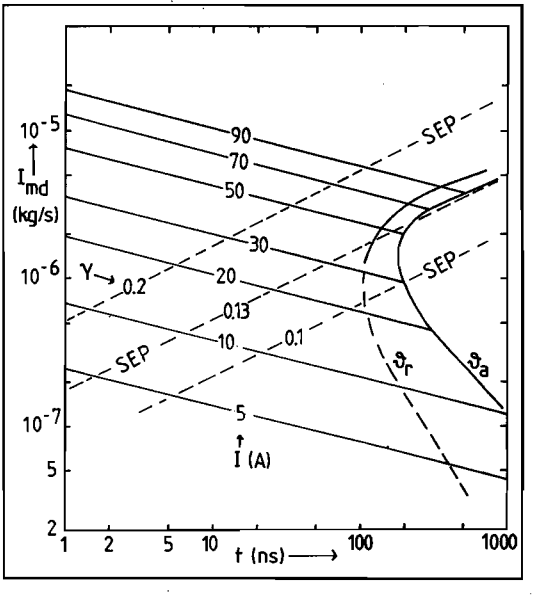

Fig. 7.7: Calculated mass flow (I_{md}) caused by the crater excavation process - for some arc currents (I) - as a function of time after crater initiation. SEP: line dividing the plane in an area with sufficient (left) and insufficient (right) mass flow. τ: ratio of total ion current to arc current ; ϑ_a, ϑ_r estimated crater formation times, see text.

Also given in fig. 7.7 is the time (ϑ_a) calculated from eq. (7.17) that elapses before the final (measured) crater radius (r_a) has been reached:

$$r_c(\vartheta_a, I) = r_a(I) \qquad \text{or alternatively:}$$

$$\int_0^{\vartheta_a} I_{md}(t)dt = \frac{2}{3}\pi \rho_m [r_a(I)]^3 \qquad (7.22)$$

This results [with eq. (7.11)] in a function $\vartheta_a(I)$ that expresses the time after which the crater formation theoretically stops. It can be seen, that for $10 < I < 100$ A these crater formation times are in the order of 0.1 - 1 μs.
A number of both experimenters and theoreticians report crater formation times from 1 ns up 10 μs. It is therefore easy to cite several authors who find times in the mentioned range. At the same time it must be realized that in most investigations - ϑ_a is only derived indirectly.

The interpretation of fig. 7.7, is that the crater excavation process can only provide a sufficient mass flow ($I_{md} > I_n$) up to a critical time (t_{cr}) that is a strong function of arc current (and τ). When a minimum value of $\tau_{min} = 0.13$ is chosen, it is clear that for currents $I \geq 45$ A, a sufficient mass flow (I_{md}) is assured during the entire crater formation time: $t_{cr} \approx \vartheta_a$. Below 45 A, $t_{cr} < \vartheta_a$, which means that a new crater must have been formed at t_{cr} in order to fulfil the mass flow criterium.
At still lower currents, the required repetition frequency of crater formation increases drastically. For these currents, it is conceivable, that a conglomerate of small craters (with radii $<< r_a$) is active more or less simultaneously, each for a very short time (some ns).
At times $t < t_{cr}$, it is evident from fig. 7.7 that an excess of mass is produced. This can be associated with the peaks in probe- (and shield) ion current as well as in the light intensity, described in chapter 5. There, these peaks were attributed to sudden charge releases in the cathode spot. In view of the high degree of ionization ($\alpha_i \approx 1$), these charge bursts may be caused by the repetitive crater formation mechanism, giving an excess of mass in its early ($t < t_{cr}$) stage. A fine-structure in the light signal with a repetition time of about 200 ns ($\approx \vartheta_a$) is easily recognized in oscillograms like fig. 5.16, possibly a direct evidence of repetitive crater formation.

Another method of estimating the repetition time of crater formation is equating the mass that leaves the cathode (in ionized from) per second, with the mass of the emptied craters, formed per second. The first quantity has been measured by Daalder (78) and can be expressed by IE_{ri}, E_{ri} being the erosion rate (in kg/C) and I the arc current.

The ionized mass of the emptied crater that definitely leaves the cathode is only half the totally removed mass [cf. eq. (7.1d)]. The equation then states: (assuming one active crater at a time)

$$E_{ri}\ I = \frac{1}{2}\frac{2}{3}\pi\ [r_a(I)]^3\ \rho_m\ \vartheta_r^{-1}\ , \qquad (7.23)$$

giving (with the experimental crater radius) the estimated repetition time ϑ_r as a function of current. Substitution of $E_{ri} = 4.10^{-8}$ kg/C in eq. (7.23) (Daalder 78), yields repetition times $\vartheta_r(I)$, also plotted in fig. 7.7. This curve deviates from the theoretical crater formation time (ϑ_a), but most interesting is the observation that for low currents ($I \ll 40$ A) again a large discrepancy arises between critical times for sufficient mass flow, and crater repetition time ($t_{cr} \ll \vartheta_r$).

f. The origin of vacuum arc instabilities

In this section, it will be tried to explain the occurrence of low-current instabilities, based on the arguments, collected in the previous sections.

In chapter 4, it was argued that a transient arc resistance (R_a) can describe the peak interelectrode voltage ($\hat{u}_{ac}$) at an instability as well as the simultaneous decay in current (and the subsequent recovery) in purely electrical terms. The essential question arising, is what process may provoke such a stepwise change in resistance.

In fig. 7.8 the specific electrical resistance (ρ_e) is given for copper at elevated temperatures. In the liquid phase [from melting temperature ($T_m = 1356$ K) up to the critical temperature ($T_{cr} = 8500$ K)] the specific resistance rises steeply (Grosse 66); in the plasma state, ρ_e drops at increasing temperature (Kovitya 85). As can be seen, a change in arc resistance might be expected caused by heating of the liquid metal layer in the crater, or cooling of the discharge plasma.

A calculation of the (time dependent) resistance (R_{ml}) of the thin, but very hot molten copper layer (Δr_c) is possible with the following expression:

$$R_{ml} = \int_{r_c-\Delta r_c}^{r_c} \frac{\rho_e[T(r)]}{2\pi\ r^2}\ dr \qquad (7.24)$$

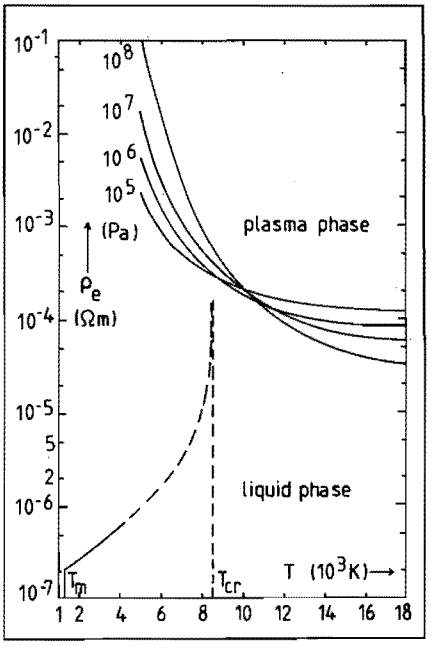

Fig. 7.8: *Specific electrical resistance (ρ_e) of Cu in the liquid phase (Grosse 66) and the plasma phase (Kovitya 85) for different pressures as a function of temperature. T_m: melting temperature; T_{cr}: critical temperature.*

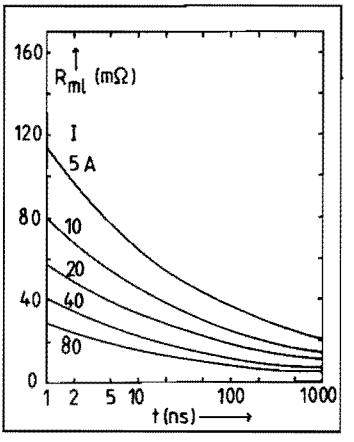

Fig. 7.9: *Resistance of the molten layer (R_{ml}) for some arc currents (I) as a function of time after crater initiation.*

On thermodynamical grounds, Daalder (78) derived a constant ratio of molten layer thickness and crater radius (see fig. 7.6; dr_c should now be read as Δr_c):

$$\Delta r_c \; / \; r_c \approx 0.1 \qquad (7.25)$$

Within the molten layer, a linear temperature profile is assumed:

$$T(r) = T_m + (T_{cr} - T_m)\,(r_c - r)/\Delta r_c \qquad r_c - \Delta r_c \le r \le r_c \qquad (7.26)$$

$\rho_e(T)$ is given by (see fig. 7.8, liquid phase):

$$\rho_e(T) = (T + 1559)/(1.7\ 10^{10} - 2.1\ 10^6\ T) \qquad T_m < T < T_{cr} \qquad (7.27)$$

Now, with eqs. (7.17), (7.24) - (7.27) the molten layer resistance can

be calculated as a function of time and current. The result is given in fig. 7.9. From this figure it can be concluded, that the voltage drop over the liquid metal - immediately (1 ns) after crater initiation - is only 10% (at the most) of the total arc voltage. This value can only account for the fluctuations in voltage (cf. fig. 5.7), but for explaining instabilities, changes in arc resistance are required from a (steady state) value of $R_a < 100$ mΩ up to $R_a \approx 50 - 100$ Ω (for large instabilities).

Cooling of the interelectrode plasma can realize a change in specific resistance over 2 - 3 orders of magnitude (cf. fig. 7.8). The time scale of such a temperature change can be approximated by a time constant:

$$\tau_{pc} = \rho_m \, c_p \, s^2 / \lambda \qquad (7.28)$$

with ρ_m the density, c_p the specific heat, s the characteristic (radial) dimension and λ the thermal conductivity of the plasma column at a certain temperature and pressure. These material functions are calculated (for copper) by Kovitya (85) and from his data, a range for τ_{pc} can be derived:

$(6.10^4$ K, 10^5 Pa) 1.5 μs $< \tau_{pc} <$ 530 ms (5.10^3 K, 10^8 Pa) (s = 1 mm)

It is very probable, that temperature and pressure of the discharge plasma are within the indicated range, so that it is clear, that τ_{pc} is always much larger than the risetime of the transient arc resistance (<100 ns). It is therefore unlikely, that a temperature fall of the conducting plasma can cause the observed instabilities.

The rapidity of the onset of instability rather suggests a disturbance of a very delicate balance in the discharge. The current conducting path (called "column" in high pressure arcs) in a stable vacuum discharge is essentially free of a net electrical field. This is due to an extremely efficient neutralization of the current carrying electrons by ions. These ions are forced to move (by ambipolar fields) towards the anode. For a given electron- and ion density (n_e, n_i resp.) and electrode distance (δ), the voltage-drop over the discharge (u_{ac}) is the sum of

the cathode voltage-drop (u_c) and conducting path voltage-drop (u_{cp}) in a rough approximation given by:

$$u_{ac} = u_c + u_{cp}; \qquad \text{with} \quad u_{cp} = \left[\frac{9}{4\epsilon_o} \delta^2 e (n_e - z_i n_i) \right]^{2/3} \tag{7.29}$$

Eq. (7.29) is a modification of the well-known Child's space charge law (Child 11).

Application to our case, taking a 30 A current in a conducting channel with a radius of 1 mm, implies already a voltage drop of 100 V by an unbalance of space charge in this channel of $n_e = (1 - 10^{-5}) z_i n_i$ (δ = 5 mm). With this in mind, a suitable (fictitious) arc resistance can now be defined:

$$R_a = u_{cp}/I, \tag{7.30}$$

Instability of the discharge may now arise following the reasoning summarized below:

1. A certain current level is imposed by the external circuit; in the discharge this current consists primarily of electrons.
2. This means that a certain minimum electron density in the plasma must guarantee continuity of the circuit current.
3. This minimum electron density requires a delicate neutralization by an ion density in order to assure that $u_{cp} = 0$.
4. The ions are produced out of a neutral mass flow (I_{md}), completely ionized in the cathode spot.
5. This mass flow strongly decreases in time as the crater (the only source of material) grows larger and larger (fig. 7.7).
6. After some time (t_{cr}), the mass production by crater excavation is no longer sufficient to meet the demands, set by the neutralization of the (circuit required) electron density in the conduction region.
7. As the electron current density wil not instantaneously adapt itself to the ion deficiency, the voltage over the discharge (u_{cp}) increases steeply, coinciding with a fall of current through the discharge.

Because of the introduction now of a time dependent electric field, the circuit current (I) should be considered here as a sum of a discharge current ($j_d S$) and a displacement current:

$$I = j_d S + \epsilon_o S \frac{dE_a}{dt} \tag{7.31}$$

Herein, j_d is the plasma current density, S an (effective) conducting area and E_a the electric field that arises in the ion-depleted zone. A rough estimation, using a voltage rise of several hundreds of volts in 100 ns indicates that the displacement term in eq. (7.31) is of a negligible magnitude. It is therefore concluded, that a rapid fall in circuit current coincides with a similar fall of current, carried by electrons in the discharge.
In a stable discharge - generally carrying a current above 40 A - the repetition rate of crater formation is such, that a new crater is active before the previous one would fail to produce sufficient mass, as is made plausible in fig. 7.7.

A possible explanation can now be given of how an instability may be removed after a certain instability duration (or decay time) (Δt). Plasma potential rises to a value up to several hundreds of volts during the decay phase. As a result, the (positive) space charge sheath at the cathode side is stressed with a considerably higher voltage. The electric field outside the actual emission zone - called E_s in eq. (7.14) - is enhanced by at least one order of magnitude, so enabling breakdown (and subsequent crater formation) at sites not initiating breakdown at lower plasma potential. As an example, the microprotrusions in fig. 7.5, not causing breakdown in a stable discharge, may do so during an instability decay phase. The breakdown process is accomplished on a (sub)nanosecond timescale and cannot be detected by the optical measuring method described in chapter 5.
An increasing number of ions, forced to move towards the anode, escape from the conducting channel at an increased distance from the point source.Therefore, in the conducting channel between cathode and anode, the region directly in front of the anode has the smallest ion density, so being the first candidate for an ion deficiency due to a failing source. The duration of an instability (Δt) in this picture, merely reflects the time needed to transport newly created ionic charge towards the ion-depleted zone. This is corroborated by the measurements, discussed in sect. 4f, showing a direct dependence (see fig. 4.16) of the instability duration upon the gap distance. It was found, that the ions cover the distance from cathode spot to anode during an instability with a velocity in the order of 2.10^4 m/s, i.e. twice the average velocity of ions, present in the plasma outside the gap (see sect. 5b).

g. Concluding remarks

Summarizing, instabilities are believed to be manifestations of an ion deficiency in the discharge plasma near the anode. This deficiency, in its turn, results from an unsuccessful repetitive crater initiation.
In sect. d it was hypothesized that candidates for the take-over of electron emission are surface irregularities that must be located in a circle, having radius x_m [cf. eq. (7.15)] around an existing active rater. It is then reasonable to assume that the probability for a successful emission take-over is proportional to x_m^2, and thus to I [eq. (7.15)]. Further, the number of times that a new crater must be initiated can be taken equal to $(t_{cr})^{-1}$. With eqs. (7.19) and (7.21) this required repetition frequency becomes proportional to I^{-2}.
These two factors may account for the strong dependence of the DC arc lifetime on current

With the explanation for the occurrence of sudden (and short lasting) jumps in arc resistance, given in the previous section, it is now possible to understand why DC arc lifetime ($\bar{\tau}$) is dependent on electrode distance (δ), as described in sect. 2g. Recalling the dependence of the instability duration on δ , it is clear [verified by the data collected in fig. 4.15 and formulated in eq. (4.5)], that a given voltage u_{cp} (or transient resistance R_a) causes higher values of relative current reduction ($\Delta I/I$) at increasing electrode distances. Such higher values of $\Delta I/I$ reduce the average lifetime considerably. Besides, it is likely, that at larger distances more and more ions may "escape" from the anode region, leaving only a bare minimum of ion density intact to balance the necessary electron density. A higher frequency of occurrence of instabilities can thus be expected, also reducing the lifetime.
A similar effect can be observed by applying a magnetic field, in a direction perpendicular to the symmetry-axis of the discharge. At δ = 3 mm, a small field of only 7 mT reduced the DC lifetime (at 38 A) by a factor 5 to 10 (Schulpen 86). A transverse B-field bends the ion trajectories away from the anode region, so provoking large net electrical fields in the conducting region (Kimblin 77).

There is a certain similarity between the low-current instabilities, treated in this thesis, and the voltage hash, preceeding anode spot

formation in high-current ($I \geq 1$ kA) discharges (Sherman 72). The latter voltage rise may also be attributed to a deficiency of positive ions, needed to neutralize the increasing electron density at the anode (Mitchell 70). In a high current discharge, however, the energy input into the anode surface can vaporize anode material, subsequently ionized by electrons accelerated in the extra anode voltage drop. This mechanism of deficiency self-removal cannot act in a low-current discharge, where the energy input into the anode is at least two orders of magnitude smaller. Hence, the necessary ions must be supplied by the cathode.

The main features of the "instable arc model" may be summarized as follows. In order to guarantee a sufficient supply of conducting medium, the repetition frequency of crater formation must increase rapidly at low currents. It is assumed that new emission centres (craters) are formed following breakdown between the near-crater plasma and surface irregularities. The area of the region, where the electric field is high enough to cause breakdown, is determined by arc current and surface micro-structure. This high-field region is large for high currents and rough surfaces, and so contains (on the average) a large number of possible breakdown sites, favouring an easy take-over of the emission. At low currents and/or "smooth" surfaces, the opposite is true.
Thus, continuity of mass supply is endangered at low currents both by a smaller probability of creation of a suitable successor to an old crater and (more important) by the necessity of creating such a successor much more often per time unit.
A discontinuity in mass supply leads to a net electric field in the conductive interelectrode plasma, leading to a higher plasma potential. At the same time however, this process facilitates breakdown between the near-crater plasma and cathode. After a very short time, dependent on the actual cathode-to-anode distance, sufficient ionized material, released after breakdown, again restores the stable situation.
Instability of a low current vacuum discharge seems to be caused rather by the processes, outlined above, than by the inability to maintain the electron emission at low currents. In sect. d it was shown that such an inability does not arise in the solution of the equations describing relevant cathode spot processes. Besides, such a stationary model cannot explain instabilities in a DC arc, contrary to the dynamic "instable arc model", presented here.

Experimental confirmation of the reasoning given in this chapter is summed up below:

- The average repetition time of instabilities increases drastically when arc current is lowered (cf. fig. 4.6 or fig. 4.17).
- Arc lifetime is strongly reduced when the electrode distance increases (cf. fig. 2.14, 2.15) or effectively increases by a transverse magnetic field.
- Large fluctuations of ionic mass productions are suggested by probe- and shield current measurements, as well as by light intensity observations (ch. 5).
- Overvoltages due to an instability, are probably generated outside the cathode spot area (sect. 5e).
- Limiting the rate of rise of the (restoring) overvoltage (e.g. by a parallel capacitance) reduces the chances of survival of a DC discharge (fig. 2.10).
- Discharges "on" a cathode having good mass producing properties (high vapour pressure) always have a long DC lifetime (e.g. Cd, sect. 2g).
- Rough cathodes produce longer lifetimes than smooth ones (fig.2.16). The motion of the cathode spot is preferably along surface scratches and other structures having a high field intensification.
- The duration of an instability is a function of the distance between the temporarily ion depleted region and the ion source - the cathode spot - (fig. 4.16).

Appendix

Here, the cathode electric field (E_c) is derived as a function of $j^{\varepsilon}_{i,c}$, j_e and u_c. When the initial particle velocity $(v_{e,i})^2 \ll (2eu_c/m_{e,i})$ [justified by Beilis (70)] the average electron- and ion-velocity at a distance y from the cathode can be written as (see fig. 7.10):

$$v_e = (2eu/m_e)^{1/2} \; ; \qquad v_i = [2z_i e(u_c - u)/m_i]^{1/2} \qquad v_i = 0 \text{ at } y = \delta_c \qquad \text{(A1)}$$

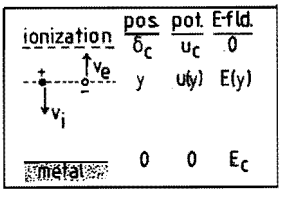

Fig. 7.10: Definitions of position (y), potential (u) and electric field (E) in the sheath. v_e, v_i: electron- and ion velocity.

Substitution of this in the Poisson-equation (ρ: net charge density):

$$\frac{d^2u}{dy^2} = \frac{-\rho}{\epsilon_o} = \frac{-1}{\epsilon_o}\left[\frac{j^{\varepsilon}_{i,c}}{v_i} - \frac{j_e}{v_e}\right] = \frac{1}{\epsilon_o\sqrt{(2e)}}\left\{ j^{\varepsilon}_{i,c}\left[\frac{m_i}{z_i(u_c - u)}\right]^{1/2} - j_e\left[\frac{m_e}{u}\right]^{1/2}\right\} \qquad \text{(A2)}$$

$$\frac{d}{dy}\left(\frac{du}{dy}\right)^2 = 2\,\frac{du}{dy}\,\frac{d^2u}{dy^2} \qquad \text{(A3)}$$

So that integrating the left-hand side of eq. (A3) yields:

$$E_c^2 \Big]^{E_y^2} d\left(\frac{du}{dy}\right)^2 = 2\int_o^u \frac{d^2u}{dy^2}\,du = \frac{-4}{\epsilon_o\sqrt{(2e)}}\left| - j^{\varepsilon}_{i,c}\left[\frac{m_i(u_c - u)}{z_i}\right]^{1/2} - j_e(m_e u)^{1/2}\right|_o^u \qquad \text{(A4)}$$

With $(du/dy)^2 = [E(u)]^2$, E(u) can be expressed:

$$E^2(u) - E_c^2 = \frac{4}{\epsilon_o\sqrt{(2e)}}\left\{ j^{\varepsilon}_{i,c}\left[\frac{m_i(u_c - u)}{z_i}\right]^{1/2} + j_e(m_e u)^{1/2} - j^{\varepsilon}_{i,c}\left[\frac{m_i u_c}{z_i}\right]^{1/2}\right\} \qquad \text{(A5)}$$

With boundary condition $E\,[u(y=\delta_c)] = E(u_c) = 0$:

$$E_c^2 = \frac{4}{\epsilon_o}\left[\frac{u_c}{2e}\right]^{1/2}\left\{ j^{\varepsilon}_{i,c}\left[\frac{m_i}{z_i}\right]^{1/2} - j_e(m_e)^{1/2}\right\} \; , \qquad \text{(A6)}$$

this being identical to (7.5).

The sheath thickness (δ_c) is now obtained from eqs. (A5) and (A6):

$$\left|\frac{du}{dy}\right| = \frac{2}{\sqrt{\epsilon_o}}\left[\frac{m_e}{2e}\right]^{1/4}\left\{ j^{\varepsilon}_{i,c}\left[\frac{m_i(u_c - u)}{z_i m_e}\right]^{1/2} + j_e(\sqrt{u} - \sqrt{u_c})\right\}^{1/2} = t(u) \qquad \text{(A7)}$$

so that δ_c is obtained from (A7) by integration:

$\delta_c = \int_o^{u_c} [t(u)]^{-1}\,du$, identical to eq. (7.6). The calculation, applied here, is a modification of the work, given first by Mackeown (29).

References:

- Andanson P. and Lefort A., J. Phys. D: Appl. Phys., vol. 17 (1984) 2377-86
- Beilis I.I, Lyubimov G.A. and Rakhovskii V.I., Sov. Phys. - Doklady, vol. 14 (1970) 897-900
- Bloomer R.N. and Cox B.M., Vacuum, vol. 18 (1968) 379-82
- Child C.D., Phys. Rev., vol. 32 (1911) 492
- Czarnecki L., Ph.D. Thesis, Technical University of Braunschweig (1986)
- Daalder J.E. and Vos C.W.M, TH report 73-E-32, Dept. of Elec. Eng. Eindhoven University of Technology (1973)
- Daalder J.E., IEEE Trans. Pow. App. Syst., PAS-93 (1974) 1747-57
- Daalder J.E., Ph.D. Thesis, Eindhoven University of Technology (1978)
- Daalder J.E., J. Phys. D: Appl. Phys., vol. 11 (1978*) 1667-82
- Davis W.D. and Miller H.C., J. Appl. Phys., vol. 40 (1969) 2212-21
- Ecker G., report no. 71-C-195 (1971) General Electric Corporation (unpublished)
- Ecker G., Z. Naturforsch., vol. 28 (1973) 417-28
- Ecker G., Beitr. Plasmaphys., vol. 14 (1974) 67-78
- Ecker G., IEEE Trans. on Elec. Insul., EI-18 (1983) 243-52
- Fearn D.G., Brit. J. Appl. Phys., vol. 2 (1969) 527-33
- Grosse A.V., Rev. Hautes Tempér. et Réfract., vol. 3 (1966) 115-46
- Hantzsche E., Physica 104C (1981) 3-16
- Hantzsche E., Beitr. Plasmaphys., vol. 23 (1983) 77-94
- Hantzsche E. and Jüttner B., XIth Int. Symp. on Disch. and Elec. Insul. in Vac., Berlin DDR (1984) 101-6
- Harris L.P. and Lau Y.Y., report no. 74-CRD-154 (1974) General Electric Corporation (unpublished)
- Jüttner B., Pursch H. and Anders S., J. Phys. D: Appl., vol. 17 (1984) L 111-4
- Jüttner B., Pursch H. and Shilov V.A., J. Phys. D: Appl. Phys., vol. 17 (1984*) L 31-4
- Jüttner B., XIIth Int. Symp. on Disch and Elec. Ins. in Vac., Shoresh (1986) 90-8
- Kimblin C.W., EPRI report EL-393, Electric Pwr. Inst. (1977)

- Knudsen M, "The kinetic theory of gases; some modern aspects", Methuen, London (1952)
- Kovitya P., IEEE Trans. on Plasma Sci., PS-13 (1985) 587-94
- Lafferty J.M., "Vacuum arcs, theory and application", Wiley and Sons, New York (1980)
- Lee T.H. and Greenwood A., J. Appl. Phys., vol. 32 (1961) 916-23
- Lippmann H.J. and Schuöcker D., Siemens Forsch. - u. Entwickl. Ber., Bd. 5 (1976) 21-4
- Lippmann H.J., Schuöcker D. and Reif W., Siemens Forsch. - u. Entwickl. Ber., Bd. 6 (1977) 252-9
- Mackeown S.S., Phys. Rev., vol. 34 (1929) 611-4
- McClure G.W., J. Appl. Phys., vol. 45 (1974) 2078-84
- Mesyats G.A., IEEE Trans. Elec. Insul., EI-20 (1985) 729-34
- Mitchell G.R., Proc. IEE, vol. 117 (1970) 2315-32
- Mitterauer J. and Till P., VIIth Workshop on Electrode Phen., Novosibirsk (1986)
- Murphy E.L. and Good R.H., Phys. Rev., vol. 102 (1956) 1464-73
- Prock J., Ph.D. Thesis, Technical University of Munich (1986)
- Rakhovskii V.I., IEEE Trans. on Plasma Sci., PS-12 (1984) 199-203
- Reif W., Appl. Phys., vol. 21 (1980) 169-71
- Schroeer J.M., Gündüz D.H. and Livingston S., J. Chem. Phys., vol. 58 (1973) 5135-40
- Schulpen F.J.H., M.Sc. Thesis EG.86.A.7, Dept of Elec. Eng., Eindhoven University of Technology (1986) (unpublished)
- Sherman J.C., rep. no. ULAP - T 10, University of Liverpool (1972)
- Tuma D.T., Chen C.L. and Davies D.K., J. Appl. Phys., vol. 49 (1978) 3821-31

8. SUMMARY AND CONCLUSIONS

In this thesis, a connection has been established between microscopic processes in the cathode spot of a vacuum (copper) discharge, and the phenomenon of current chopping, inherent to the interruption of AC power currents. This connection is illustrated below; each bloc of the diagram is briefly discussed hereafter.

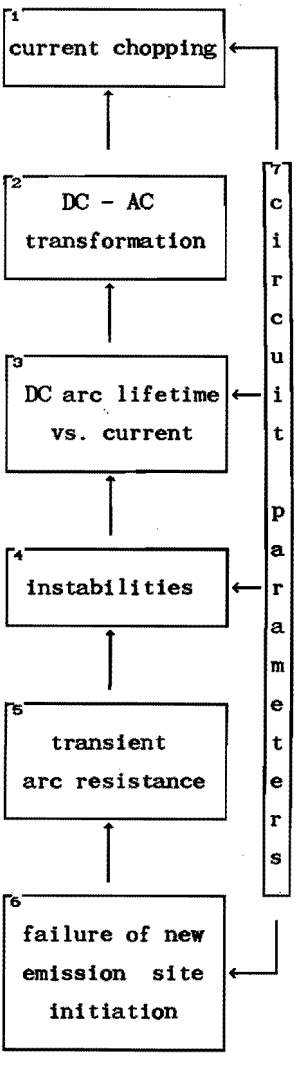

1. The chopping phenomenon may generate high overvoltages so endangering the insulation of high voltage circuits and components, normally guaranteeing the supply of electric energy. It is therefore of great practical importance to understand the physical mechanisms leading to current chopping in a vacuum interrupter. (sect. 3a).

2. It was shown, that current chopping of an AC current is equivalent to the inability of a DC arc to maintain itself indefinitely at low currents. An average DC lifetime ($\bar{\tau}$) after which the arc extinguishes spontaneously, can be defined and easily measured (ch. 2). This lifetime is a function of arc current: $\bar{\tau} = F(I)$.
   An important practical quantity is the current level (I_c) at which a falling AC current - having an amplitude $\hat{i}$ - chops before its natural sine zero. The chopping level determines the resultant overvoltage, and is a function of AC amplitude: $I_c = G(\hat{i})$.

A transformation was developed that constructs the functional dependence $I_c = G(\hat{i})$ (within certain boundaries) out of the experimentally determined dependence $\bar{\tau} = F(I)$. It was made plausible and proved that

this DC → AC transformation can give good results in predicting chopping levels, provided that the contact distance under AC and DC conditions is of a similar magnitude (sect. 3b, d).
The advantage of expressing AC data in DC quantities is twofold:
For testing purposes, essential in the development of low-chopping contact material, the necessity vanishes of using voluminous high-power circuits to measure chopping levels directly. As shown in sect. 3c, d, table-top DC experiments, using currents not higher than 10 A can predict chopping levels of AC currents up to 500 A.
For research purposes, DC experiments eliminate circuit imposed variations of arc current, allowing a more clear view on arc induced changes in externally measurable parameters.
It is the latter advantage, that is exploited in this work in order to clarify the relevant processes.

3. After a lifetime, ranging over 6 orders of magnitude at arc currents from 4 - 40 A, a DC arc always extincts spontaneously even without a change of any external parameter. This extinction is due to an accumulation of instabilities, that reduces the current more or less step wise to zero. Typical instabilities occur during the entire lifetime, but the more frequently and severely the lower the arc current is. The average lifetime seems to be determined by the probability that two or more instabilities coincide in a sufficiently short time interval (sect. 4d).

4. One such typical arc instability manifests itself as a steep rise of arc voltage (in the order of 2 kV/μs), and a circuit induced decay of current simultaneously. Although the instability proper is removed after some hundreds of ns, the external circuit prevents an instantaneous recovery of arc current. During a certain (circuit determined) time an increased probability of repeated instability remains (sect. 4c, d).

5. Electrically, the observed phenomena that accompany an instability, can be described by a transient arc resistance. This (fictitious) resistance is smaller than some tens of mΩ in a steady state arc, but may step to some ohms or even tens of ohms so causing the observed voltage and current behaviour (sect. 4e, f).

6. In order to assure a continued operation of the discharge as a whole, a sufficient amount of metal vapour must be supplied. This can only be done by the cathode spot. Visual inspection of the cathode after arcing shows emptied craters as remnants of vapour producing sites. A time dependent evaluation of the crater excavation process during arcing makes clear that one single crater can only supply sufficient vaporized mass up to a critical time after initiation. This means, that a new crater must have been initiated before that moment (sect. 7e). For low currents this critical time becomes extremely short, so that the repetition time of crater initiation must increase. Given a certain probability of successful crater initiation, a failure to initiate a new crater becomes more likely at low currents.
It is thought, that crater initiation is a result of breakdown between the discharge plasma and surface irregularities. The field, required for breakdown is only high enough close to the active cathode crater.
Failure to have an active crater ready in time, may result in an ion deficiency in the conducting interelectrode plasma. This leads to a building up of (negative) space charge at the anode side. Externally, this space charge is noticed as a voltage peak, or (after division by current) as a transient arc resistance. Internally, the voltage peak stresses the cathode sheath and facilitates breakdown at surface irregularities, so restoring stability (sect. 7f).
The necessity of the emission site, to displace itself pseudo-contineously over the cathode, is considered here as the main cause of arc instability. A semi-empirical evaluation of relevant emission processes indicates that an easy displacement is obstructed before the emission itself would become impossible, when current is reduced from high to low (sect. 7d).

7. The interaction between the discharge and the circuit is very important. A large inductance enhances arc stability, because the arc current response to an arc resistance-step of a given value and duration is less severe than in a resistive circuit. On the other hand, a large parallel capacitance - when located close to the discharge - impairs the restoring mechanism by reducing the rate of rise of the transient voltage (sect. 2e; 3e; 4f).

Time resolved measurement of the ion current, drawn from the plasma of a stable discharge shows large fluctuations, probably originating from a pulse-wise production of mass in the cathode spot. Light intensity measurements add to this picture; large fluctuations in light intensity coincide with small variations in arc voltage (chapter 5).

Recovery of the gap after interruption is initially determined by the charged particle density decay. After approx. 1 μs, the diffusion of neutrals becomes dominant, and lasts for some tens of μs. A galvanic connection between the vapour shield and either electrode may impair the breaking capacity of a vacuum interrupter. This is because an inductive shift of plasma potential allows the vapour shield to become an anode temporarily. Post-zero emission can then arise, the duration of which is determined by the magnetical energy, stored in the parasitic inductances of the electrode supports (sect. 6c, d).

SAMENVATTING

Dit proefschrift bevat een studie naar de fundamentele processen die leiden tot het verschijnsel "stroombreking" in vakuum vermogensschakelaars. Stroombreking is het abrupte doven van een metaal-(hier: Cu) damp ontlading die ontstaat bij het onderbreken van stromen in netten voor de elektrische energievoorziening. Dit abrupte doven is ongewenst, omdat in induktieve circuits er hoge overspanningen door kunnen ontstaan.

In dit werk is aangetoond dat stroombreking in wisselstroom circuits overeen komt met het spontane doven (na een karakteristieke levensduur) van een gelijkstroom ontlading. Deze equivalentie is mathematisch geformuleerd en kan dienen als recept waarmee stroombrekingswaarden in hoogspanningscircuits voorspeld kunnen worden uit eenvoudige laagspannings-gelijkstroom metingen. Digitale oscillografie met hoge tijdresolutie (100 MHz) heeft aangetoond dat het spontane doven van een gelijkstroom ontlading (beneden ca. 40 A) een gevolg is van akkumulatie van typische instabiliteiten. De gemiddelde herhalingsfrekwentie blijkt sterk stroom-afhankelijk. Monte Carlo simulatie van zeer veel instabiele ontladingen laat zien dat boogdoving geheel statistisch bepaald wordt.

Ter verklaring van de fysische oorsprong van een instabiliteit, zijn optische- en stroom-injektie meettechnieken gebruikt met hoge tijdresolutie. Interpretatie van deze metingen, o.a. met kruiskorrelatie- en frekwentie-analyse methoden, maakt duidelijk dat metaaldamp sterk gepulst door het ontladingsvoetpunt geproduceerd wordt. De noodzaak van dit voetpunt om zich snel over de kathode te verplaatsen, om zo een kontinue massastroom naar het ontladingsplasma te garanderen wordt als oorzaak van instabiliteit gezien. Uit een theoretisch model van relevante processen in het voetpunt blijkt dat bij afnemende stroom dit verplaatsingsmechanisme eerder bemoeilijkt wordt dan de emissie op zichzelf. Aldus is verband gelegd tussen mikroskopische, fysische processen in het ontladingsvoetpunt, en de praktische "stroombreking".

Zeer belangrijk is de interaktie tussen de ontlading en het voedende circuit. Deze is bestudeerd en (kwalitatief) gemodelleerd met behulp van experimenten, zowel op sub-microsekonde als op millisekonde tijdschaal.

Tot slot is het gedrag bestudeerd van het diëlektrisch herstel na de onderbreking. De eerste microsekonde van dit herstel is van essentiëel belang voor het slagen van de onderbreking. Bij een ongunstige elektrode geometrie kan een na-emissie effekt het herstel nadelig beïnvloeden.

Levensloop:

René Smeets werd op 29 juni 1955 geboren te Venlo. Gedegen basis onderwijs onder leiding van zijn vader legde de fundamenten voor een gymnasium bèta opleiding aan het Collegium Marianum te Venlo, van 1967-1973. In die tijd werd de belangstelling voor de natuurkunde gewekt; een logisch gevolg was dan ook een studie aan de (destijds) Afdeling der Technische Natuurkunde van de Technische Hogeschool Eindhoven. Daar studeerde hij in mei 1981 (met lof) af in de groep "Magnetische Ordeningsverschijnselen" onder leiding van prof.dr.ir. W.J.M. de Jonge. Het afstudeerverslag was getiteld: "Lokale en kollektieve excitaties in magnetische systemen".
Na een langdurige reis door Noord-, Midden- en Zuid-Amerika trad hij in mei 1983 als wetenschappelijk assistent in dienst bij de Technische Hogeschool Hogeschool Eindhoven. In de vier daarop volgende jaren kwam dit proefschrift tot stand, onder begeleiding van prof.dr.ir. W.M.C. van den Heuvel in de vakgroep "Elektrische Energiesystemen" van de Fakulteit Elektrotechniek.

Stellingen bij het proefschrift

"Low-current behaviour and current chopping of vacuum arcs" van René Smeets

-1-

De konklusie van Ecker, dat een vakuumontlading voor lage stromen een negatieve stroom-spannings karakteristiek heeft, is onjuist. Hieruit volgt dat stroombreking in vakuumschakelaars niet veroorzaakt kan worden door ontladingsstroom-oscillaties met een toenemende amplitude.

Ecker G., Beitr. Plasmaphys., vol. 14 (1974) 67-78

-2-

Verkleining van de korrelgrootte van het minderheidsbestanddeel in binaire kontaktmaterialen van vakuumschakelaars leidt tot een aanzienlijke reduktie van het breekstroomnivo. Een geschikte technologie hiervoor is het lokaal snel smelten en stollen van het oppervlak met een elektronenbundel van hoog vermogen.

Schellekens H., EUR-Contract No. SUM-027 Nl (1986);
van Heeren A.H., Kool W.H. en Kievits F.J., EUR-Contract No. SUM-028 NL (1986)

-3-

Gefascineerdheid door apparatuur en een kritiekloos vertrouwen in de resultaten van het gebruik ervan gaan veelal hand in hand.

-4-

Het ontstaan van kathode spots op de vatwanden van Tokamak installaties in de stabiele plasma fase is niet waarschijnlijk. In de instabiele fase echter kan kathode spot emissie het fusie plasma aanzienlijk verontreinigen en kunnen stralingsverliezen door metaalionen een ernstig probleem vormen.

Ertl K. et al., Nuclear Fusion, vol. 25 (1985) 1413-19

-5-

Voorstanders van grootschalige toepassing van kernenergie zouden moeten beseffen dat een wellicht irrationele angst onder grote bevolkingsgroepen voor deze manier van energieproduktie ook een angst is.

-6-

Op grond van de stelling van Van den Heuvel: "Als kunst een scheppende aktiviteit is en esthetica de normatieve leer daarvan, kunnen nieuwe normen in de kunst uitsluitend achteraf door de esthetica geëvalueerd worden", kan de benaming "vernieuwend" voor hedendaagse kunst-uitingen nooit een inhoudelijk waarde-oordeel bevatten.

Van den Heuvel W.M.C., proefschrift Eindhoven (1966)

Het nut van kontakt-konditionering met hoge spanning in het produktieproces van vakuumschakelaars moet worden betwijfeld.

-8-

De benaming van planeten naar figuren uit de mythologie is in het verleden op zuiver willekeurige gronden gebeurd. Het verbinden van bepaalde planeetstanden ten tijde van geboorte met persoonseigenschappen, overeenkomstig die van de mythologische figuren, waarnaar de planeten in kwestie genoemd zijn, tast de geloofwaardigheid van de serieus beoefende astrologie dan ook aan.

-9-

Het verdient aanbeveling in toekomstig onderzoek op het gebied van vakuum-ontladingen kathode-, anode-, en interelektrode-fenomenen niet afzonderlijk te bestuderen, maar de gehele ontlading (inklusief het voedende circuit) als een dynamisch systeem te beschouwen.

Dit proefschrift

-10-

Het ontstaan van hoogfrequente overspanningen over zowel lage stroom vakuumontladingen als hoge stroom ontladingen vlak voor anodespotvorming heeft een gelijke oorzaak: negatieve ruimtelading voor de anode. Het neutraliseren hiervan (door de ontlading zelf) gebeurt daarentegen op geheel verschillende wijze.

Dit proefschrift hoofdstuk 7; Fischer R., proefschrift TU Aachen (1985)

-11-

De bliksem slaat niet in maar uit; bolbliksem daarentegen slaat wel aan maar tevens nergens op.

"Lightning", ed. by Golde R.H., Academic Press, London, (1977), vol. I

-12-

Om het karakter van een land te leren kennen is het noodzakelijk zich te begeven onder de "lagere" klassen, de manier van leven van de rijken is immers bijna overal eender. (Naar J. J. Rousseau).

-13-

Het dreigend tekort aan ingenieurs in de energietechniek kan - bij uitstek in het huidige zg. "no-nonsense" tijdperk - worden verkleind door studenten vroegtijdig te wijzen op de relatief grote direkteuren-dichtheid in deze bedrijfstak.